3-6-2020

Composite Gel Polymer Electrolytes for Extended Cyclability of Lithium-Oxygen Batteries

Marcus Carlton Herndon
Florida International University, mhern544@fiu.edu

FLORIDA INTERNATIONAL UNIVERSITY

Miami, Florida

COMPOSITE GEL POLYMER ELECTROLYTES FOR EXTENDED CYCLABILITY OF LITHIUM-OXYGEN BATTERIES

A dissertation submitted in partial fulfillment of

the requirements for the degree of

DOCTOR OF PHILOSOPHY

in

MECHANICAL ENGINEERING

by

Marcus Carlton Herndon

2020

To: Dean John Volakis
College of Engineering and Computing

This dissertation, written by Marcus Carlton Herndon, and entitled Composite Gel Polymer Electrolytes for Extended Cyclability of Lithium-Oxygen Batteries, having been approved in respect to style and intellectual content, is referred to you for judgment.

We have read this dissertation and recommend that it be approved.

Zhe Cheng

Chunlei Wang

Shekhar Bhansali

Bilal El-Zahab, Major Professor

Date of Defense: March 6, 2020

The dissertation of Marcus Carlton Herndon is approved.

Dean John Volakis
College of Engineering and Computing

Andrés G. Gil
Vice President for Research and Economic Development
and Dean of the University Graduate School

Florida International University, 2020

DEDICATION

To my family and close friends who kept me motivated, genuine, optimistic, energetic, spontaneous and happy throughout my academic tenure. Without their love, patience, ideas and support, none of this would have been possible.

For all African Americans and Blacks, who seek a familiar face and role model, to show that we, as individuals and as a culture, are more than just scholars, entrepreneurs, or creative artists, but we are a combination of all 3. We are originators, we are trendsetters, we are beautiful, and we are unstoppable! I am proud to have come this far, and I will keep pushing the envelope forward! YAY-YAY!

~ MARC.MADE

ACKNOWLEDGMENTS

I would like to express my deepest appreciation to Dr. Sonja Montas-Hunter, Dr. Shekhar Bhansali, Dr. Jaffus Hardrick, Dr. Alla Mirzoyan and Dr. Bilal El-Zahab for their support, suggestions, and both professional and personal guidance during my graduate studies. I am grateful to all my fellowship colleagues, committee and lab-mates specifically, Dr. Amir Chamaani, Dr. Meer Safa and Dr. Neha Chawla for their invaluable help and support, in experimental technique and instruction. I acknowledge all copyright permissions for usage of their figures and illustrations in this dissertation.

I would also like to express my gratitude to all the people who have helped and given me support throughout the completion of my graduate studies. First, to God, and my amazing family (mother Darlene Herndon, father Lawrence Herndon Sr., and brother Lawrence Herndon Jr.) who have always supported and loved me unconditionally. Secondly, to my colleagues, whom I have built lasting relationships and experiences with throughout my academic tenure. Last but not least, to my close friends and creatives, who have constantly given their love, support and companionship, thank you and may all your talents, admirations and hard work pay off and gain notoriety.

I acknowledge the University Graduate School at FIU for supporting me through scholarship, namely the National Science Foundation Bridge to the Doctorate, McKnight Doctoral, Delores A. Auzenne, Start-Up FIU and GEM Fellowship programs, and the Lion Battery Technologies, Inc. grant for tuition assistance and funding during my graduate tenure.

ABSTRACT OF THE DISSERTATION

COMPOSITE GEL POLYMER ELECTROLYTES FOR EXTENDED CYCLABILITY OF LITHIUM-OXYGEN BATTERIES

by

Marcus Carlton Herndon

Florida International University, 2020

Miami, Florida

Professor Bilal El-Zahab, Major Professor

In lithium-oxygen (Li-O_2) batteries, addressing challenges like electrode degradation, cell stability and electrolyte decomposition are key to creating more practical applications. Despite many attempts to minimize anode oxidation and cathode byproduct formation, electrolyte decomposition remains the leading source for rapid capacity fading and poor cyclability in Li-O_2 batteries. Understanding the loss of functionality in electrolytes, carbon nanotube (CNT) fillers and redox mediators (RM), during cycling within Li-O_2 battery systems, could be the solution to prolonging battery lifetime. Determining the efficiency of these battery components and additives will push the medium towards lifelong, rechargeable and safe battery configurations.

Composite gel polymer electrolytes (cGPE) consisting of an acrylate-based polymer, tetraglyme based electrolyte, and glass microfibers provided a stable membrane for a dual-enhancement system consisting of (1) CNT loaded onto a porous carbon cloth at the cathode for oxygen inlet and (2) a lithium-iodide (LiI) RM to oxidize the Li-O_2 battery during charge, thus reducing overpotential.

Combining the battery performance improvements of the highly conductive CNT fillers, charge mediation of LiI RM, modified cathode loading (0.5 mg to 0.1 mg) and ionic transport properties of glass microfibers, resulted in a superior 1663% increase in charge/discharge cyclability (CCD) for maximized cGPE (423 cycles) cells, when compared to the control GPE (24 cycles) cell. Results using in-situ electrochemical impedance spectroscopy (EIS), Raman spectroscopy and cyclic voltammetry (CV) revealed that the source of the improvement was the rate of lithium carbonate formation being reduced on the surface of the cathode. Operation using thin, multi-layered concentric CNT fillers with LiI RM decreased Li_xRCO_3 (R- carbon and hydrogen groups) formation rates due to the decreased electrolyte and cathode decomposition rates. This stabilization during cycling helped prolong battery life to 401 cycles (in comparison to 75 cycles from other CNTs) by maintaining lower charge potentials, since higher potentials have been associated with rapid cell deterioration.

In this dissertation, Li-O_2 battery cyclability was extended by improving ionic transportation in the electrolyte, and charge mediation and conductivity in the cathode from LiI RM and CNT fillers, respectively. These batteries provide a wealth of application primarily in electric vehicles, grid and consumer electronics.

TABLE OF CONTENTS

LIST OF TABLES

TABLE PAGE

LIST OF FIGURES

FIGURE PAGE

1 INTRODUCTION

Batteries, or electric cells, are devices that produce electricity from a chemical reaction. A single cell battery is comprised of a negative anode, an electrolyte for ion conduction, and a positive cathode [1]. Batteries are primarily categorized into 3 different types including: household, industrial and vehicle batteries. The household battery is the most commonly used battery, which includes non-rechargeable (AA, AAA, etc.) and rechargeable (typically lithium or lithium-ion, used in electronics) [2-4], allowing the battery to be recharged after discharge for multiple uses before being recycled. Industrial batteries are used to power heavy duty applications and backup generators for telecommunication utilities, while vehicle batteries (commonly lead acid batteries) are used to power our boats, cars and motorcycles on a commercial scale. Improved battery development and optimization techniques must be considered to offer more practical, user-friendly applications [5-23].

1.1 Transportation Impact of Batteries

Transitioning from gasoline-based vehicles to the partial electric vehicles like hybrid electric vehicles (HEVs) and plug-in hybrids (PHEVs), or fully electric vehicles (EVs), has begun [24-27]. Li-ion batteries have been in demand for electric vehicles for many years. Despite many developments in the Li-ion battery field, the current state-of-the-art Li-ion batteries cannot meet many requirements for emerging applications such as future EVs. Energy density of 2 to 5 times greater than current Li-ion batteries are needed to meet the performance requirements of PHEVs with a 40-80 mile and EVs with a 300-400 mile

driving range [24]. Table 1 shows various Li-ion chemistries developed by different companies, which is currently being used in EVs ranked by present sales in the United States [26].

Manufacturer	Model	Battery Size (kWh)	Supplier	Vehicle Range (mi)	Vehicle Range (km)
Tesla	S	60-100	Panasonic/Tesla	208-315	334-508
Tesla	X	60-100	Panasonic/Tesla	208-315	334-508
BMW	I3	22, 33	Samsung/Bosch	80, 114	129, 183
Nissan	Leaf	24, 30	AESC/LG Chem	84, 107	135, 172
Volkswagon	e-Golf	24, 358	Panasonic	83, 124	135, 200
Chevrolet	Spark	19	A123	82	132
Fiat	500e	24	Samsung/Bosch	87	140
Kia	Soul EV	27	SK Innovation	90	145
Smart	Fortwo EV	17.6	LG Chem	68	109
Ford	Focus EV	35.5	LG Chem	100	160
Mercedes	B-Class Electric	28	Panasonic/Tesla, SK Innovation	85	137
Mitsubishi	I	16	Toshiba	62	100

Table 1. Batteries for present-day electric vehicles (EVs) sold in US [26].

Current commercial batteries are approaching the performance needed for PHEVs; however, the recent developments in energy density (approximately 350 km performance) and price reduction of Li-ion batteries by Tesla Motors and Panasonic's partnership is not sufficient for future EVs. Beyond Li-ion batteries (BLIs) such as Li-sulfur and metal-air batteries have been developed to replace the current Li-ion batteries. Figure 1 shows some of the recent advances in Li-ion energy density and price packs along with the future battery chemistries [27].

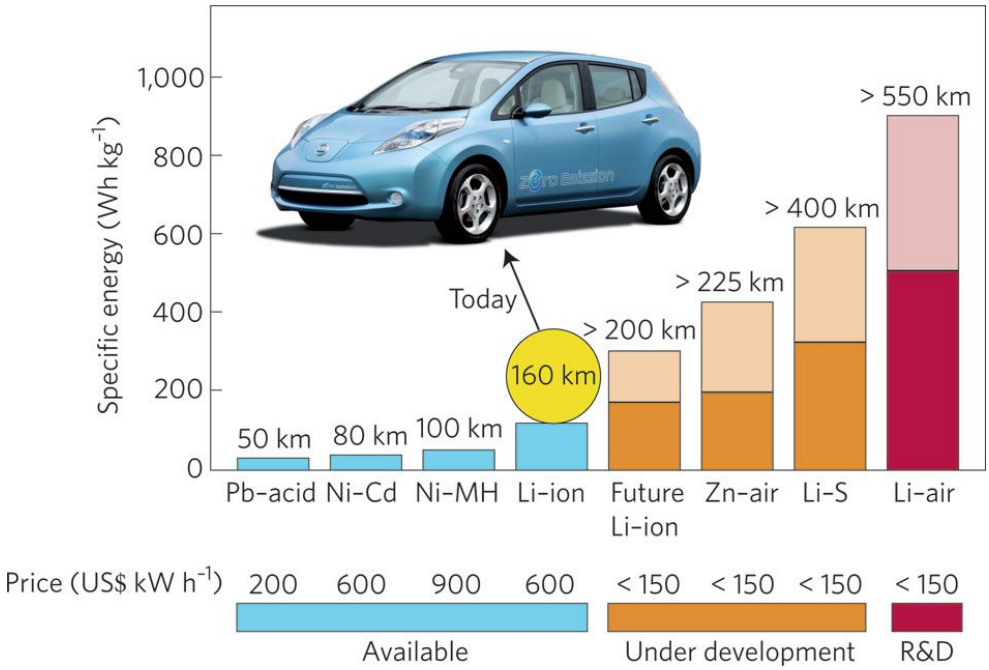

Figure 1: Practical specific energies for some rechargeable batteries, along with estimated driving distances and pack prices. Permission from [27].

In 2013, it was estimated that transportation technology was responsible for 25% of air pollution and greenhouse gas emissions (GHG) due to its distribution of particulate matter in urban areas, causing important human health impacts [28, 29]. The international energy

agency (IEA) estimated that the transportation sector could potentially achieve a reduction of 18% of GHG until 2050 [30]. An attractive advantage of electric vehicle (EV) operation is its power-train efficiency of 60-80% (no tailpipe emissions), [31] in comparison to internal combustion engine vehicle (ICEV) that only have a 20% to 35% efficiency. As reported by Hawkins *et al.* [32], the average European electric-vehicle lifetime approximated to 150,000 km. Utilization of EVs entirely could reduce global warming potential (GWP) by approximately 20% compared to ICEVs [29]. Unlike ICEVs, EVs use the installed battery system for complete vehicle operation including auxiliary ports, propulsion, electronic functionality and HVAC and radio functionality [33].

The environmental scalability of EV battery systems, when compared to ICEVs, depend on the capability of future battery technologies to increase energy, power density and battery life while decreasing cost [34]. Commercial traction batteries are heavy and expensive devices that consist of raw materials, that are high in energy (e.g., aluminum, copper, nickel, cobalt, graphite) [35]. These 2 factors, environmental scalability and high-energy raw material sources, combined with increased demand for more capable energy storage system technologies, have inspired research efforts to improve our technological standpoint on energy capacity and cost [34, 36, 37].

1.2 Environmental Impact of Batteries

Due to wide-scale commercializing of batteries, there have been significant economic and environmental impacts. Without proper disposing methods i.e. battery recycling, batteries can be extremely harmful to the environment due to the many chemicals (cadmium, lead,

zinc, manganese, nickel, silver, aluminum, lithium, various acids, etc.) [38] used to make them. These chemicals act as toxins to the environment causing air, water and soil pollution, [39-42] and body damage. Batteries that decompose in landfills experience a photochemical reaction that emits greenhouse gases effecting climate change.

Lead/ lead dust is probably the single largest soil contaminant worldwide because it has been widely introduced into soil and local water supplies from anthropogenic sources like gasoline, paint, mining and other industrial activities [43]. Lead can be absorbed into the body through inhalation and ingestion (drinking or consuming fish from contaminated water), both of which are equally dangerous. Health problems attributed to lead in adolescents (among others) are well documented [44, 45] and are of growing public health concern. Lead contamination in urban areas, where children have a high risk of exposure and contamination are at the top of these concerns [46, 47]. Mass lead poisoning was recently reported in Senegal [48] and Nigeria [49] in villages that participated in informal recycling of used lead-acid batteries. In 2016, lead was found to be in the drinking water of Flint, Michigan, and could be associated with improper recycling of chemicals (that have an association with batteries), ultimately effecting people [50, 51]. While not reported to be the determining suspect, lead poisoning in Flint, Michigan could be attributed to poor battery recycling and decomposition [52]. Long term health effects (5+ years) from this instance has yet to been evaluated in patients, however, common high-level exposure to lead has been seen to cause anemia, weakness, kidney and brain damage, damage a developing baby's nervous system and even death [53].

Sulfuric acid (commonly found in car batteries) is highly corrosive and can cause permanent blindness when exposed to the eyes. Ingestion of crops contaminated by sulfuric acid or cadmium, which is commonly used in nickel-cadmium batteries, can fatally damage internal organs [38, 42, 54]. Industrial waste depositions and poor crop fertilization inspection (sewage and superphosphate exposure) has led to an abundance in cadmium contamination in soil and plant tissue [55, 56]. This contamination affects food and crop toxicity which are considered harmful to humans and animals when consumed. Soil-contamination diseases like the itai-itai ("it hurts-it hurts") disease were documented in Japan in the early 1900s, while workers mined the Japanese Toyoma Prefecture [55]. It is stated that improper mining techniques led to large cadmium deposits into the Jinzu river, which was a common source for rice irrigation. Neighboring residents who subsequently consumed the cadmium-absorbed rice were reported to have extreme leg and spinal pain, as well as infections and kidney failure.

1.3 Economic Impact of Batteries

The average household in America consumes about 897 kWh per month at an $0.12/ kWh, in electricity, resulting in roughly 10,765 kWh (29.5 kWh/ daily) and $1,291.80 annually [57]. This equates to roughly 2.93 times more than common households in southern European countries (Portugal, Italy, Spain, Greece) whose common household has an average consumption of 3673 kWh/year, translating into roughly 10 kWh/daily [58]. EV batteries have 10-85 kWh of capacity [59]; enough to power a home. Table 2 presents battery options for current-market EVs and their potential 2nd life capacities after automobile use. According to [60], repurposing electric vehicle batteries for residential

applications verified that second life applications (up to 70% degradation) can satisfy the energy containment needs of modern European households (and about half an American household consumption, not considering the Tesla Model S) [60].

Electric Vehicle	Initial Capacity (kWh)	2nd Life Capacity (kWh)
Nissan Leaf	24	16.8
Chevy Volt	16.5	11.55
Tesla Model S	85	59.5
BMW i3	18.8	13.16
Citroen C0	14.5	10.15

Table 2. Remaining capacity of the battery of some EV, considering 70% degradation of its initial capacity.

The cost of secondary battery utilization in battery management systems (BMS), capable of controlling complete charge and discharge cycling (maximizing its lifespan) [61-64], has become dependent on cell packaging. Packaging (monitoring and safety) and installation costs ("Other") were defined as 5% of the total repurposing cost. The final end-consumer pricing acquisitions for EV battery energy storage systems are presented in Table 3 (re-evaluated for the USD; 1 pound (€) = 1.3 dollar ($)).

EV	Battery ($)	BMS ($)	Other ($)	Total ($)
Chevy Volt	510.51	1950	123.03	2583.54
BMW i3	581.67	1404	99.28	2084.95
Citroen C0	448.63	1404	92.63	1945.26
Nissan Leaf	742.56	1950	134.63	2827.19

Table 3. Cost of the storage system for the end user, in $ [60].

With annual costs, at an average $0.12 per kWh, totaling $1,291, and assuming the BMS would last longer than 2 years, consumers would see positive gain from using a modern-day battery system after just 2 years of use under current conditions. According to [65, 66], a solar panel produces about 1 kWh per day (365 kWh annually). When partnered with an energy storage system, this total cost would be reduced by $110/ year, equivalent to a month of complete solar energy consumption each year in the United States.

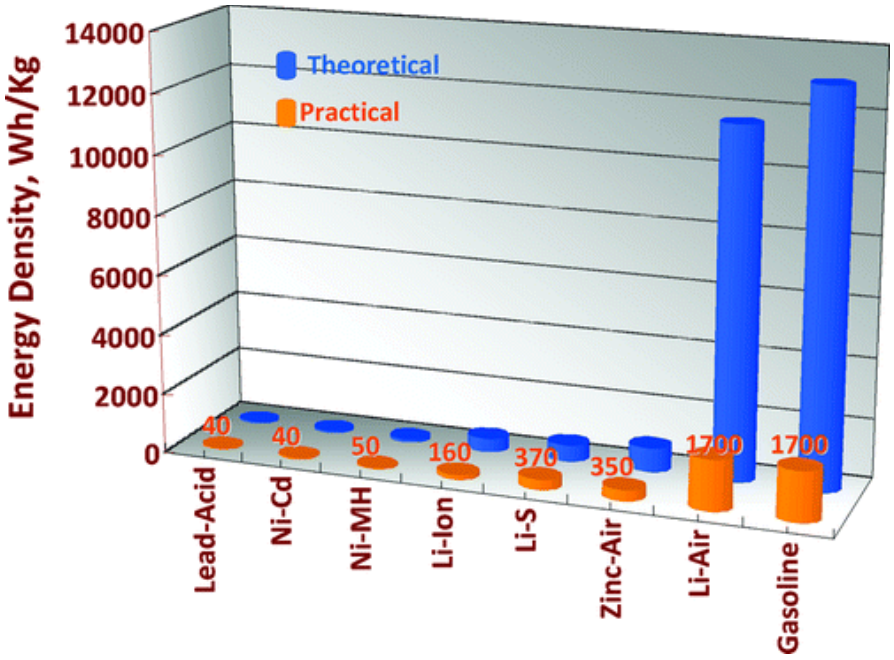

Figure 2. Practical and theoretical gravimetric energy densities (Wh/kg) of different rechargeable battery compositions compared to gasoline. Practical values for most rechargeable batteries are still in its infancy, therefore considered an estimation, while gasoline's value represents its average tank-to-wheel efficiency of cars. Permission from [67].

Rechargeable batteries have revolutionized industry due to their storage capabilities and reusable battery life. Despite their initial cost being more than the disposable, non-rechargeable batteries, their total cost of ownership and environmental impact are significantly reduced due to their inexpensive means of recharging before needing to be replaced [67]. Examining ownership costs (per kWh) include cost per cycle, longevity, replacement and disposal. Table 4 analyzes the costs and energy comparisons in modern day batteries. In 2017, Tesla, Inc. began manufacturing of its Model 3 EPA-rated all-electric Standard Range (220 miles (354 km)) and Long Range (325 miles (523 km)) vehicle [68, 69]. According to reports, Tesla's battery cell cost is at $111/ kWh at its

Nevada Gigafactory with aims to be at $100/ kWh by end of the year, enabling standard Model 3 battery packs [70-72].

Battery	Specific Energy (Wh/kg)	Cycle Life	$USD per kWh (powertrain)
Lead Acid	30 to 50	Moderate	$100 to $200
NiCd	45 to 80	High	$300 to $600
NiMH	60 to 120	High	$300 to $600
Li-ion	100 to 250	High	$300 to $1000

Table 4. Energy and cost comparison for rechargeable batteries.

1.4 Architectural Impact of Li-O_2 Batteries

While this report thus far has summarized the battery's environmental and economic impact due its commercialization over time, the future of battery technology and energy generation is dependent upon lithium-oxygen and lithium-air battery practicality. Practicality of the Li-O_2 and Li-air batteries depend on the optimization of its oxygen reduction reactions (discharge) and oxygen evolution reactions (charge). Figure 3 details different battery architectures that effect charge and discharge reactions in Li-O_2 batteries.

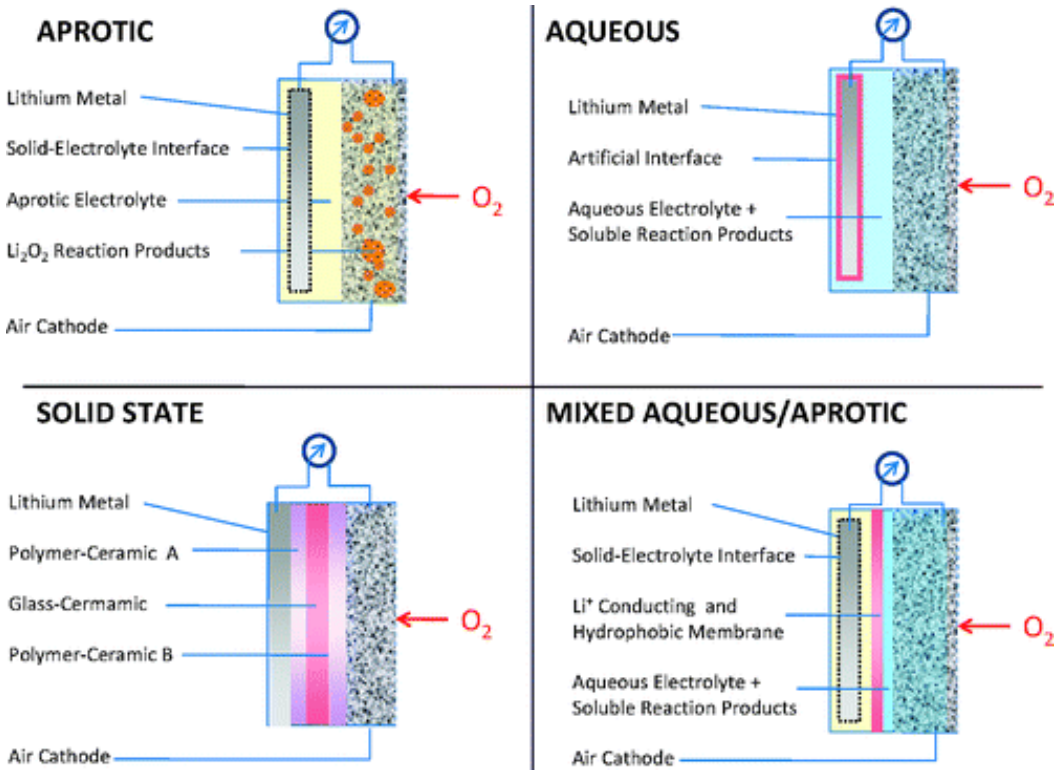

Figure 3. Principal architectures of Li-O_2 batteries: aprotic, aqueous, mixed aprotic-aqueous and fully solid-state architecture are labeled. Surface electrolyte interfaces (SEI) along the lithium anode are given as dashed and solid lines. Permission from [67].

Solution-mediated Li_2O_2 formation on Li-O_2's electrode surface is due to the aprotic liquid electrolyte's intermediate donor number (DN). The DN compatibility with the lithium metal anode sustains its oxidation potential stability up to 4 V versus Li/Li^+, allowing for safe, consumer friendly and reduced pressure for higher molecular weighted solvents [73]. Solid-state electrolytes are generally categorized into two general classes depending on their materials used: (1) Li^+ ion conducting inorganic ceramics and (2) organic polymers. Solid-state electrolytes can sustain functionality under high temperature and act as substantial barriers against ambient gas diffusion and moisture toward the Li metal anode. The high interfacial resistance between ceramic electrolyte/electrodes prevent practical

application usage due to its reactivity with ambient atmospheres. Solid polymer electrolytes (SPEs) could be a safe and viable substitute to ceramic electrolytes due to their high thermal, mechanical and electrical stability, and considerable anode protection. According to [74], the chemical stability of polymers used in SPEs could negatively react with discharge byproducts, suggesting focus should primarily attack stable SPE-carbon interfaces. Figure 4 illustrates the common polymers and their structures used in SPEs. Common polymers include: Polyacrylonitrile (PAN), Polymethyl methacrylate (PMMA), Polyvinyl chloride (PVC), Polytetrafluoroethylene (PTFE), polyethylene oxide (PEO), Polyvinylpyrrolidone (PVP), Polyvinylidene fluoride (PVDF) and Polyvinylidene fluoride-co-hexafluoropropylene (PVDF-HFP).

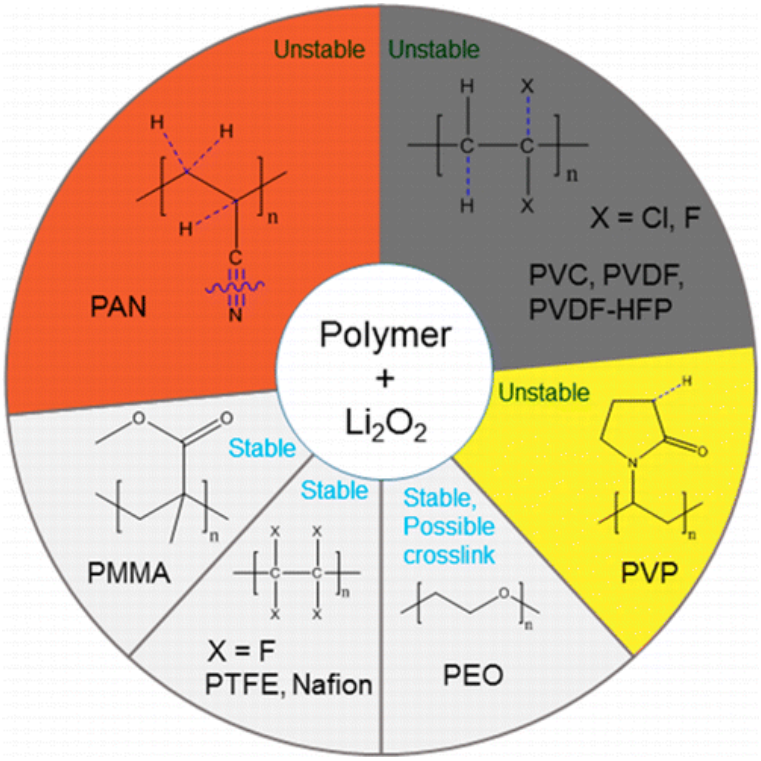

Figure 4: Common polymers and their structures used in SPEs. Permission from [74].

The lack of liquid solution in Li-O_2 batteries obstruct the overall capacity in SPEs, extending to a poor reversibility and low ionic conductivity [75]. SPEs can be swollen with a liquid plasticizer to form gel polymer electrolytes (GPEs). These GPEs offer the ideal mechanical properties of SPEs along with the high ionic conductivity of its liquid counterparts. However, using organic carbonates as plasticizers in GPEs is questionable due to their tendency to decompose in the presence of oxygen radicals. Different GPEs using various polymer hosts and aprotic liquid electrolytes have been developed for Li-O_2 batteries [76].

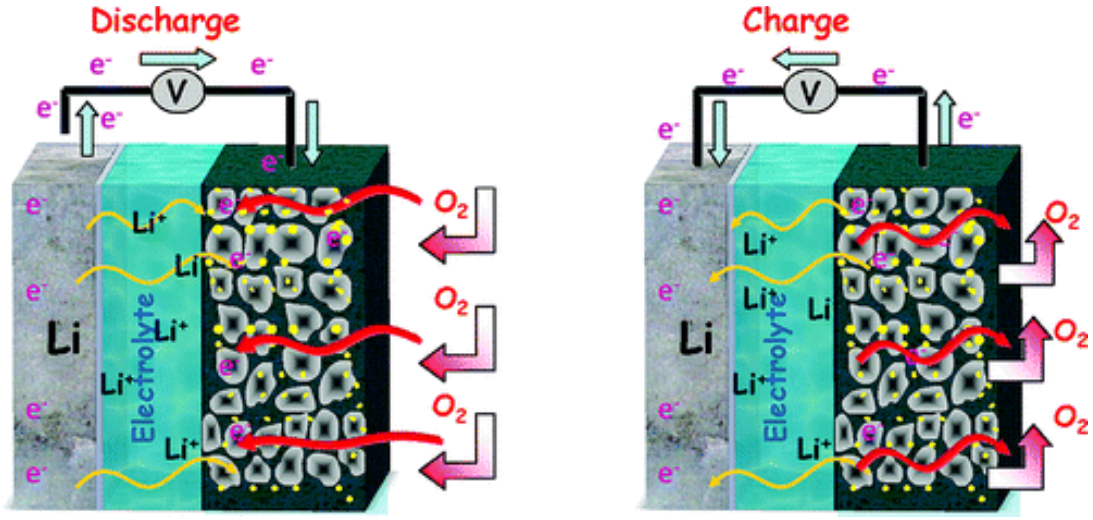

Figure 5. Schematic operation proposed for the rechargeable aprotic Li-O_2 battery. Permission from [67].

The most commercially ideal usage of the aforementioned configurations would be an electrolyte that can make contact with an air-ambient atmosphere, while deterring unwanted contaminants and reactions. Cycling electrochemical reactions between

discharge and charge should generate an equilibrium voltage of 2.96 V to approximately 4 V, respectively. Optimizing and sustaining the electrochemical stability between the electrolyte and electrodes (specifically the cathode) are the deciding factor in Li-O_2 battery system practicality and commercialization. Experimental facts, summarized by [77], all suggest the formation of small, glassy carbon (~ 40 nm thick) and Li_2O_2 byproduct (~ 100 nm long) deposits on the CNT cathode [67, 78, 79] during discharge cycling.

1.5 ORR (Discharge) in Li-O_2 Batteries

Rechargeable Li-air batteries were introduced by Abraham and Jiang in 1996 [80], and since has been a cornerstone for our practical understanding of rechargeable technology. Many electrolyte configuration systems have been reported like Read's [79] non-hydrolytic lithium salts with low volatile, highly stable aprotic organic solvents, Zhang *et al.*'s [81] moisture resisting (hydrophobic) composite gel polymer electrolyte membrane to protect the lithium anode from atmospheric contamination, and Wang *et al.*'s [82] dual electrolyte system separated by a super-ionic glass conductor. In all reports, it has been documented that negligible change in polarization occurs at the lithium anode current density during discharge (> $mAcm^{-1}$) [80, 83] suggesting research should address the cathode voltage loss primarily and explore catalysts to stabilize the cathode during oxidation reduction reaction (ORR) [84]. Unfortunately, connecting reported normalized currents of examined catalysts with the intrinsic activity of ORR has proven difficult [85]. This is because the catalyst particle sizes and loadings can be significantly different among these studies. Carbonate-based electrolytes used in these studies [78, 85-88] have created additional complications

due to their instabilities against superoxides, forming Li_2CO_3 instead of LiO_2 or Li^+ friendly oxides during ORR [89-95].

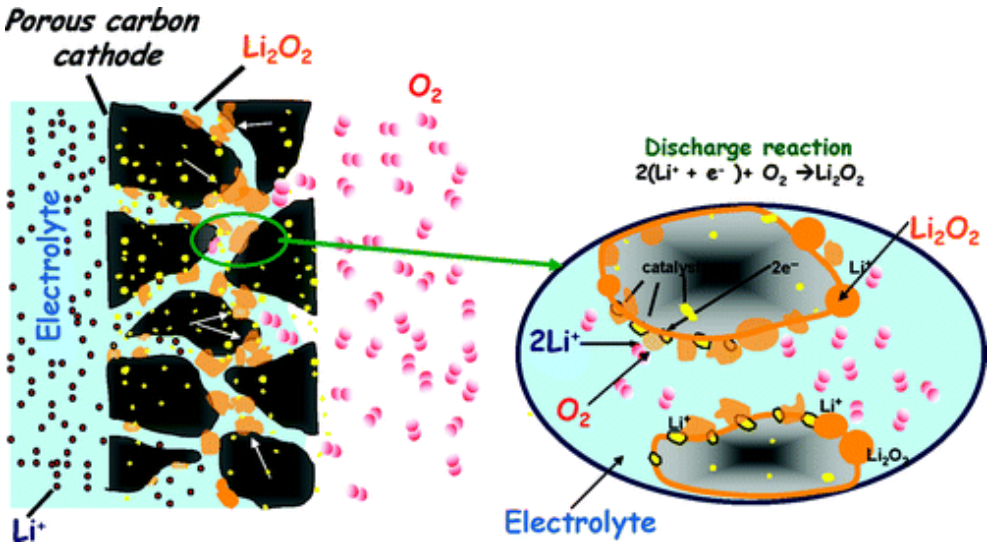

Figure 6. Schematic representation of the proposed chemistry in the porous carbon cathode (left) and an expanded view of the cathode discharge reaction (right). Permission from [67].

During discharge, or ORR, the lithium anode is oxidized by releasing an electron into the battery system producing lithium ions, while oxygen is reduced at the cathode forming lithium peroxide (Li_2O_2) or lithium oxide (Li_2O) [27, 67, 81, 96-98]. Reduction of O_2 to Li_2O_2 at the cathode during discharge normally proceeds via the intermediate LiO_2 in a Li-O_2 cell [99]. As reported by Lu [100], cyclability is improved by limiting LiO_2 byproduct formation during discharge at the expense of specific energy (1 e^-/O_2 for LiO_2 instead of 2 e^-/O_2 for Li_2O_2). The extra electron formed on the O_2 molecule orbital during this process allows for a stepwise transformation of highly reactive, superoxide and peroxide ions that are only stable on inorganic surfaces with non-reactive centers [91, 101]. During charge, oxygen evolution reaction (OER) occurs, causing the lithium oxide discharge products to

be reconverted to lithium and oxygen singlet molecules in the cell atmosphere. Iodide in lithium acts as a redox (reduction oxidation) mediator to assist with the spare electron during charge (OER) from Li_2O_2 to Li^+ and O^-, overall helping reduce overpotential of the charge/discharge cycles.

1.6 OER (Charge) in Li-O_2 Batteries

Superoxide specie attacks typically occur on the carbon cathode, which result in radical nucleophilic reactions and oxidation of olefins with activated double bonds [102, 103]. As reported previously [90, 104], a highly reversible one-electron process ($O_2 + e^- \leftrightarrow O_2^-$) during discharge of the Li-O_2 cell is initiated with the transient formation of O_2^-. The O_2^- tends to attack the positively charged components of the present organic species within the system [105] thereby stabilizing the O_2^- in the CNT cathode due to its soft acidity of the cation [106, 107]. Introducing Li^+ cations disproportionate the O_2^- ions to peroxide or O_2 molecules [108]. Li^+ ions transported from the GPE into the CNT cathode are incorporated with all of the super-oxides, forming LiO_2, and then decompose to produce the Li_2O_2 obeying the hard-soft acid base theory of Pearson [109, 110]. Any water (H_2O) molecules permeated through this cell's atmosphere promotes partial Li_2O_2 decomposition, therefore facilitating the charging process by improving Li^+ ions transference through the GPE into the CNT cathode [111]. Studies by McCloskey [112] and Gallant [113] conclude that lithium peroxide reacts with carbon leading to carbonate byproduct formation, however, carbon's unique physical properties keep graphene [95], carbon nanotubes [114], etc. highly attractive as cell conductors.

#	Equation	Type
1	$Li^+ + O_2 + e^- \rightarrow LiO_2$	Oxygen Reduction Reaction (ORR)
2	$2Li + O_2 \rightarrow Li_2O_2$	ORR at the cathode
3	$2Li + 2H_2O \rightarrow 2LiOH + H_2$	Corrosion of Li anode
4	$2LiO_2 \rightarrow Li_2O_2 + O_2$	
5	$2Li_2O_2 + 2H_2O \rightarrow 4LiOH + O_2$	Hydration
6	$2LiOH + CO_2 \rightarrow Li_2CO_3 + H_2O$	
7	$Li_2O_2 \rightarrow 2Li^+ + O_2 + 2e^-$	Oxygen Evolution Reaction (OER)
8	$4LiOH \rightarrow 4Li^+ + O_2 + 2H_2O + 4e^-$	OER
9	$2Li_2CO_3 \rightarrow 4Li^+ + O_2 + 2CO_2 + 4e^-$	OER
10	$I_3^- + 2e^- \rightarrow 3I^-$	
11	$2Li + I_3^- \rightarrow 2Li^+ + 3I^-$	Redox Mediator

Table 5. Speculated reactions of the Li-O_2 cell.

1.7 Fundamental Mechanisms of Li-O_2 batteries

The first primary lithium-air batteries were introduced by Littauer and Tsai in 1974, in which an aqueous alkaline solution was used as an electrolyte [73]. In their batteries, typical open circuit voltage (OCV) was about 2.9-3.0 V, and cell voltage of 2.0 V was achieved at current densities of approximately 200 mA/cm^2. In their batteries, at OCV and low current density, self-discharge of the lithium anode was rapid, so electrochemical efficiency of the cell was very low. The first rechargeable Li-air battery was developed by Abraham and Jiang [80] using a GPE containing a nonaqueous electrolyte. The cell

consisted of a lithium metal anode, a GPE and a carbon air cathode with a catalyst. Their GPEs consist of polyacrylonitrile (PAN) and carbonate-based electrolyte containing $LiPF_6$ lithium salt. The observed OCV was around 3.0 V at room temperature and the formation of lithium peroxide (Li_2O_2) on the surface of cathode, after discharge, was also confirmed. The capacity of the nonaqueous Li-air battery depends on the weight of the carbon cathode and its surface area as the discharge product Li_2O_2 is insoluble in nonaqueous electrolytes. In 2002, Read [79] developed a high capacity carbon air electrode using super P carbon black in carbonate-based electrolyte (propylene carbonate (PC) and diethyl carbonate (DME)) containing $LiPF_6$ lithium salt. In 2006, Bruce [4] and his coworkers reported the possibility of improved cycling of Li-air battery by using Super P carbon black with an electrolytic manganese dioxide. However, in 2010, Mizuno [94] reported that lithium carbonate (Li_2CO_3) and lithium alkyl-carbonate are the main discharge products, instead of Li_2O_2 in carbonate-based electrolytes.

In typical Li-O_2 batteries, the cell consists of Li metal as the anode, porous carbonaceous air as the cathode and Li^+ containing aprotic electrolyte separating the cathode and anode. During discharge, an oxidation reaction occurs at the anode ($Li \rightarrow Li^+ + e^-$) and electrons flow through an external circuit. Li^+ ions generated from this reaction are transferred to the cathode through the electrolyte. At the cathode, the Li^+ reduce oxygen to form Li_2O_2. Standard potential for the overall cell reaction, U_0, can be calculated by the Nernst equation as follows:

$$\text{Nernst Equation: } U_0 = 2.96 \text{ V vs. Li} \qquad (1)$$

In charge, the ($Li \rightarrow Li^+ + e^-$) reaction is reversed, lithium metal is plated out on the anode, and O_2 is evolved at the cathode. Figure 7 shows a typical charge/discharge curve known as the voltage profile of Li-O_2 battery [67]. As illustrated, the working voltage of this cell during discharge is approximately between 2.6 V and 2.7 V, which is significantly less than the thermodynamic cell voltage (also known as OCV), 2.96 V. This difference is called the discharge overpotential (ηdis). During galvanostatic charging of the cell, the voltage increases to approximately 4.0 V. Hence the charge overpotential (ηchg) is significantly greater than the discharge overpotential (ηdis). The electrical energy efficiency for a charge/discharge cycle is only 65% (2.6 V/4.0 V=65%) [67].

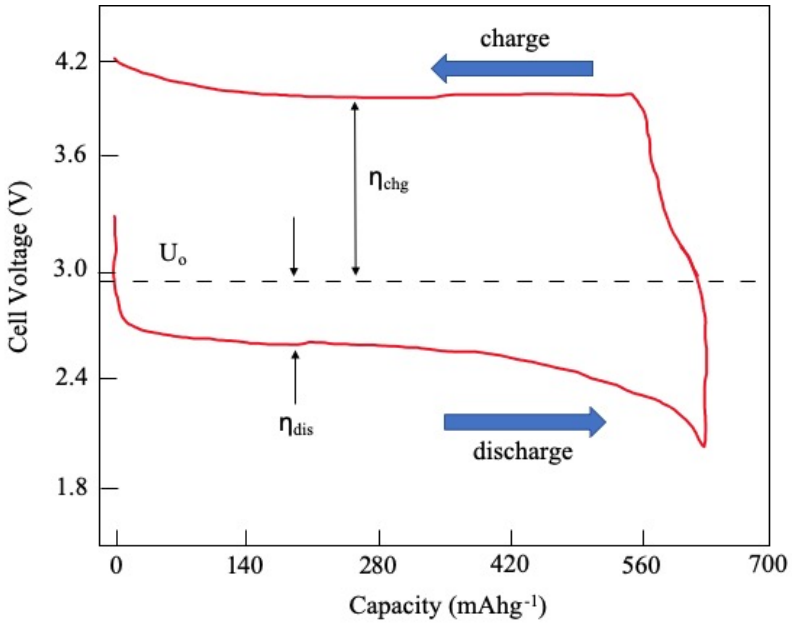

Figure 7: Typical voltage profile (charge/discharge curve) of Li-O_2 batteries along with its overpotentials [67].

Many factors influence the charge or discharge overpotentials, such as the deposition of side reaction products from the electrolyte and electrode degradation [112, 115]. For example, the discharge processes depend on some competitive factors such as effective current density, voltage cut-off (overpotential), and whether the LiO_2 intermediate, which is formed during discharge, is dissolved in solution or adsorbed on the electrode surface. At high overpotentials and high current densities, O_2 is reduced to form Li_2O_2, which grows as a film on the electrode surface [116, 117]. At low current densities and overpotentials, Li_2O_2 can grow as surface films or large toroid-shape particles from a solution process, depending on the solvent or salt from which the electrolyte solution is formed, depending on the additives in the electrolyte solution [118, 119]. Figure 8 illustrates two different Li_2O_2 formation mechanisms at low current density depending on the donor number (DN) of solvents used in electrolyte [115].

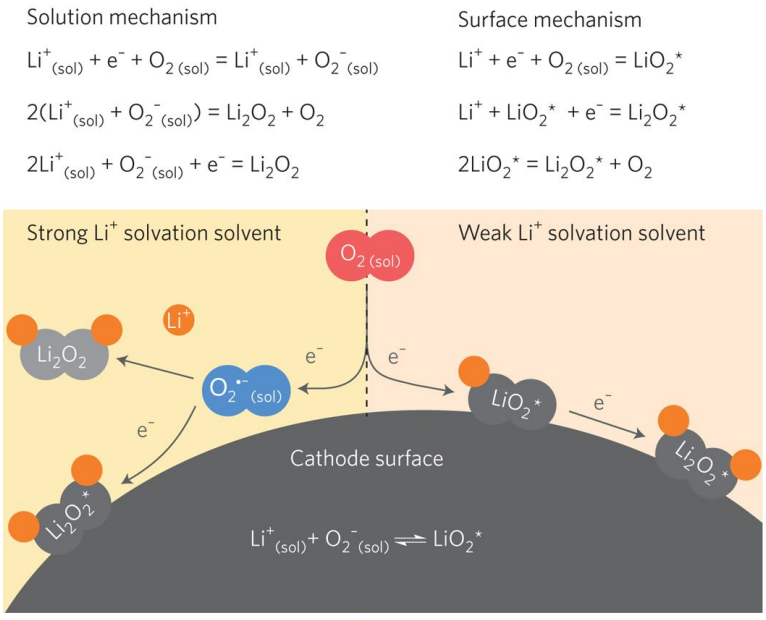

Figure 8: Reduction mechanisms in a Li-O_2 cell at low overpotentials depending on the donor number (DN) of solvent. Permission from [115].

In a high DN solvent, O_2 is generated during discharge and dissolved in electrolyte. Once the concentration of O_2 reaches the solubility limit, it precipitates with Li^+ to produce LiO_2 on the cathode surface and gets reduced or disproportionate to Li_2O_2 (solution-mediated formation). Large toroid-shaped Li_2O_2 [118] can be formed via this mechanism, and accordingly large discharge capacities can be obtained. On the other hand, in a low DN solvent, LiO_2 is generated and deposited on the cathode surface and further reduced via a disproportional or electrochemical process to form Li_2O_2 film on the cathode (surface-mediated formation).

1.8 Challenges with Li-O_2 batteries

Despite a number of studies, Li-O_2 batteries are still in their infancy. Many technical and fundamental challenges still remain to be addressed before their commercialization [119, 120]. Figure 9 depicts the summary of current challenges in Li-O_2 batteries. Up until now, most of the research studies on Li-O_2 batteries have used only limited current densities (one or two orders of magnitude lower than those utilized in commercial Li-ion batteries), so the rate capability of Li-O_2 batteries must improve significantly to make them competitive with current Li-ion batteries. If the higher current densities cannot be achieved, the increase in O_2 flow can be considered as an alternative solution for transport.

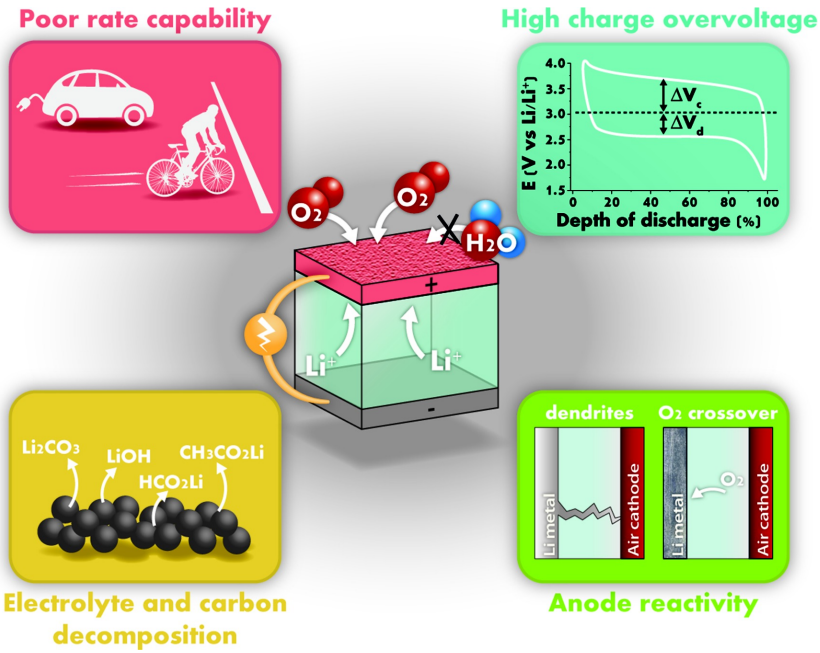

Figure 9: Summary of challenges in Li-O_2 battery applications. Permission from [120].

Advanced chemical and electrochemical techniques have revealed that, to some degree, all components of Li-O_2 batteries undergo undesirable chemical/electrochemical changes during discharge/charge cycling. These challenges and changes are detailed in the sub-sections 1.9-1.12.

1.9 Lithium Anode Degradation

Metallic lithium is the main anode material used in Li-O_2 batteries due to its extremely low weight, low negative potential (-3.04 V vs. standard hydrogen electrode (SHE)) and high specific energy (11,680 $Wh \cdot kg^{-1}$). The usage of Li metal has its own safety concerns as formation of lithium dendrites during repetitive lithium dissolution/deposition can result in poor cycling stability and internal short circuiting. However, Li-O_2 battery failure owing to the dendrite growth has not been reported yet [121]. Recent studies have identified that

reaction of Li metal is due to charge/discharge products and O_2 crossover from the cathode in Li-O_2 batteries [122-125]. Figure 10 illustrates the possible reaction happening at the anode surface in Li-O_2 batteries.

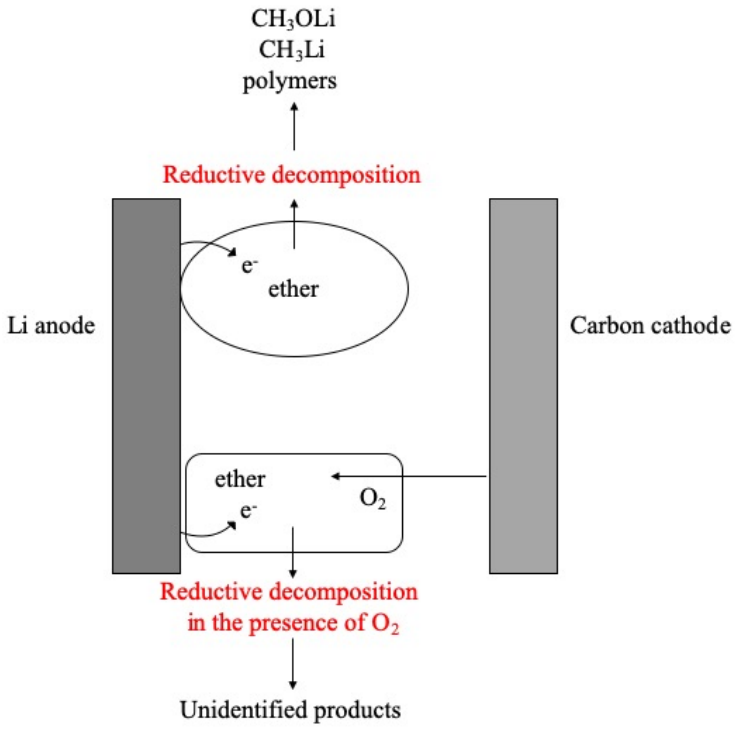

Figure 10: Possible Li metal reactions with and without O_2 [122].

Advanced approaches such as using oxygen and humidity impermeable separators [126] and artificial protective films [127] on the Li anode have been proposed to minimize Li anode degradation. Furthermore, replacement of lithium metal anode with lithiated carbon composites has also been proposed [128, 129].

1.10 Cathode Degradation

While the main discharge product (Li_2O_2) of aprotic Li-O_2 batteries are insoluble in electrolyte, they must be stored in a porous conductive matrix. Carbon in different

allotropes has been used as the cathode material due to its high electronic conductivity, low cost, ease of fabrication and ability to catalyze the ORR/OER [130, 131]. However, recent studies confirmed that carbon can react with discharge products and decompose during both discharge and charge in Li-O_2 batteries. It has been reported that carbon is chemically unstable above 3.5 V in the presence of Li_2O_2 and decompose to lithium carbonates [112]. McCloskey *et al.* [112] reported that lithium carbonate (Li_2CO_3) and lithium alkyl carbonates ($LiRCO_3$) can be produced at the carbon- Li_2O_2 interface and Li_2O_2-electrolyte interface, respectively due to the reaction of discharge product with carbon cathode and electrolyte. Carbonate formation leads to an extra overpotential during charge and subsequently carbon reacts chemically with Li_2O_2 during charge, to produce more lithium. Figure 11 illustrates this process.

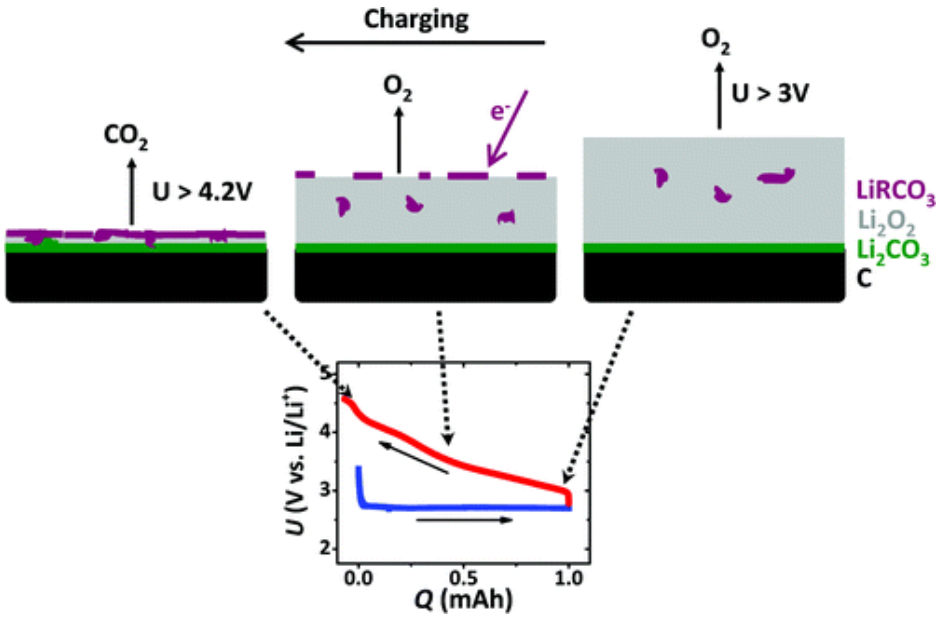

Figure 11: Proposed carbonate formation mechanism due to the reactivity of discharge products with carbon and electrolyte. Permission from [112].

Due to the instability of carbon as the cathode material, many researchers have devoted effort to replacing carbon completely. Peng *et al.* [132] proposed a nano-porous gold (NPG) cathode as a stable cathode for Li-O_2 batteries. Although, NPG was stable and the kinetics of oxidation formation of Li_2O_2 was demonstrated to be faster than that of carbon cathodes, NPG cathodes are not suitable for the cathode due to their high mass of gold, which in turn reduced the specific energy of Li-O_2 batteries significantly. Metal oxides [132, 133] and metal carbides [134] have also been suggested for cathode materials. However, other side reactions were also reported for non-carbon cathodes [134].

1.11 Electrolyte Decomposition

Despite many technological developments of stable cathodes and anodes for Li-O_2 batteries, electrolytes remain a leading cause for rapid capacity fading and poor cyclability [135, 136]. Reactive oxygen species are expected to coexist with molecular O_2 in the electrolyte owing to the ORR/OER, and possible reaction between Li metal and dissolved O_2 [98, 137]. The reaction between these reactive oxygen species with electrolytes have been considered as the main reason for electrolyte decomposition [138]. In general, the electrolyte decomposition pathways can be categorized into five groups as illustrated in Figure 12: (1) nucleophilic attack, (2) auto-oxidation, (3) acid-base reactions, (4) proton mediated degradation, and (5) reduction by Li [137].

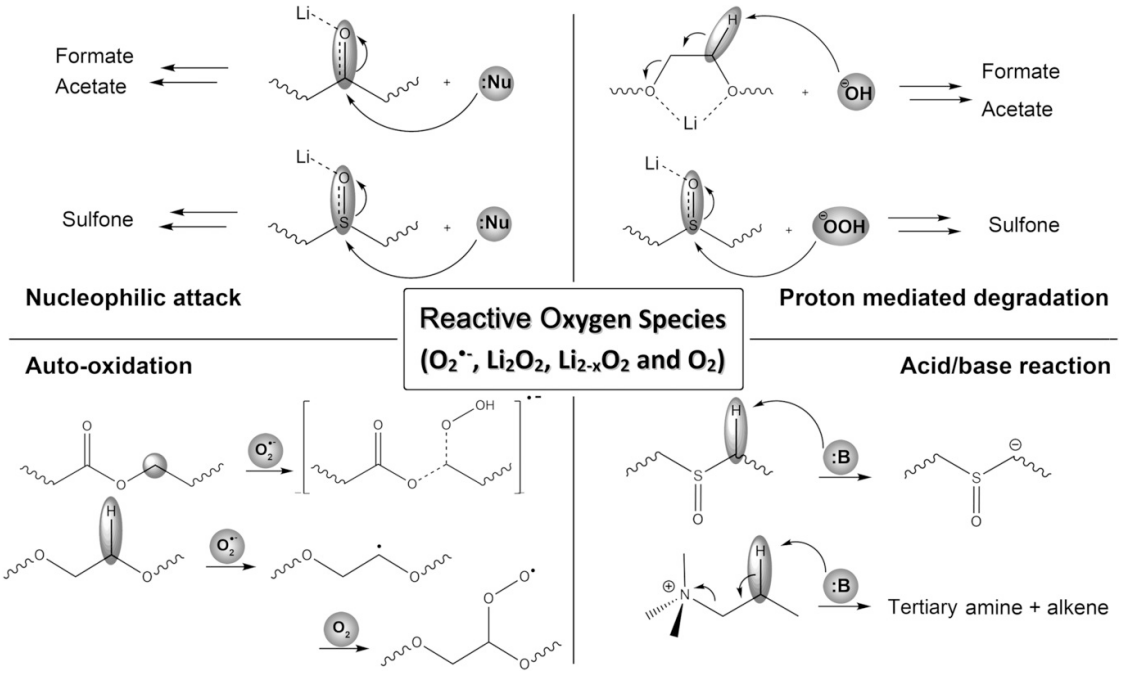

Figure 12: Schematic pathways of electrolyte decomposition by reactive oxygen species. Decomposition mechanisms are dependent on the electrolyte chemistries in the solvent. Permission from [137].

1.12 Electrolytes for Li-O_2 batteries

As mentioned earlier, the electrolyte has a profound influence on the reactions that occur at the anode and cathode, and hence, the overall cell operation of nonaqueous Li-O_2 batteries. Electrolytes in Li-O_2 batteries need to have some certain requirements, as detailed in Table 6.

Equation	Type
Conductivity	Sufficiently high for the anticipated rate capability
Stability	Within potential window used on discharge and charge In contact with O_2 and its reduced species on discharge In contact with Li_2O_2 and its intermediates on charge In contact with the anode or a stable SEI formed
Low Volatility	To minimize evaporation at the porous O_2 cathode
O_2 solubility and diffusivity	To ensure adequate rate of mass transport to the cathode
Electrode surface soaking	Promotes ion transfer and reduces electrolyte volatility
Solubility of Li_2O_2	Interaction with intermediates for high rate and packing density of Li_2O_2
Safety, low cost and toxicity	Provides more applicable and consumer ready usage

Table 6. Requirements on electrolytes for the nonaqueous Li-O_2 battery [5].

In the early stages of Li-O_2 battery research, organic carbonate-based electrolytes were widely used. However, it has been shown that organic carbonates are unstable in Li-O_2 cells, with little to no evidence for Li_2O_2 formation during discharge [90]. The nucleophilic attacks by O_2^- to the C=O groups of carbonate-based electrolyte produce Li-alkyl carbonates and Li_2CO_3 [90, 137]. Therefore, much attention shifted to other aprotic electrolytes for Li-O_2 battery application. GPEs can improve the Li-O_2 battery performance in many ways. For example, it has been reported that the GPE in Li-O_2 cells minimize electrolyte evaporation. GPEs could hinder the Li dendrite growth and form stable surface electrolyte interfaces (SEIs) on the surface of the Li metal anode [139]. They could also prevent Li metal corrosion by inhibiting the O_2 and humidity crossover [126, 140, 141]. Table 7 lists performance properties of various GPEs and solid polymer electrolytes (SPEs) used in Li-O_2 batteries.

Electrolyte Type	Polymer Matrix	Ionic Conductivity ($x10^{-4}$ S cm^{-1})	Voltage Window (V vs. Li/Li^{+})	Operating Atmosphere	Cycles/ Cycle Capacity
SPE	PVA	2.85 (RT)	-	Ambient Air	-
SPE	PEO	3 (RT)	Up to 4.6 V	O_2	20 cycles/ 500 $mAhg^{-1}$
GPE	P(VDF-HFP)	10 (RT)	Up to 4.6 V	O_2	50 cycles/ 500 $mAhg^{-1}$
GPE	PMMA/PSt	1.27 (RT)	Up to 5.3 V	Ambient air, RH= 5%	100 cycles/ 500 $mAhg^{-1}$
GPE	PVDF	-	Up to 4.7 V	O_2	6 cycles/ 500 $mAhg^{-1}$
GPE	PVDF/pBQ	49.8 (RT)	-	O_2	40 cycles/ 500 $mAhg^{-1}$
GPE	P(VDF-HFP)	-	-	Ambient air, RH= 5%	180 cycles/ 500 $mAhg^{-1}$
GPE	P(VDF-HFP) /ETPTA	2.843	-	O_2	100 cycles/ 500 $mAhg^{-1}$

Table 7. List of SPEs and GPEs used in Li-O_2 batteries [76].

1.13 Gel Polymer Electrolytes in Li-O_2 Batteries

Li_2O_2 is deposited on the surface of the cathode via forward ORR discharging, while reverse OER charging decomposes Li_2O_2 [67]. Li-O_2 batteries suffer from poor cyclability due to the reactivity of lithium anode with oxygen crossover, cathode decomposition, and electrolyte evaporation and decomposition [91, 112, 122, 138, 142-144]. Optimization maneuvers to improve performance like lithium anode protection [127], controlled cathode micro-structuring [145] and cathode material substitutions [146] are small examples of advancements in Li-O_2 battery technology. Electrolyte decomposition has been previously reported to yield a solid byproduct microlayer on the surface of the electrode causing rapid capacity fading in Li-O_2 batteries [123, 147]. Electrolyte properties like ionic conductivity, transference number, and surface interface interactions affect the electrochemical performance of Li-O_2 batteries [75, 148, 149].

High interfacial resistances and low ionic conductivity limit the practical applications of both ceramic electrolytes and SPEs at ambient temperature [23]. The high ionic conductivity and low interfacial resistance of GPE, which place liquid electrolytes in a polymer medium, have been a successful technique used in Li-ion battery applications [75, 150-152], and combinations of polymer-solvent pairs in GPEs have shown to efficiently protect the lithium anode from oxygen crossover, while limiting electrolyte evaporation [126, 140, 141, 153-157]. Inorganic filler additions to both liquid and polymer electrolytes (SPEs and GPEs) has resulted in improved Li^+ transport properties through the interaction of fillers with the polymer, solvent, and salt [141, 156-162]. While little attention has been placed upon one-dimensional fillers, zero-dimensional (nanoparticle) fillers have been

suggested as the most significant GPE filler configuration for battery applications [163-168]. As reported in [81, 169, 170], microstructural characterization of the micro-fillers exhibited a broadened peak (glass fillers used in study had an amorphous phase), a surface area of ~ 0.5 m^2/g, non-porous, impurity-free and could be uniformly distributed with no apparent cluster in any particular direction.

AC impedance spectroscopy is used to determine ionic conductivity, σ = L/A·R where, L and A is the thickness and area of surface electrode, respectively, and R is the bulk resistance obtained by high frequency intercepts during electrochemical impedance spectroscopy (EIS). The initial current (I_0), steady-state current (I_{SS}), initial resistance (Z_0) and steady-state resistance (Z_{SS}) are obtained from DC polarization and AC impedance spectroscopy, respectively. Bruce-Vincent method [34] is used to determine lithium transference number, t_{Li+}, by the following equation:

$$t_{Li+} = \frac{I_{SS}\,(\Delta V - (Z_0 \times I_0))}{I_0\,(\Delta V - (Z_{SS} \times I_{SS}))} \qquad (2)$$

Both σ and t_{Li+} values have been reported to act proportional with the increase in micro-filler content until 1%, before noticeable decreases in result. The formation of ion-ceramic structures at the glass micro-filler surface are caused by the cGPEs polymer matrices and its ability to adsorb its TFSI counter-ions.

1.14 CNT in Li-O_2 Batteries

According to [144], conductive filling versus conductive coating at the cathode further confirm that infusing fillers into the battery system improve the lifespan (almost doubling) of the Li-O_2 cell. EIS studies on the palladium coated and palladium filled CNTs (in study [144]) provided insight into the kinetics operating the battery illustrating that R_{ion} had the highest resistance, suggesting battery failure was due to pore-clogging at the cathodes. Additionally, the increasing R_b within this particular study indicates more electrolyte decomposition in the case of palladium coated, rather than palladium filled, CNT cathodes.

As reported by Freunberger [147], Raman shifts at 790 cm^{-1} confirm Li_2O_2 formation on the cathode surface of Li-O_2 cells that utilize cGPE/GPE during discharge, with low frequencies in EIS spectrums/ Warburg resistances due to lithium ion diffusion at the porous carbon cathode [171, 172]. Heterogeneous lithium plating/stripping tests indicate overpotential decreases during initial cycling using both GPE and cGPE-1% [173]. A continuous increase in overpotential would indicate a growth formation created by the electrochemical reaction byproducts of the GPE and electrode overtime [173]. High ionic conductivity and transference numbers, commonly attributed to cGPE-1%, improve cell cycling potential, due to improved mechanical properties which block dendrite growth and stabilize the Li interface by decreasing the interfacial resistance (R_{int}) [124, 160, 174-181]. Accounts of poor rechargeability suggest low OER activity of CNT cathodes, and would need to be accompanied by fillers or redox mediators for improvement in Li-O_2 batteries [144, 182-186].

Other reports [177, 187] have stated that initial anode/electrolyte interface stability is a primary factor in R_{int} of Li-O_2 batteries. Consequently, the initial decrease in the R_{int} is attributed to the dissolution of the passivating film at the anode/electrolyte interface [174], however, the accumulation of irreversible byproducts on the electrode/electrolyte interfaces [123, 177] in later cycles, cause the increase in R_{int}. Studies suggest low salt concentrations are proportional to high concentrations of R_{int} [97, 188]. According to [189, 190], reactions of salt anions and solvent, at low salt concentration, result in faster growing, thicker SEI layers and increasing R_{int}. Further increases in Li salt concentration are proportional to strong contact ion pair (CIP) formations and electrolyte viscosity reduction [191-195]. Therefore, increasing the formation of CIPs with weak Li^+ and $TFSI^-$ interactions, could liberate Li^+ and improve transport properties [196]. The formation of carbonate species in Li-O_2 batteries have been associated with the decomposition of carbon cathodes and electrolytes [112, 131, 197]. Increasing LiTFSI concentration slows the growth of lithium carbonates formation and mitigates TEGDME decomposition. Previous research studies have shown that the superoxide species formed during cycling of Li-O_2 batteries can attack uncoordinated solvent molecules to form lithium carbonates [131, 197, 198]. Appropriate solvation of solvent/lithium salt can protect radical solvent molecules from superoxide attacks [131, 186, 197-201].

1.15 Redox Mediation in Li-O_2 Batteries

Studies have shown that redox mediated batteries (RMBs) show signs of scalability even when combined as two different half cells [202, 203]. While polymeric membranes have good mechanical and chemical stability, a highly Li^+ conductive, impermeable redox

mediated membrane is desired for the operation of RMBs, which is compromised in non-aqueous RMBs. Iodide in lithium acts as a redox mediator to assist with the spare electron during charge (OER) from Li_2O_2 to Li^+ and O^-, overall helping reduce overpotential of the charge/discharge cycle. Operation of RMBs rely on the chemical reactions between redox mediators and Li storage materials and demonstrate extremely high energy densities when paired with a suitable membrane capable of blocking the crossover of redox molecules [204]. Mass transport across an electrolyte circulated membrane would effectively accelerate the transport of redox species and Li^+ within the cell. According to Jennings [205], combining a low concentration of redox mediated molecules with a high concentration of Li^+, in a solid material, could achieve more practical, high-energy density battery functionality.

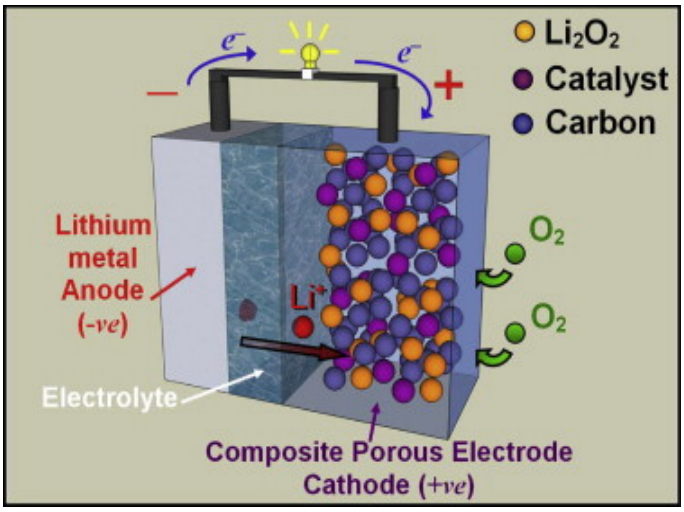

Figure 13. Schematic of a rechargeable Li-O_2 battery consisting of a lithium metal anode, GPE and porous CNT cathode with catalyst (redox mediator, filler, etc.). Permission from [206].

1.16 Future Work: Dual-Enhancement Systems

Practical development of Li-O_2 batteries are prevented by electrochemical reactions on the electrode surfaces, and electrolyte, demanding a higher focus on effective and consumer-friendly battery designs. The Li anode suffers from byproduct (including water) formation while the air cathode is affected by electrochemical reaction mechanisms, resulting in Li_2O_2 clogging. The use of selective, high cost catalysts [78, 207] are required to assist battery charge/discharge cycling, by controlling atmospheric reactivity, to improve cell life. Engineering advances are needed to optimize the geometric structuring of the cathode and prevent uneven byproduct deposits (and atmospheric contaminants) which can be transferred to, and react, with the anode [208, 209]. Accounting for these necessary changes could catalyze the inclusion of Li-O_2 batteries in practical applications.

Addressing the challenges of Li-O_2 batteries would offer a great deal of improvements in commercial applications of common electronics. Potentially combining solutions that address these challenges: (1) electrode degradation, (2) electrolyte stability, and (3) ionic interaction, would optimize the output performance of such batteries and create an entirely new system altogether. Use of GPE [97, 150, 169, 187, 210, 211] in a dual-enhancement system comprised of lithium-iodide (LiI) redox mediation [78, 203-206] and loaded carbon nanotube (CNT) fillers [144, 212, 213], would improve battery life by reducing resistance growth and maintaining system stability. Dual-enhancement systems are specifically beneficial due to the absence of the blocked pores caused by the flooding liquid electrolyte and LiI redox mediated solutions causing an enhanced oxygen diffusion at the cathode suppressing byproduct formation and GPE deterioration during charge/discharge cycling.

Polarization factors due to the kinetic and diffusion barriers were reported by Xu [93] to affect the discharge product distribution greatly, indicating that the reduction of the diffusion barrier by increasing Li^+ ions content (through redox mediation) is an important factor in facilitating the reversible charging process at the electrolyte/cathode interface. This will increase the ionic conductivity in the CNT cathode by increasing the Li^+ ions content, and according to Nernst equation, increasing Li^+ ions concentration tends to cause the electrode potential of the half-reaction OER ($Li_2O_2 \rightarrow 2Li^+ + O_2 + 2e^-$) to be nearer to its equilibrium value, overall optimizing the Li-O_2 cell.

1.17 Purpose of Dissertation

The purpose of this study is to extend cyclability of Li-O_2 batteries by implementing a dual-enhancement (redox mediated and CNT filled) system at the cathode with a composite gel polymer electrolyte (cGPE-1%, GPE filled with 1% wt. glass microfibers). The use of cGPE will stabilize the cell thermally, mechanically, chemically and electrically, while improving the ionic conductivity of the cell. Great insulating properties and low volatility allow the cGPE to maintain wetness, improve oxygen solubility and protect the anode. CNT fillers increase conductivity in the cathode thus improving rechargeability, while maintaining a high specific surface area. Large surface areas allow for more active sites for lithium-oxide formation across the cathode. LiI redox mediation improves electron transfer by oxidizing the cell during charge. This reaction assistance ultimately reduces overpotential, extending cell cyclability.

2 EXPERIMENTATION

2.1 Li-O_2 Battery Chemistry

Pairing lithium, and oxygen (from air), can theoretically lead to electrochemical cells with the highest specific energy possible. The theoretical specific energy of a non-aqueous Li-air battery (in the charged state with Li_2O_2 product and excluding the oxygen mass) is approximately 11.7 kWh/kg, comparable to the theoretical specific energy of gasoline of approximately 13 kWh/kg. Practically, Li-air batteries have achieved only 1.7 kWh/kg at the cell level. Lithium is a chemical element with the symbol Li and atomic number 3. It is a soft, silvery-white alkali metal. Under standard conditions, it is the lightest metal and the lightest solid element. Like all alkali metals, lithium is highly reactive and flammable, and is stored in mineral oil or under inert gases such as argon. When cut, it exhibits a metallic luster, but moist air corrodes it quickly to a dull silvery gray, then black tarnish. It never occurs freely in nature, but only in (usually ionic) compounds, such as pegmatitic minerals, which were once the main source of lithium. Due to its solubility as an ion, it is present in ocean water and is commonly obtained from brines. Lithium metal is isolated electrolytically from a mixture of lithium-chloride and potassium-chloride.

Oxygen is the chemical element with the symbol O and atomic number 8. It's a member of the chalcogen group on the periodic table, a highly reactive nonmetal, and an oxidizing agent that readily forms oxides with most elements as well as with other compounds. By mass, oxygen is the third-most abundant element in the universe, after hydrogen and helium. At standard temperature and pressure, two atoms of the

element bind to form dioxygen, a colorless and odorless diatomic gas with the formula O_2. Diatomic oxygen gas constitutes 20.8% of the Earth's atmosphere. As compounds including oxides, the element makes up almost half of the Earth's crust.

2.2 Salt, Solvent and Polymer

Salt is an ionic compound composed of cations (positively charged ions) and anions (negatively charged ions) that results from the neutralization reaction of an acid and a base. It is considered as the electrolyte of the cell system. Solvent is a substance that dissolves a solute (a chemically distinct liquid, solid or gas), resulting in a solution. The quantity of solute that can dissolve in a specific volume of solvent varies with temperature. A polymer is a large molecule, or macromolecule, composed of many repeated subunits called monomers created via polymerization. Their consequently large molecular mass relative to small molecule compounds produces unique physical properties: toughness, viscoelasticity, semi-crystalline formation, etc.

2.3 Anode and Cathode

Anodes are electrodes through which the conventional current enters into a polarized electrical device. This contrasts with a cathode, an electrode through which conventional current leaves an electrical device. The direction of conventional current (the flow of positive charge) in a circuit is opposite to the direction of electron flow, so (negatively charged) electrons flow out the anode into the outside circuit. In a galvanic cell, the anode is the electrode at which the oxidation reaction occurs. Cathodes are the electrode from which a conventional current leaves a polarized electrical device. A conventional current

describes the direction in which positive charges move. Electrons have a negative electrical charge, so the movement of electrons is opposite to that of the conventional current flow.

2.4 Materials

Lithium-oxygen batteries were made using a lithium foil anode, a GPE/cGPE (comprised of lithium bis(trifluoromethanesulfonyl)imide (LiTFSI) salt, tetraethylene glycol dimethyl ether (TEGDME) solvent, ethoxylated trimethylolpropane triacrylate (ETPTA) monomer, 2-hydroxy-2-methyl-1-phenyl-1-propanon (HMPP, photo-initiator to be cured with λ=365 nm), N-methylpyrrolidine (NMP) and polyvinylidene fluoride (PVDF), and glass fibers (for cGPE)), lithium iodide (LiI) redox mediator, and a carbon cloth with CNT fillers at the oxygen cathode. All materials were purchased from Sigma-Aldrich and Fisher Scientific.

2.5 Preparation of GPE/cGPE, LiI Redox Mediator, and CNT Cathode Disks

Liquid electrolyte was prepared using 1.0 mol/kg LiTFSI salt in TEGDME solvent, 80:20 by weight polymer liquid electrolyte was used to create the GPE substrate. One percent to weight glass fibers were mixed to create the cGPE solution. GPE/cGPE solutions were spread over a PDMS template and polymerized under UV light for 10 minutes, forming thin, flexible discs of approximately 150 μm in diameter. Liquid electrolytes containing 50 mM LiI was prepared and used as redox mediator in the cathodes. CNT carbon-cloths (CC) were cut in 0.5" discs then dipped in 90:10 wt% CNT (SW, HR, MW_1 and MW_2) + PVDF in NMP and dried to produce the cathode. Cathode loadings were established by repeatedly dipping and drying until the desirable loadings (0.1 - 0.5 mg) of CNT were achieved.

2.6 Fabrication of Li-O_2 Cell

Lithium-foil disk anode was placed in an open Swagelok cell. Prepared GPE films were soaked in LiTFSI -TEGDME (electrolyte) and pressed on top of the lithium-foil disk. A porous cathode disc was then placed on top of the GPE film and soaked with LiI redox mediator. A stainless-steel mesh serving as a current collector was placed on top of the cathode. Constructed Swagelok cells displayed an open circuit voltage (OCV) of > 2.8 V before testing. The cell was then sealed and allowed to rest overnight. After construction, cells were kept at +10 psi gauge pressure under ultra-high purity oxygen gas (Airgas, purity > 99.994%) and operation tests were completed under a specified current density (50 or 250 mA/g, depending on CNT loading). In galvanostatic charge/discharge tests, batteries were cycled in the voltage range of 2-4.5 V and at constant cycle capacity (100 or 500 mAh/g). All preparations and fabrications were performed in an argon-filled glove box (< 1 ppm O_2 and < 0.1 ppm H_2O).

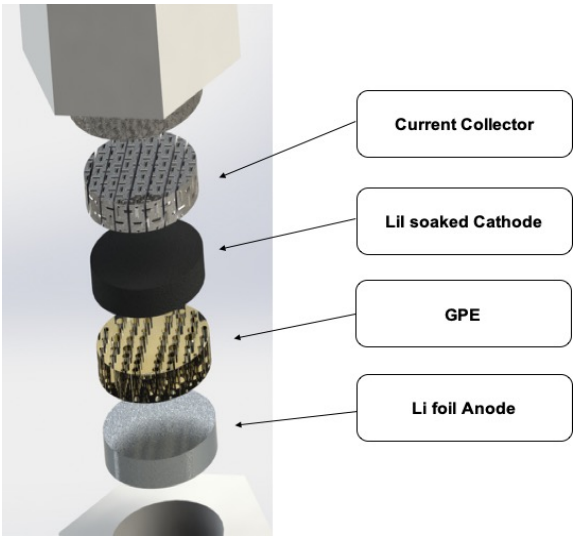

Figure 14. 3D schematic of the cell assembly.

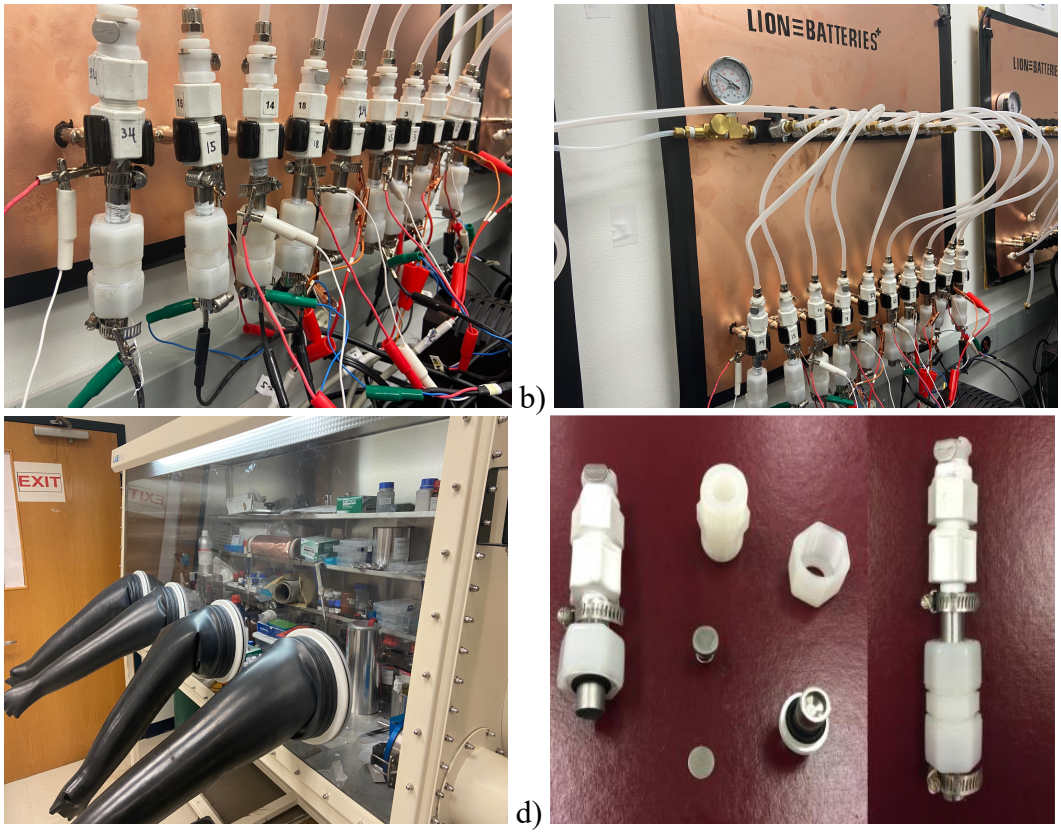

Figure 15. Pictures of a) Swagelok cell mounts, b) oxygen inlet tubes, c) Argon-filled Glove box, and d) disassembled cell (left) and assemble cell (right).

2.7 Instrumentation

Analytical testing equipment include: Gamry Reference 600 Potentiostat electrochemical interface (interfacial impedances 0.1–10^6 Hz frequency range), JEOL JSM-6330F, MTI BTS8- MA (10mA) and MultiView 2000TS (with built-in Raman), performing electrochemical impedance spectroscopy (EIS) and cyclic voltammetry tests (CV), charge/discharge cycling (CCD), and Raman spectroscopy, respectively. These tests are described in more detail in the next sections.

2.8 Open Circuit Voltage (OCV)

Open-Circuit Voltage (OCV) is the difference of electrical potential between two terminals of a device when disconnected from any circuit. There is no external load connected or any external electric current flows between terminals. Alternatively, the open-circuit voltage may be thought of as the voltage that must be applied to a solar cell or a battery to stop the current. It is sometimes given the symbol V_{OC} or electromotive force (emf), which is the maximum potential difference when there is no current and the circuit is not closed.

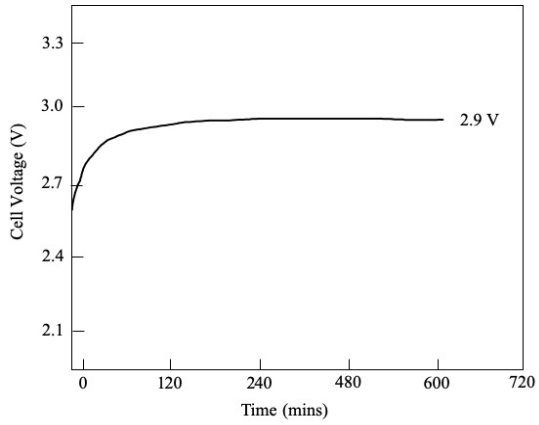

Figure 16. Typical OCV stabilization plot prior to testing.

2.9 Cyclic Charge/Discharge (CCD)

Cyclic Charge/Discharge (CCD) is the process of charging a rechargeable battery and discharging it as required into a load. The term is typically used to specify a battery's expected life, as the number of charge cycles affects life more than the mere passage of time. Discharging the battery fully before recharging may be called "deep discharge"; partially discharging then recharging may be called "shallow discharge". In general, number of cycles for a rechargeable battery indicates how many times it can undergo the

process of complete charging and discharging until failure or when it cannot hold the set capacity. In this dissertation, CCD tests were monitored via galvanostatic mode in which voltage was measured during charge and discharge to obtain voltage profiles.

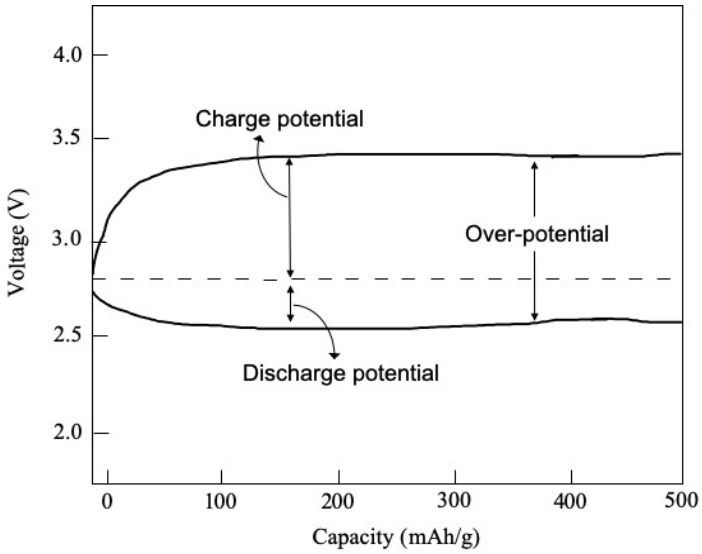

Figure 17. Typical CCD of a Li-O_2 battery containing GPE.

2.10 Cyclic Voltammetry (CV)

Cyclic Voltammetry (CV) is a type of potentio-dynamic electrochemical measurement where the working electrode potential is ramped linearly versus time. Unlike in linear sweep voltammetry, after the set potential is reached in a CV experiment, the working electrode's potential is ramped in the opposite direction to return to the initial potential. These cycles of ramps in potential may be repeated as many times as needed. The current at the working electrode is plotted versus the applied voltage (that is, the working electrode's potential) to give the cyclic voltammogram trace. CV is generally used to study the electrochemical properties of an analyte in solution or of a molecule that is adsorbed

onto the electrode. CV voltammograms are often used to identify the oxidation and reduction potentials. For Li-O_2 batteries, CV is used to determine both the magnitude and potential of the ORR and OER peaks. In this dissertation, CV was also used to determine current stability ranges of the electrolyte using the Gamry Reference 600 Potentiostat.

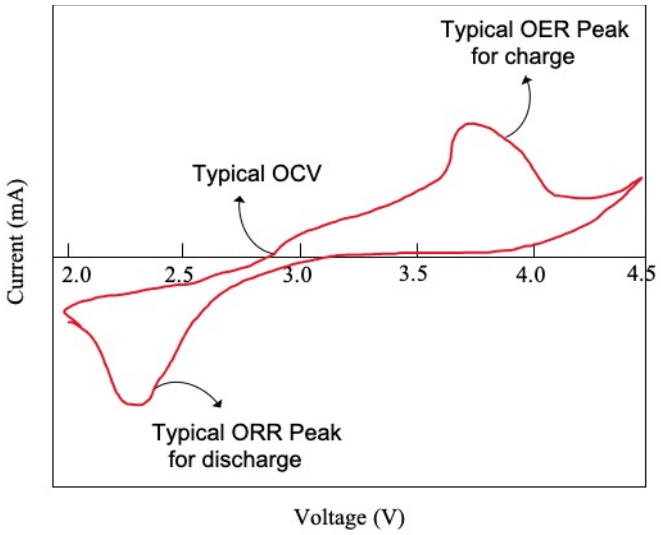

Figure 18. Sample CV of GPE batteries.

2.11 Electrochemical Impedance Spectroscopy (EIS)

Electrochemical Impedance Spectroscopy (EIS) measures the impedance of a system over a range of frequencies, and therefore the frequency response of the system, including the energy storage and dissipation properties, are revealed. The data obtained is often expressed graphically in a Bode or Nyquist plot. Impedance is the opposition to the flow of alternating current (AC) in a complex system. A passive complex electrical system comprises both energy dissipater (resistor) and energy storage (capacitor) elements. If the system is purely resistive, then the opposition to AC or direct current (DC) is simply

resistance. In this dissertation, EIS was used to quantify the individual resistances (ionic, interfacial and bulk), within the battery. R_b (bulk resistance) corresponds to the electrolyte resistances at, on, and in-between the anode, cathode and GPE; R_{int} (interfacial resistance) represents the charge transfer resistance at the electrode/GPE interfaces. The R_{int} (semi-circle of the Nyquist plot illustrated in Figure 19) corresponds to the resistance afforded by the interfaces between the electrolyte and electrodes; R_{ion} (ionic resistance) corresponds to the lithium-ion migration resistance of the electrolyte within cathode's pores.

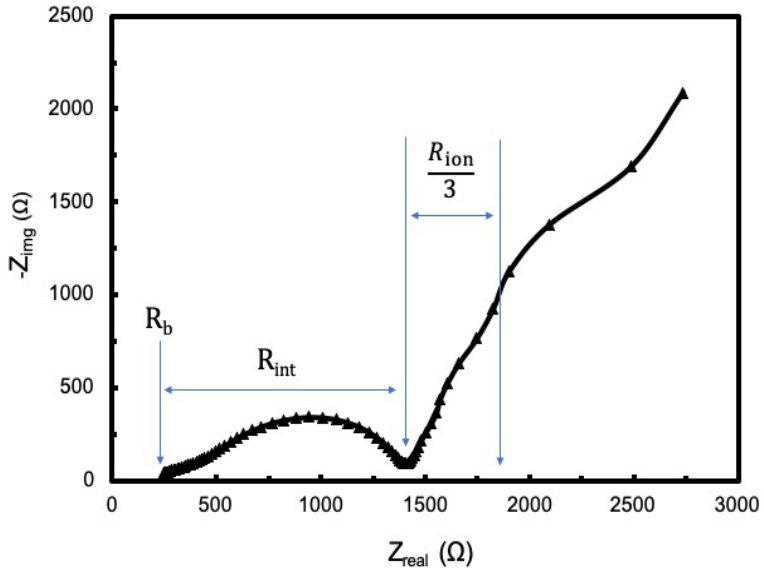

Figure 19. Sample EIS Nyquist plot from GPE batteries.

2.12 Scanning Electron Microscopy (SEM)

Scanning Electron Microscopy (SEM) is a type of electron microscopy that produces images of a sample by scanning its surface with a focused beam of electrons. The electrons interact with atoms in the sample, producing various signals that contain information about the sample's surface topography and composition. In this dissertation, SEM was used to

visually inspect the carbon cathode after failure, and to determine the morphology of the discharge species.

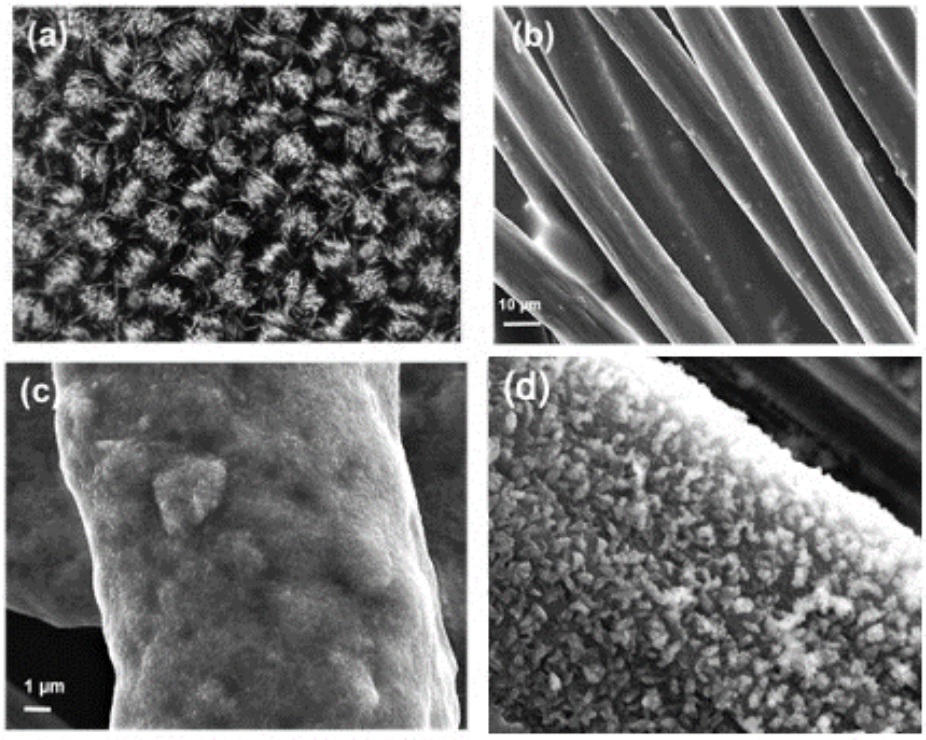

Figure 20. SEM illustration of a) pristine carbon cloth (CC), b) close-up look at CC fibers, c) CC fiber coated with CNT and d) CNT coated fiber after failure. Permission from [187].

2.13 Raman Spectroscopy

Raman Spectroscopy is a technique that relies on inelastic scattering of laser light (visible, near infrared, or near ultraviolet range) resulting in the energy of the laser photons being shifted up or down to observe vibrational, rotational, and other low-frequency modes in a system. This provides a structural fingerprint by which molecules (byproducts) can be identified. In this dissertation, Raman was used to characterize the discharge species in the cathodes after cycling.

3 REDOX-MEDIATED BATTERIES USING GEL POLYMER ELECTROLYTES

3.1 Introduction

Rechargeable lithium-oxygen (Li-O_2) batteries theoretically have 150-200% more energy storage capabilities than modern lithium ion batteries [67, 98, 199, 214-216]. Li-O_2 batteries ($2Li + O_2 \rightleftharpoons Li_2O_2$) operate at 5-15 times more than commercial Li-ion batteries, with a considerably high theoretical specific energy of 3.5-5.2 kWh/kg and working open-circuit voltage (OCV) of 2.96 V [217]. In an ideal Li-O_2 battery practicality, the oxygen could be accessed through ambient air thus significantly improving the theoretical specific energy of the Li-Air battery to 11.7 kWh/kg [74, 80, 96, 132, 217]. Optimizing the solid electrolyte configuration could improve oxygen transport, minimize evaporation and protect the anode from ambient impurities in the cell's atmosphere [115].

Oxygen reduction reaction (ORR) refers to the discharge cycling process where the lithium anode is oxidized to produce lithium ions in the electrolyte and oxygen is reduced at the cathode surface to form lithium peroxide (Li_2O_2) or lithium oxide (Li_2O) [67, 80, 96-100, 215]. Extra electrons on the O_2 orbitals can produce superoxide and peroxide ions which can be extremely reactive when in contact with organic materials [91, 101]. Oxygen evolution reaction (OER) occurs during the charge cycling process allowing the discharge products (Li_2O_2 or Li_2O), to reconvert back into lithium metal and oxygen gas.

Carbon cathode surfaces primarily house superoxide byproducts that could potentially allow spontaneous electrochemical reactions and oxidation, however there is a lack of

evidence solidifying carbons reactivity with radical superoxide ions [103]. Recent studies conclude the lithium peroxide compounds react with the carbon cathode to create lithium carbonates (Li_2CO_3), which can be detrimental to cell life [112, 113]. Despite lithium carbonate's growth being a negative influence on a battery's functionality, if produced in deposits of high surface area, it can mitigate some of its negative effects [95, 114]. Polymeric membranes in the electrolyte are praised for their chemical, electrical, thermal and mechanical stabilities while providing anode protection from organic material and high ionic transfer due to its permeability in fuel cells [218].

Iodide's high solubility, speedy kinematics and great reversibility in both aqueous and non-aqueous Li batteries have identified it as an ideal reduction oxidation mediator to assist with the spare electron created during OER, reducing overpotential [47, 218-221]. LiI has a high solubility of up to 8.2 M in H_2O, making it significantly more considerable in LiI aqueous flow battery systems than conventional Li-O_2 batteries [221-224]. According to Zhao *et al.[220]*, the high solubility of the triiodide (I_3^-)/iodide (I^-) redox couples results in a reversible redox reaction without the formation of resistive solid products promotes rechargeability. As iodide is stripped from the cathode through electron absorption, Li^+ ions travel through the salt to combine with the I^- ions (at the cathode surface), generating electricity in the cell system [225].

In this chapter, GPE membranes are used to extend Li-O_2 battery life by reducing resistance growth, using a dual-enhancement system consisting of a LiI redox mediator soaked,

porous CNT-filled cathode to improve system oxidation, ionic transfer and ionic conduction.

3.1.1 Ion-Solvent Interaction in Electrolytes

The solvation is an important parameter in the dissolution of solute (MX). It has been reported that ions of solute (MX) can interact with solvent molecules in different ways [226, 227]. Hence the solvent properties can significantly affect the electrolyte solution properties. The most important solvent properties in considering solvent effects are the solvent permittivity, acidity and basicity. For instance, if the permittivity of one solvent is high ($\varepsilon_r > 40$) and the other is low ($\varepsilon_r < 10$), the difference in chemical processes of the two solvents is usually attributable to the influence of permittivity. On the other hand, in two high-permittivity solvents, ($\varepsilon_r > 40$) are often attributable to the influence of the acidity or basicity of the two solvents rather than the influence of permittivity. Table 8 shows ion-solvent interaction influencing ion solvation, with their contribution percentage of total ionic solvation energy. The values with percentages in Table 8 show the rough estimate of the contribution from each factor to the total solvation energies of univalent ions (300-500 kJ/mol) in a solvent of ε_r = 25-100. Electrostatic interaction has the major contribution in ion-solvent interaction and can be defined as the difference between the electrostatic free energy of an ion in vacuum and that of the ion in a solution of relative permittivity. It has been shown that the difference between the electrostatic ion-solvent solvation energy in two high-permittivity solvents is often less important than the difference in the solvation energies caused by other interactions [226, 227].

# Interaction	Contribution
Electrostatic interactions as expressed by the Born equation	>80%
Electron (-pair) donor-acceptor interactions	<10%
Interactions of anions and hydrogen bond donor solvents	<10%
Interactions based of HSAB concept	<20%
Interactions by back-donation from d^{10} -cation to solvent molecules	<10%
Interactions related to the structure-making and breaking of solvents	<5%

Table 8. Different ion-solvent interactions along with their contribution percentage [226].

Another important contribution in ion-solvent interaction is electron pair donor (EPD) and electron pair acceptor (EPA) interactions. In ion solvation processes, the solvent molecules approach a cation with their negative charge and approach an anion with their positive charge. Therefore, cation solvation is mainly related to the electron pair donor capacity (Lewis basicity) of the solvents and becomes stronger with the increase in donor number (DN) of solvent. The anion solvation, on the other hand, is closely associated with the electron pair acceptability (Lewis acidity) of the solvents and becomes stronger with the increase in acceptor number (AN) [226, 227]. The ion-solvent interactions can be studied by spectroscopic techniques like infrared (IR), Raman and nuclear magnetic resonance (NMR) spectroscopy [228].

3.1.2 Ion-Ion Interaction in Electrolytes

The Coulombic force of attraction between two oppositely charged ions (M^+ and X^-) are inversely proportional to the relative permittivity of the solvent. Thus, solvents with high relative permittivity ($\varepsilon_r > 40$) will be able to reduce the strong electrostatic attraction between oppositely charged ions and dissociate them into free solvated ions [227]. However, in relatively low permittivity solvents, the complete dissociation becomes difficult and part of the dissolved solute (MX) are not dissociated. The undissociated ions in low permittivity solvents contribute in chemical reactions and ion transport in electrolyte solution. The ion association/dissociation of solute (MX) is strongly depended on the ion-association constant (K_A), which could be defined as follows:

$$M^+ + X^- \leftrightarrow M^+X^- \text{ (ion pair)} \qquad (2)$$

$$K_A = \frac{[M^+X^-]}{[M^+] + [X^-]} \qquad (3)$$

Upon solvation, based on the mutual geometric arrangement of the two ions and the solvent molecules, different ion pairs can be formed. Figure 21 shows different ion pairs formed in electrolyte solution. In contact-ion pairs (CIPs), no solvent molecules intervene between the two ions that are in close contact. The ion pair separated by the thickness of only one solvent molecule is called a solvent shared ion pair. In solvent separated ion pairs (SSIPs) the primary solvation shells of the two ions are in contact, so that some overlap of secondary and further solvation shells takes place. Further dissociation of the two ions lead to unpaired (free) solvated ions with independent primary and secondary solvation shells.

In dilute solution using low-permittivity solvents, the presence of ion-pairs, even in dilute solutions, were reported.

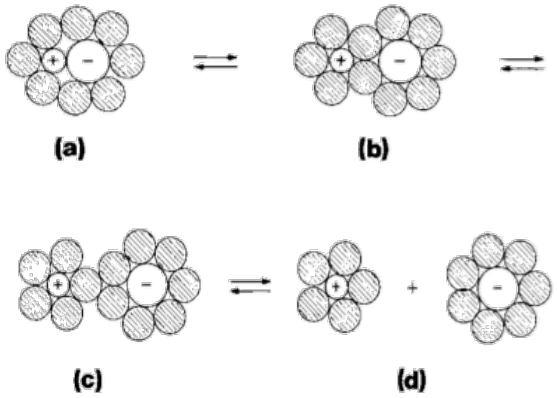

Figure 21. Schematic representation of different ion-pairs: (a) Contact ion pair (b) Solvent shared ion pair (c) Solvent separated ion pairs (d) Free solvated ions (shaded circles denote the solvent molecules). Permission from [227].

With the increase of solute concentration, the formation of aggregate ions was also observed in high-permittivity aprotic solvents. For alkali salts (LiX), ionic association strength can be affected by the negative charge delocalization, size, and steric effects of the anion X^-. They could be categorized in three different classes [229]: (1) dissociated salts: $LiN(SO_2CF_3)_2$ (LiTFSI) (2) intermediate salts: $LiClO_4$ and $LiBF_4$ and (3) associated salts: $LiCF_3SO_3$, $LiNO_3$ and $LiCF_3CO_2$.

3.1.3 Ionic Transport Properties in Electrolytes

The value of conductance for a segment of solution immersed in an electric field is directly proportional to the cross-sectional area, A, perpendicular to the field vector, Z, and is inversely proportional to the length, L, of the segment along the field. The proportionality constant is the conductivity, σ, which is an intrinsic property of the solution [230]:

$$\sigma = \frac{L}{A \cdot Z} \qquad (4)$$

Ionic conductivity, σ, is the sum of contributions from all ionic species as the passage of current through the solution is accomplished by the independent movement of different species. Therefore, it is acceptable that each component of σ is proportional to the concentration of the ion, the magnitude of its charge $|Z_i|$, and the mobility, which is the limiting velocity of the ion in an electric field of unit strength. Once an electric field in the strength of ξ is applied to an ion, it accelerates under the force imposed by the field until the frictional drag force exactly counterbalances the electric force. Then, the ion continues its motion at that terminal velocity. The magnitude of the force applied by the field is equal to $|Z_i|e\xi$, where e is the electronic charge. The frictional drag force can also be approximated using Stokes law as $6\pi\eta r v$ where η is the viscosity of the medium, r is the radius of the ion, and v is the velocity. When the terminal velocity is reached, the ion mobility can be defined as [230]:

$$u_i = \frac{\mathrm{v}}{\xi} = \frac{|Z_i|\mathrm{e}}{6\pi\eta\mathrm{r}} \qquad (5)$$

The proportionality factor relating an individual ionic conductivity to charge, mobility, and concentration turns out to be the Faraday constant, so the ionic conductivity can be defined as [226, 230]:

$$\sigma = F \sum |Z_i| u_i C_i \qquad (6)$$

The transference number for species i, which the fractions of the current carried by species i and j are called their transference numbers, is merely the contribution to conductivity made by that species divided by the total conductivity:

$$t_i = \frac{|Z_i| u_i C_i}{\sum_j |Z_j| u_j C_j} \qquad (7)$$

3.2 Results and Discussion

3.2.1 Cyclic Voltammetry and Charge/Discharge Cycling

The aim of this chapter was to characterize and compare LiI redox mediator's effect on a Li-O_2 cell using a lithium anode, gel polymer electrolyte, and CNT carbon cloth cathode. The presence of redox mediator at the electrolyte-cathode surface layer has shown to reduce the charge overpotential thus making the charge reaction more efficient. At lower charge and discharge rates, LiI redox mediator stabilized the electrolyte and reduced the formation of the lithium carbonate passivating layer at the cathode. Battery cells are

expected to display an OCV of > 2.8 V before cyclic testing under a current density of 250 mA/g_{CNT} and 10 psi oxygen gauge pressure.

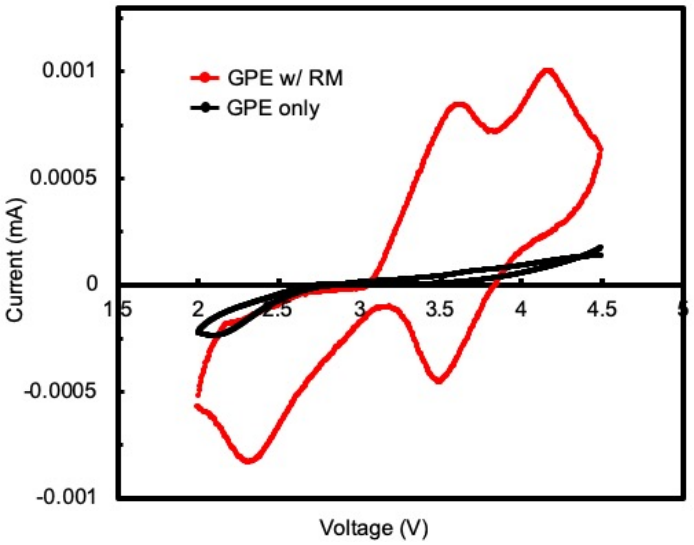

Figure 22. CV of GPE batteries. The black line represents the GPE without RM, and the red line represents GPE with RM. The addition of RM increases the cell's redox activity. Scan rate was 5 mV/s over a sample area of 0.71 cm^2.

Typically, batteries are rested for 10 hours after assembly. After rest, OCV of the fabricated batteries were between 2.80 - 2.90 V. Li-O_2 batteries with GPE only exhibited a cyclability of 24 cycles (control) at a current density of 250 mA/g between 2.00- 4.50 V. However, 30 µL 0.05 M LiI redox mediator (RM) showed significant improvement in the battery performance, as illustrated by the larger area in Figure 22. Huang *et al.* [203, 231] reported LiI undergoes two-electron redox reactions in 1M LiTFSI-TEGDME based electrolytes. The I^-/I_3^- reaction occurs at ~3.5 V (*vs.* Li/Li^+) and the I_3^-/I_2 reaction at ~4.25 V (*vs.* Li/Li^+) [232]. The redox potential of Li-O_2 (3.85-4.09 V *vs.* Li/Li^+) [232] sits right in between the potentials of I^-/I_3^- and I_3^-/I_2. Therefore, it is energetically favorable for O_2 to be chemically reduced by I^- and for Li_2O_2 to be chemically oxidized by I_2 [233]. During

charge, oxidation peaks at approximately 3.5 V and 4.25 V correspond to oxygen (O_2) evolution reactions. During discharge, reduction peaks at 3.5 V and 2.3 V correspond to lithium-iodide (LiI) and lithium-peroxide (Li_2O_2) reduction reactions, respectively. However, the 3.5 V peak did not yield any plateau during the discharge. Figure 22 indicates 2 peaks during both OER and ORR, confirming that LiI RM did not completely oxidize nor reduce the Li_2O_2 at 3.5 V, and instead completed Li_2O_2 oxidation and reduction at 4.2 V and 2.4 V, respectively [185].

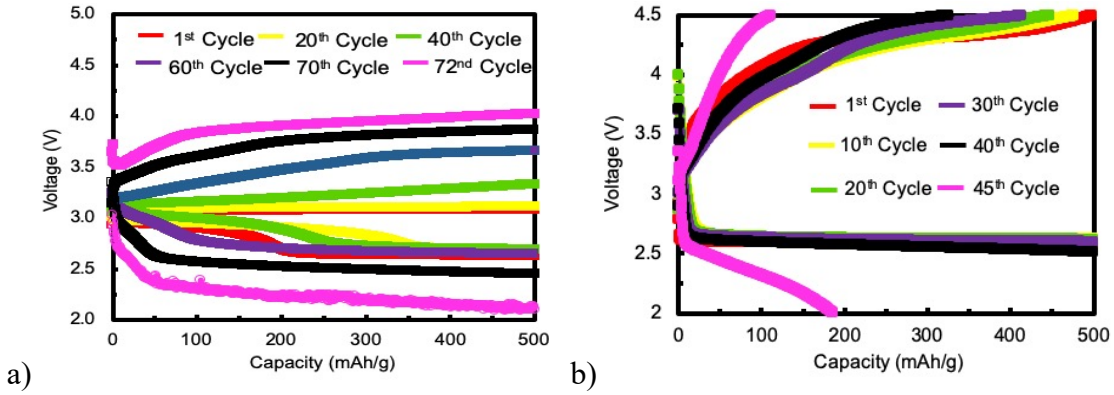

Figure 23. Voltage profiles of the CCD tests for a) GPE with CNT and LiI RM [B1] and b) GPE with CNT only [B2]. The batteries were cycled at 500 mAh/g cycle capacity between voltage window of 2.0-4.5 V.

As charge/discharge electrical stimulation is applied to the GPE substrates, byproduct formation may have occurred and potentially changed the internal and external substrate properties over time. Initial overpotential charge decreased from 4.30 to 3.15 V and initial discharge increased from 2.60 to 2.70 V, respectively, under RM on cathode as seen in Figure 23. Thus, the initial overpotential has reduced to approximately 0.50 V from 1.7 V. Reduced overpotential resulted in significant cycling improvements from 24 cycles to 72 cycles. This improvement is attributed to a higher voltage efficiency when using RM,

which in turn reduces the electrolyte decomposition [97] and cathode byproduct formation rates. Additional cycling tests soaking 10 μL, 20 μL, and 40 μL RM into the cathode showed negative to minor improvements and was not pursued further. Creating an internal open-circuit due to delamination within [B1] is assumed to have caused the battery to become spontaneously unstable overtime. During charge (OER), LiI redox assisted in oxidizing the battery system reducing the potential for battery failure due to electrolyte decomposition (R_b) [89, 116, 122, 147, 234-236]. During discharge (ORR), CNTs assisted in ionic conduction within the cathode, reducing battery failure due to ion transfer between the electrodes (R_{ion}).

Theoretical OCV for traditional Li-O_2 and Li-I_2 battery systems are approximately 2.96 V and 3.55 V [220], respectively. Hence, the oxidization of Li_2O_2 by I_3 is considered to be thermodynamically favorable with a driving force of 0.59 V (3.55 V - 2.96 V = 0.59 V), resulting in additional stability [237]. Within the Li-O_2 system using LiI redox in this chapter, an OCV of approximately 2.8-3.1 V was obtained. The larger potential in this system is due to the redox additive iodide reacting with the low ionic conductivity of TEGDME at high current rates of 2.5 mA/cm^2. Significant discharge potential drops from 3.0 V to 2.7 V indicate that the 0.05 M LiI redox concentration was not enough to sustain low discharge/ charge potential, resulting in potential drop suppression and reduced mass transport loss due to electrolysis of GPE, which otherwise would cause battery deterioration at higher current rates. Eventually the power density of the system approached the theoretical charge/ discharge potentials of Li-O_2 batteries indicating reduced LiI redox reactions within the GPE over time.

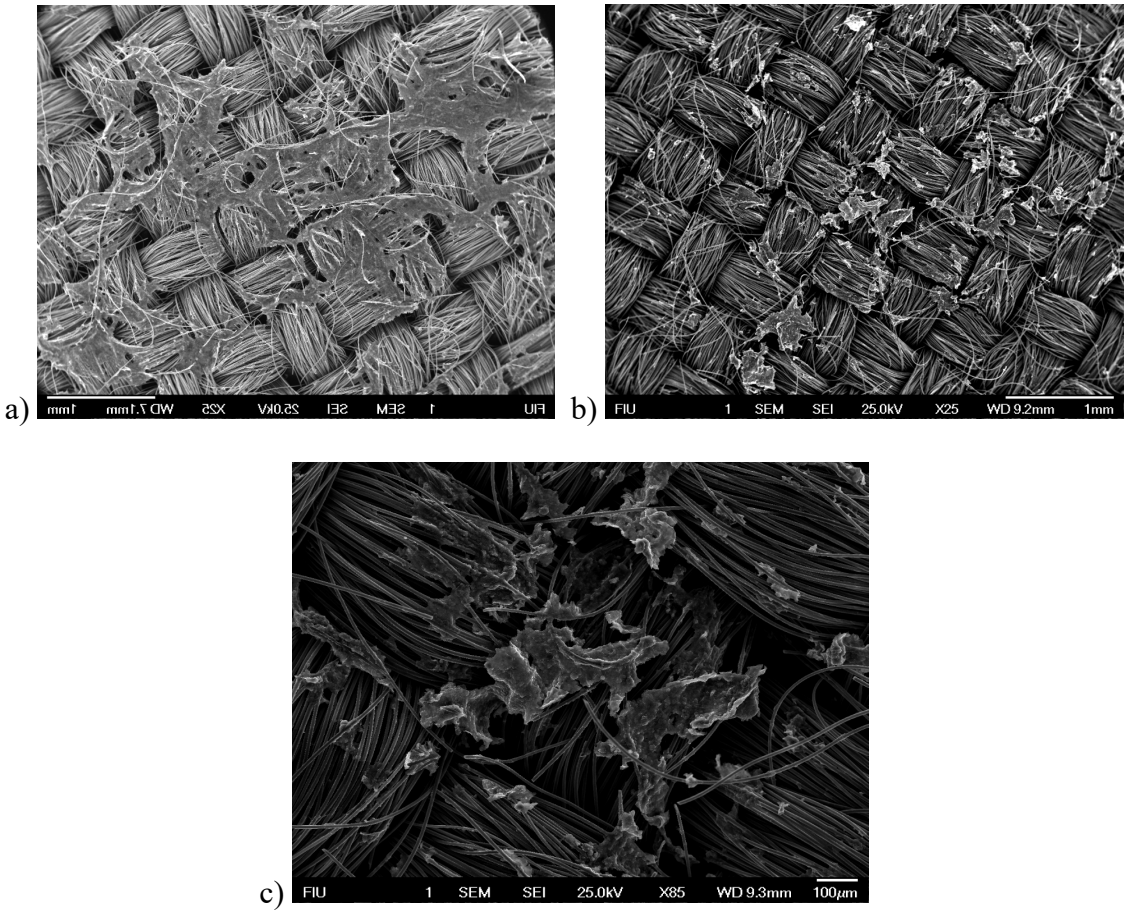

Figure 24. SEM micrographs of the carbon cathodes after discharge for a) Carbon cloth with 0.5 mg CNT only [B2] at 25x magnification, b) GPE with 0.5 mg CNT and RM [B1] at 25x magnification and c) 85x magnification.

Figure 24 shows that cells without LiI RM have increased byproduct buildup within the cathode, suggesting that LiI reduces undesirable cathode and electrolyte degradation, and helps facilitate redox reactions across the system. Being a solution, LiI redox leaves no solid product, which leads to zero volume expansion at the cathode and promotes adequate rechargeability. Wu *et al.* claims LiI radicals generate and react with TEGDME, polymerizing into a thin, permeable layer at ≈ 3 V on the electrode/GPE interface, creating

a protective layer at both the anode/GPE and cathode/GPE surfaces, protecting each from direct contact with organic and inorganic material [238].

3.2.2 Electrochemical Impedance Spectroscopy

EIS measurements investigated the cathode/electrolyte potentiostatic property behaviors during discharging and charging processes at a rate of 5 mV/s. R_b (bulk electrolyte resistance) corresponds to the resistances at, on and in-between the anode, cathode and GPE; R_{int} (interfacial resistance) represents the charge transfer resistance at the electrode/GPE interface (associated with the semicircle in Nyquist plots, Figure 25); R_{ion} (ionic resistance) corresponds to the lithium-ion migration resistance within the porous carbon cathode in the cell system [81, 104, 173, 180, 239, 240].

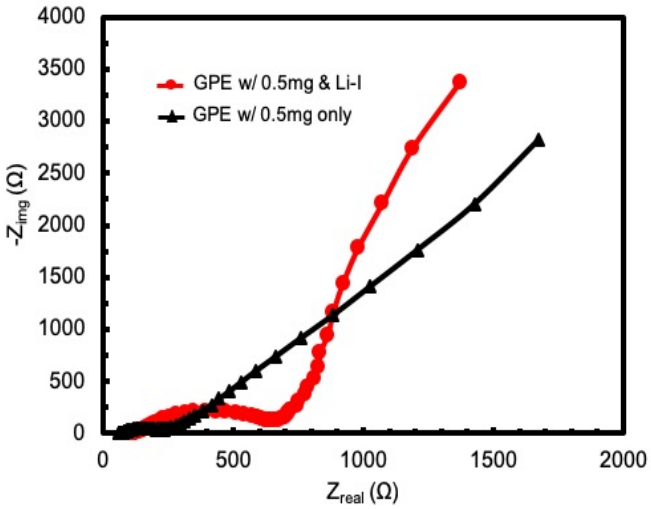

Figure 25. Nyquist plots of batteries with GPE and LiI and GPE only. The batteries were cycled at 250 mA/g for both charge and discharge between 2.0-4.5 V.

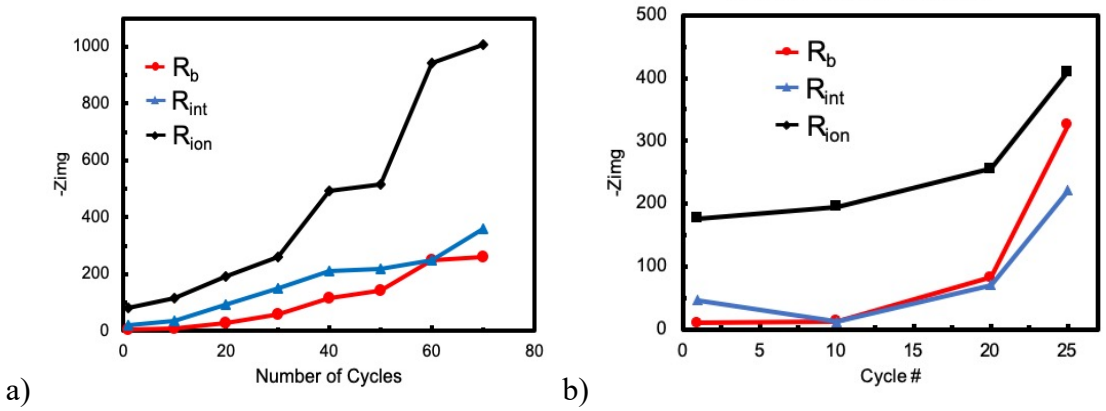

Figure 26. Resistance profiles of R_b, R_{ion}, and R_{int} during cycling for a) GPE with 0.05 M LiI on CNT cathode [B1] and b) GPE without LiI [B2]. Plots were obtained using EIS Bode plots before discharge.

From Figure 25, the Nyquist plot exhibits a bigger diameter of semicircle for [B2], after discharge to 500 mAh/g, indicating slower charge transfer kinetics due to higher resistance. High-frequency resistance shifts for both cathodes are clearly visible in Figure 26 after

discharge, as cycle number increase. After the last discharging cycle, which is 72 and 24 cycles for [B1] and [B2], respectively, R_b has shifted from 101 Ω [B1] to 249 Ω [B2]. The rate at which R_b increases is proportional to the amount of pore blockage and byproduct formation (primarily lithium carbonate (Li_2CO_3)) of the cell, with steep increases indicating complete cathode blockage preventing O_2 reduction [63,66, 68]. R_{ion} was the major resistance in [B1] and [B2] and it increases as the number of cycles increases (lifetime of the battery increases). As seen in Figure 26, [B1] has a more proportional increase in R_{ion} due to having almost the same number of charge and discharge cycles. R_{int} in [B1] has shown to be almost ½ the approximated value of [B2], indicating that byproduct formation on the electrodes (including byproducts formed due to CNTs at the cathode) increase the surface resistance between the anode/GPE and cathode/GPE, however, [B1] shows that R_{int} can be reduced further with the aid of a redox mediator component. Increased R_{int} on the cathode/electrolyte interface in Li-O_2 batteries could be the result of Li_2CO_3 byproduct formation during cycling, leading to cell death [50, 70-72].

3.2.3 Raman Spectroscopy

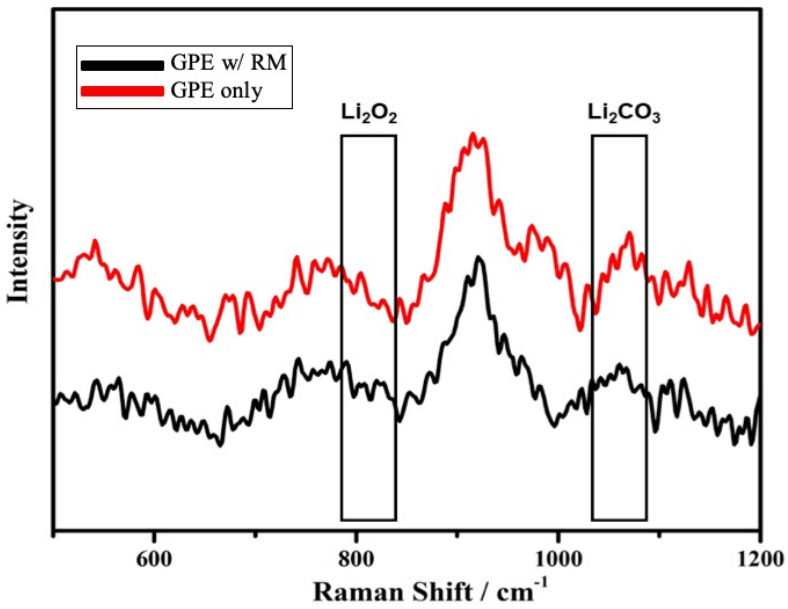

Figure 27. Raman spectra of cathodes after discharge using GPE with 0.5 mg CNT fillers with and without 0.05 M LiI RM.

Cycled cathodes, after their respective failures, illustrated Raman bands at 1082 cm^{-1} corresponding to the formation and clogging of lithium carbonate species in the cathode pores, causing cell decomposition and R_{ion} increase [171, 241]. Raman peaks at 920 cm^{-1} indicate the formation of an unexpected byproduct specie of Li_xRCO_3 [171, 242] in the cathode pores, causing addition electrode decomposition and R_{ion} increase. R is considered to be either radical hydrocarbon or hydrogen ions, which may have been cured into the carbon cathode during preparation and become reactive while cycling. Increasing LiTFSI concentration has been reported to protect the TEGDME solvent from superoxide attack and decomposition, improving Li^+ transport properties [112, 131, 187, 197-202]. Relatable

works have implemented the use of various salt concentrations [92, 197], polymers and electro-catalytic fillers, carbon-less cathodes [141], Li-air wire batteries [243], dual and redox mediators [99, 244], and the most effective GPE concentrations for significant ion transfer within the cell [187, 244].

3.3 Conclusion

This chapter addresses Li-O_2 battery life improvement by reducing resistance growth, using LiI as a RM, to maintain system stability. These results confirm the benefits of using CNT fillers and LiI RM (at the cathode) within a Li-O_2 battery cell operation, to enhance cyclic stability and oxygen diffusion. The redox-mediated cell was cycled for 72 cycles before failure, in which the ORR potentials up to the 60^{th} cycle had stable voltage profiles. The impedance spectra showed that the LiI redox mediated catalyst had a significant reduction at the diffusion barrier [73] by increasing LiI concentration, thus improving ionic conductivity (in the CNT cathode) and facilitating the reversible charging process at the GPE-cathode surface interface. CNT cathodes, with LiI redox mediation, created a high energy density with a low environmental impact and could be scaled to operate with optimized separators, offering additional mechanical strength and increased ionic transport. Therefore, dual-enhancement systems (comprised of LiI RM and CNT fillers in the cathode) have shown extended cyclability and system stability, by improving the charge capacity and maintaining charge voltages within the electrochemical stability window of the electrolyte. This reveals a preliminary opportunity to utilize these systems in Li-O_2, and eventually ambient Li-air batteries, furthermore, improving safety and evolving generational lithium batteries.

4 REDOX-MEDIATED BATTERIES USING COMPOSITE GEL POLYMER ELECTROLYTES

4.1 Introduction

Several reports [100, 171, 241, 245-250] have identified various lithium oxide species such as lithium superoxide (LiO_2), lithium oxide (Li_2O) and lithium peroxide (Li_2O_2) during ORR in Li-O_2 batteries [67, 80, 96-98, 187, 215]. There is a disproportionation reaction during discharge from the superoxide-like component of Li_2O_2 (potential during charge ~ 3.2-3.5 V) compared to its oxygen-abundant Li_2O_2 component (~ 4.2 V). This disproportion is likely caused by the cathode's porosity allowing for continuous byproduct growth during discharge [67, 97-100, 215, 248]. Any lithium-oxide discharge products are reconverted to lithium Li^+ and oxygen O^- singlet molecules while the cell charges during OER. Iodine in lithium acts as a redox mediator during OER reducing cell overpotential during the charge/discharge cycle. Lithium peroxide reacts with carbon leading to lithium carbonates (Li_2CO_3) and lithium oxides as both Li_2O_2 and Li_2CO_3 have been reported in recent studies [112, 113]. Carbon properties (high surface area, low density, conductivity) make graphene, [95] carbon nanotubes (CNT), [114, 144, 211, 212] and other carbons highly considerable cell conductors despite their electrolyte decomposition attributes [89, 122, 147, 234]. Adams *et al.* [251] claimed that a parasitic reaction between the O_2^- and electrolyte would lead to a spare electron bonding with the system, causing an additional chemical reaction between Li_2O_2 and the electrolyte, further increasing disproportion, especially at low current densities [116].

Gel Polymer Electrolytes	Transference Number, t_{Li^+}	Ionic Conductivity, σ (mS/cm)	Li^+ Conductivity, σ_{Li^+} (mS/cm)
LiTFSI-TEGDME	0.50	2.56 ± 0.00	1.28
GPE	0.53	1.02 ± 0.05	0.54
cGPE-0.5%	0.58	1.12 ± 0.02	0.65
cGPE-1%	0.66	1.40 ± 0.02	0.92
cGPE-2%	0.52	0.95 ± 0.05	0.50
cGPE-5%	0.48	0.75 ± 0.02	0.36

Table 9. Conductivity and lithium ion transference number values of GPE and various cGPEs [81, 97, 252-254].

The interaction between the micro-fillers and electrolyte increase the ion-pair dissociation [158, 165, 255, 256], which increase radical Li^+ content, allowing them to travel along the intricate network created by the micro-fillers [257, 258]. Conversely, excessive filler loading can lead to the obstruction and blockage of these pro-Li^+ ion pathways, crediting the importance and dependability on optimized distribution of micro-fillers. As reported by Liao [259], micro-fillers do not change GPE oxidation stability (anodic stabilities up to 4.75 V), confirming the polymer used was electrochemically stable under an oxygen environment [260].

The purpose of this chapter is to characterize the influence of one-dimensional (nano) glass micro-fillers in gel polymer electrolytes (cGPE) with a lithium-iodide redox mediated, porous carbon cathode filled with CNT in a Li-O_2 cell.

4.1.1 Salt-Inorganic Additive Interaction in Electrolytes

Fillers can influence the ion transport mechanisms in solid polymer electrolytes (SPE) in a variety of indirect and direct ways [261]. One of the main concerns of SPEs is their low ionic transport properties at low temperatures due to lack of the amorphous phase in polymer structures. Ion transport in polymer electrolyte is due to segmental motion of polymer chains, which are significantly higher in the amorphous regions compared to crystalline counterparts [262]. Small fillers may also add free volume and speed up segmental dynamics, and in turn improve the ion transports. Inorganic fillers could also directly participate in ion transport by increasing free Li^+ concentrations, Li^+ surface conduction, anion attraction, or as a Li^+ source [261]. The mechanism of filler participation in ion conduction can be expressed as follows: (1) fillers actively interacting with the ion pairs. In this case, fillers with specific surface chemistries promote ion-pair dissociation level and increase the number of ions able to participate in conduction. It has been shown that acidic surface groups could attract anions, while basic surface groups attract cations. In either case, the corresponding counter-ion acts as a mobile specie. (2) The surface of the fillers provides an additional site for anion and/or cation migration, due to Lewis acid-base interactions between the salt and the particle surface. (3) The filler surface attracts either the anion or cation, which reduces the ion's mobility. (4) Fillers can also change the polymer chain structure at the electrolyte interface thus creating pathways for Li^+ transport independent of segmental motion.

Interaction between lithium salt and inorganic fillers in liquid electrolytes was reported in earlier studies [256]. Bhattacharyya and Maier in 2004 showed that active Li^+ surface

conduction occurs in liquid-based electrolytes with fillers known as soggy-sand electrolyte [256]. The liquid matrix allows for percolation of spherical particles at a lower loading, as in the absence of an adsorbed polymer layer, the particles readily aggregate to form networks of complex fractal dimensionalities. Due to the low particle loading (< 1-3 wt.%), soggy-sand electrolytes, with significant Li^+ surface transports, display ionic conductivity above that of pure liquid electrolytes. The mechanism of ion transport in soggy-sand electrolytes could be the attraction of the ion pair at the filler's surface and facilitates the ion pair dissociation. The counter-ion will then exist in the space charge region at the vicinity of particle liquid interface. At a threshold filler loading, ionic conductivity increases as percolation allows for long-range transport of the free ions in the space charge layer. Below the threshold filler loading, the ionic transport properties will not change as percolation does not exist. Beyond threshold filler loading, the conductivity will continue to increase with increasing filler content until it reaches maximum filler loading. Beyond this maximum filler loading, conductivity decreases due to the blocking of the percolative pathways and volume depletion effects [261]. Figure 28 shows the charge space vicinity of the fillers and electrolyte interface, with and without filler percolation.

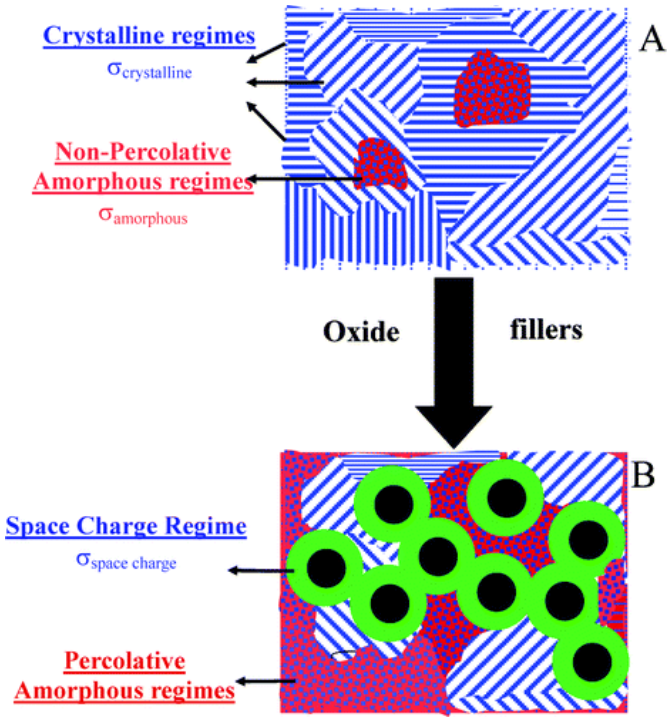

Figure 28. The inorganic filler in liquid electrolyte (a) below threshold filler loading (no percolation) (b) above or at threshold filler loading (percolation formed). Permission from [262].

4.2 Results and Discussion

4.2.1 Electrochemical Characterization

Polymeric membranes have been introduced due to their high ionic transfer abilities, rapid consumption of organic material, pro Li^+ transfer, anodic and oxidizing environment, gas barrier surfaces and effective chemical, thermal, and mechanical stabilities within the operating conditions (cold start, shut down, unplanned disruptions) of a fuel cell [150, 169, 187, 210, 218, 263]. Positive Li^+ migrate through the GPE to combine with I^- at the cathode/GPE interface [225]. The I^-/I_3^- reaction occurs at ~3.5 V (*vs.* Li/Li^+) and the I_3^-/I_2 reaction at ~4.25 V (*vs.* Li/Li^+) as shown in the Figure 29. The redox potential of Li-

O_2 (3.85-4.09 V *vs.* Li/Li^+) [232] sits right in between the potentials of I^-/I_3^- and I_3^-/I_2. Therefore, O_2 is chemically reduced by I^- and Li_2O_2 is chemically oxidized by I_2 [233]. During charge, peaks at approximately 3.5 V and 4.2-4.5 V correspond to oxygen (O_2) evolution and iodine (I_2) evolution reactions, respectively. During discharge, peaks at 3.5 V and 2.4 V correspond to lithium-iodide (LiI) and lithium-peroxide (Li_2O_2) reduction reactions, respectively. Figure 29a illustrates 2 peaks during OER confirming that LiI RM did not completely oxidize the Li_2O_2 at 3.5 V, and completed Li_2O_2 oxidation at 4.4 V. Also, 1 peak during ORR confirms that cGPE-1% completely reduced Li_2O_2 at 2.3 V. The presence of RM at the electrolyte-cathode surface layer has shown to reduce the charge overpotential thus making the charge reaction more efficient [185, 203, 205, 231, 264].

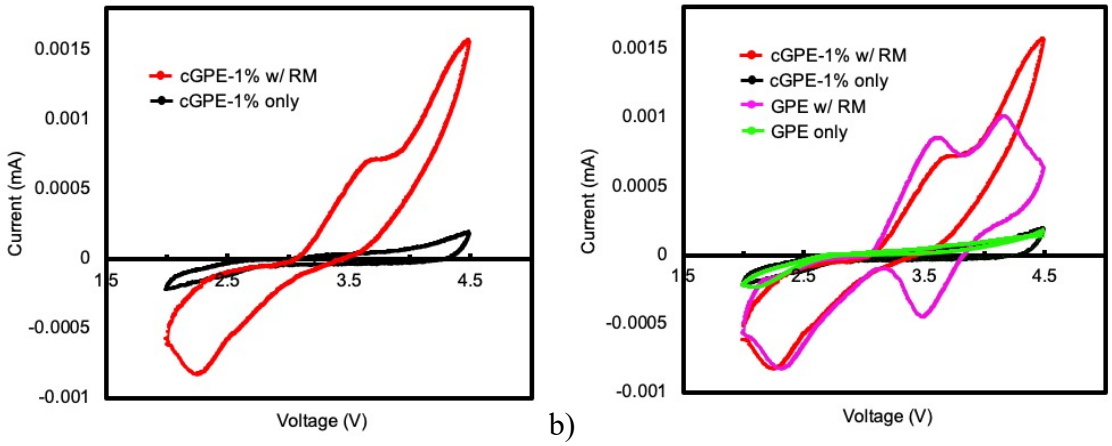

Figure 29. CV comparison of a) cGPE-1% and b) cGPE-1% vs GPE batteries with RM.

Cells exhibited an OCV of > 2.8 V before cyclic testing under a current density of 250 mA/g and 10 psi, under a voltage range of 2.0-4.5 V. CV confirmed the difference in initial potentials between cGPE and GPE batteries during charge/discharge testing. Initial

overpotential charge decreased from 4.3 to 3.05 V and 4.3 V to 3.55 V for cGPE-1% and GPE, and initial discharge increased from 2.6 V to 2.7 V for both GPE and cGPE, respectively, under 0.05M LiI redox mediation, therefore the initial charge to discharge overpotential has shown to be reduced to approximately 0.35 V and 0.85 V for cGPE and GPE, respectively, from its previous 1.7 V. Reduced overpotential resulted in significantly better cycling due to decreased charging versus discharging power, contributing to decreased electrolyte decomposition and cathode byproduct formation rates.

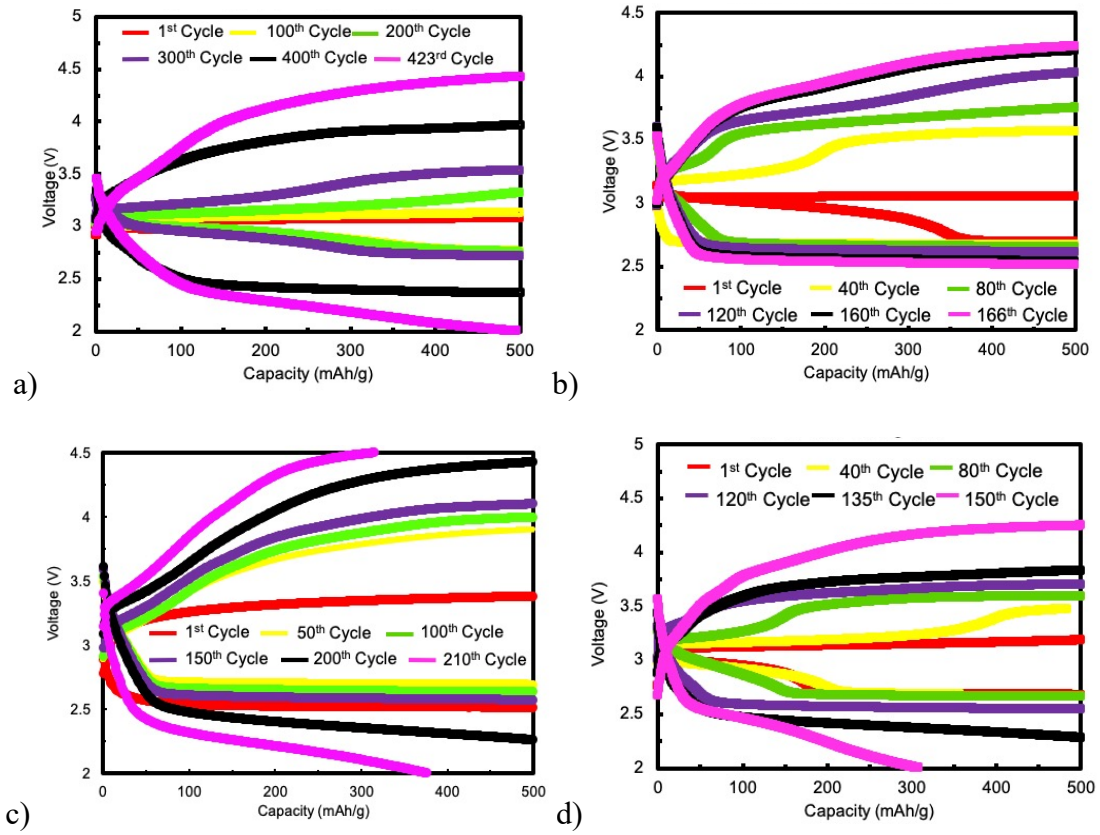

Figure 30. CCD plots (until failure) with 0.1 mg CNT cells for a) cGPE-1% with 0.05 M LiI RM [A1], b) GPE with 0.05 M LiI RM [B1], c) cGPE-1% only [A2], d) GPE only [B2], respectively. Capacity for all 0.1 mg CNT cells were 500 mAh/g, with a voltage window of 2.0-4.5 V.

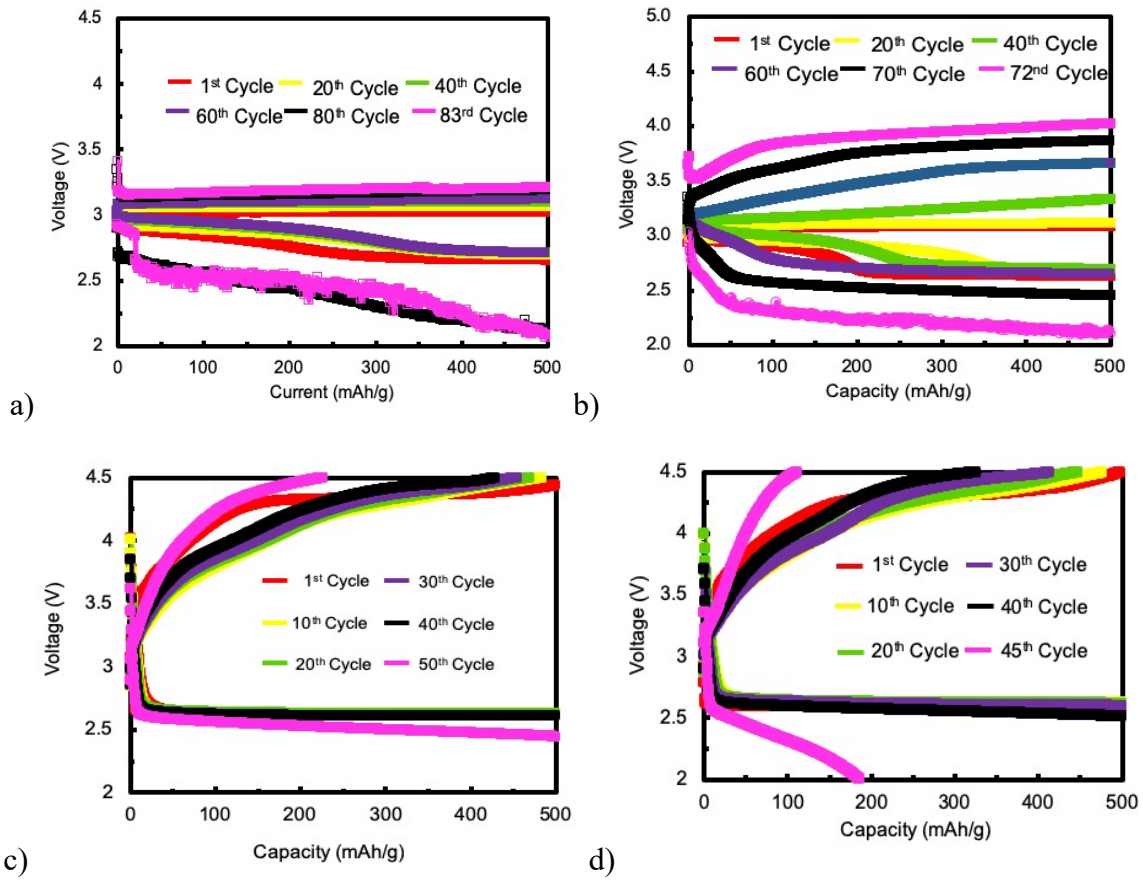

Figure 31. CCD plots (until failure) with 0.5 mg CNT cells for a) cGPE-1% with 0.05 M LiI RM [A3], b) GPE with 0.05 M LiI RM [B3], c) cGPE-1% only [A4] and d) GPE only [B4], respectively. Capacity for all 0.5 mg CNT cells were 500 mAh/g with a voltage window of 2.0-4.5 V.

As charge/discharge electrical stimulation is applied to the GPE/cGPE substrates, dendritic growth and byproduct formation occurred and changed the internal and external substrate properties over time. Charge/discharge cycling determined 423, 167, 83 and 47 cycles with batteries A1, A2, A3 and A4, respectively, using 1M cGPE-1%. Charge/discharge cycling also determined 201, 137, 72 and 24 cycles with batteries B1, B2, B3 and B4, respectively, using 1M GPE. Both A3 and B3 are illustrated to have undergone delamination causing

instant shorting. This data suggests a more stable cathode during charge and discharge using 1M cGPE-1% due to the increased conduction and energy efficiency of the glass fibers. Excellent mechanical, chemical and electrical properties of the cGPE, along with optimized conduction from the 0.1 mg CNT cathode, reduced the rate of delamination, pore clogging within the CNT cathode and byproduct formation at the cathode/cGPE interface in A1. Secondary analysis achieved 166 charge/discharge cycles before delamination occurred during charge cycle, suggesting the Li foil anode lost contact with the cGPE and/or byproduct formation at the anode caused the cell to short. It is apparent that the addition of LiI RM created less stress on the system during charge, due to the increased oxidation, assisting the overall battery system by reducing byproduct formation, and electrode and electrolyte decomposition rates.

Data indicates that LiI's effective range is between 3.0-3.7 V, and that significant Li_2CO_3 reactions occur once systematic oxidation is negligible, above 3.7 V charge [111]. Owing to the distinguishable reactions, part of Li_2O_2 and LiI (redox) were still in presence during discharge resulting in a plateau between 2.75 V and 2.5 V. Byproduct formations (due to carbon) scattered across the cathode/GPE interface effect cell life dramatically, however CNT variations on the cathode result in improved ionic conduction, cycling and transfer in the battery system.

4.2.2 Electrochemical Impedance Spectroscopy

The impedance and potentiostatic spectra confirm that CNT-LiI redox mediated cathodes have a significant reduction effect on the Li^+ diffusion. Polarization due to the kinetic and diffusion barriers affected discharge product distribution therefore, the ionic conductivity in the CNT cathode would increase and reduce barrier growth with the increase of Li^+ ions content due to redox addition [111].

According to Ryu *et al.* [246], during OER, the cathode acts as an insulator to the CNT particles restricting direct electron transfer and blockage. Optimizing catalytic placement configurations on the cathode suggest a possibility for extremely efficient Li-O_2 batteries. EIS measurements were performed during CCD to investigate the cathode/electrolyte potentiostatic property behaviors (5 mV/s). R_b (electrolyte resistance) corresponds to the resistances at, on and in-between the anode, cathode and GPE; R_{int} (interfacial resistance) represents the charge transfer resistance at the electrode/GPE interfaces; R_{ion} (ionic resistance) corresponds to the lithium-ion migration resistance inside the porous cathode structure of the cell system [180, 187, 239].

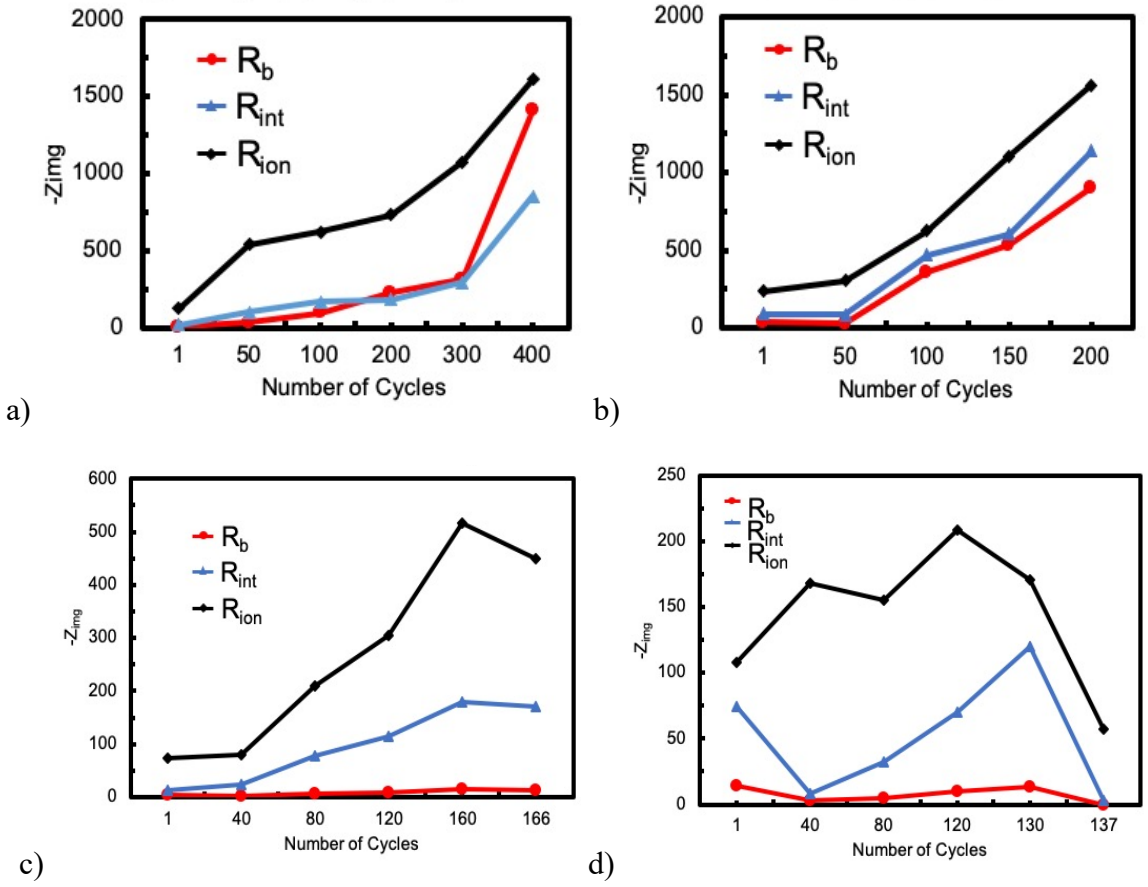

Figure 32. Resistance evolution plots obtained from EIS studies for 0.1 mg CNT a) cGPE-1% with 0.05 M LiI RM [A1], b) GPE with 0.05 M LiI RM [B1], c) cGPE-1% only [A2], d) GPE only [B2], respectively.

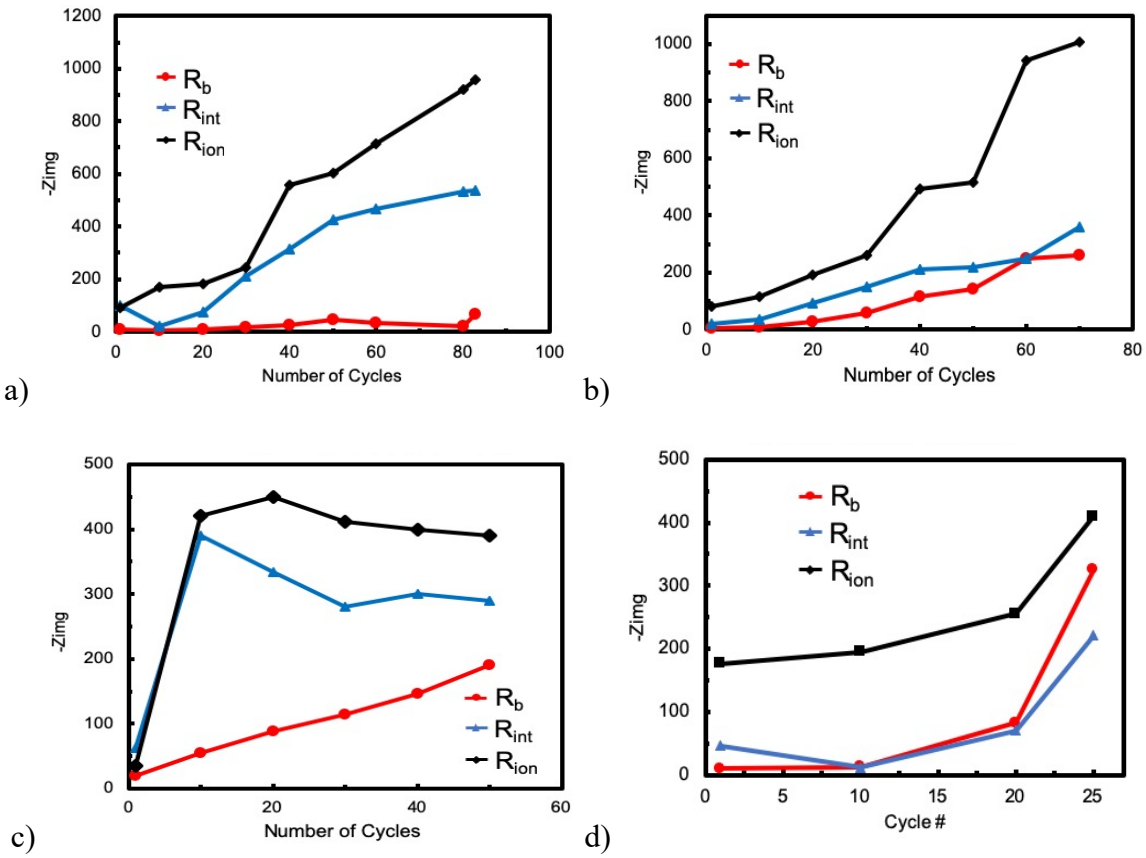

Figure 33. Resistance evolution plots obtained from EIS studies for 0.5 mg CNT a) cGPE-1% with 0.05 M LiI RM [A3], b) GPE with 0.05 M LiI RM [B3], c) cGPE-1% only [A4] and d) GPE only [B4], respectively.

Redox mediated systems had lower resistances over a similar cycle lifetime, indicating improved cell life and stability [187]. Reduced R_{ion} also assisted R_b, as indicated by the cell's reduced electrolyte decomposition and byproduct formation, in the cathode pores [239, 265]. Results indicate byproduct formation at the anode/GPE and cathode/GPE interfaces (R_{int}) can be reduced further with the aid of a RM component, extending cell life further [97, 124, 167, 181, 182, 265, 266].

4.2.3 Raman Spectroscopy

Using cathode of failed cells after their final discharge cycles, Li_2CO_3's accumulation (clogging the cathode pores) caused an increase in R_{ion} for cells without RM, as seen in Figure 34's Raman band at 1082 cm^{-1}, ultimately leading to increased cell decomposition [112, 131, 198]. During OER, the oxidation of the LiI (redox) and Li_2O_2 happened before the Li_2CO_3 corresponding to the plateau at 3.7 in the charge curve (Figures 30 and 31) [89, 93, 267-270]. Figure 34 shows that cells using RM had significantly less Li_2CO_3 formation, while sustaining a similar Li_2O_2 transference. Cell recharging processes sustained for another 50 cycles after the Li_2O_2, LiI, and $LiCO_3$ became reactive, ruling out the degradation of the GPE/cGPE. Raman peaks between 850-950 cm^{-1}, could also suggest possible PVDF $(C_2H_2F_2)_n$ chemical reactivity as was reported elsewhere [271, 272]. This phenomenon results in increased PVDF dissipation and dielectric loss of CNT conductivity (due to reduced insulation), resulting in cell failure from increased R_{ion} and R_{int} [271, 272]. PVDF dissipation (loss of energy) could cause cathode instability in cells with reduced loading (0.1 mg CNT), allowing radical R-ions (hydrogen or carbon ions) of the PVDF to bond with CO_3, resulting in an insoluble, Li_xRCO_3 byproduct (Raman peak at 920 cm^{-1}) [171]. Assuming the mechanical properties of the PVDF remained intact, the only logical reasoning for Li_xRCO_3 formation would be radical hydrocarbons cured into the porous structure of the cathode (during preparation) reacting with Li ions during ORR. This would create unwanted reactions that can significantly affect rate cyclability performance.

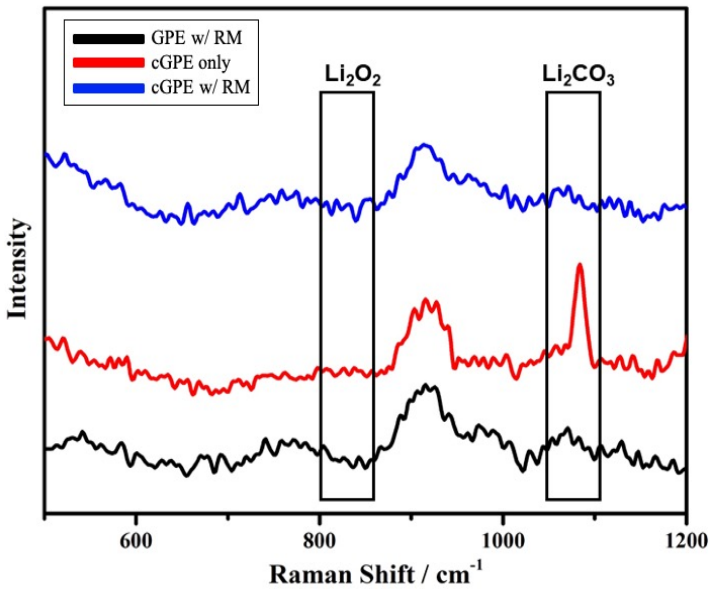

Figure 34. Raman spectra of cathodes after discharge using cGPE-1% (with and without LiI RM) and GPE with LiI RM.

4.3 Conclusion

This chapter addresses Li-O_2 battery life improvement by reducing resistance growth, using a composite GPEs based on 1-dimensional glass fibers and RMs. These experiments showcase the benefits of using a dual-enhancement system with cGPE, within Li-O_2 cells, to demonstrate enhanced cyclic stability. This is predominantly beneficial from the absence of blocked pores caused by the flooding liquid electrolyte and LiI RM solutions, enhancement of the oxygen diffusion in the cathode, anode suppressing dendrite formation, and reduced electrolyte deterioration during charge/discharge cycling, due to the high thermal, chemical, and mechanical stability properties of the GPE/cGPE allowing for high ionic conduction and transfer between the electrodes. LiI RM created electron transfer assistance at the cathode reducing the overall cell overpotential by over 1 V for early cycle

stages (Figure 30 and 31) minimizing ionic resistance and “unwanted” reaction rates, overall improving roundtrip efficiency of the battery system.

The A1 battery cell was cycled for 423 cycles, in which the ORR potential drop and OER potential increase after 300^{th} cycle was as low as 0.05 V to 0.4 V, respectively (Figure 30). Electrolyte polarity and oxygen solubility limit the viscosity and ionic conductivity of the electrolyte requiring the inclusion of a functional catalyst at the electrolyte-cathode interface to partially dissolve Li_2O or Li_2O_2 and improve discharge performance [93]. Ultimately, these results can be used to optimize cathode loading and improve electron transfer, while reducing transfer resistance across the electrolyte-cathode surface layer, thus maintaining a high specific surface area and electrical conductivity due to the cathode’s intrinsic pore structure in future Li-O_2 battery systems.

5 EFFECT OF CARBON NANOTUBE WALL COUNT AND GEOMETERY ON CATALYTIC PERFORMANCE OF Li-O_2 BATTERIES

5.1 Introduction

The introduction of lithium batteries has made a significant impact on the energy and storage industry. Creating practical, consumer friendly batteries with high energy densities and life cycles are ideal for extended use in various applications [156, 243, 273-276]. Battery performance issues primarily focus around discharge byproduct formation at the electrolyte/electrode interface and cathode stability [224, 225, 277, 278]. Implementing gel polymer electrolytes (GPE) into the cell structure adds mechanical, thermal, chemical and electrical stability and reduces electrolyte decomposition, while improving anode protection and ionic conduction [97, 150, 169, 187, 210, 211, 218, 279, 280]. Porous cathode infrastructures with carbon nanotube (CNT) fillers and redox mediators create highly conductive and oxidized cell atmospheres, with minimal flow disruption and extended life up to 3.7 V (before rapid cell deterioration occurs) [144, 212, 213, 219-223, 281-291]. Single-walled carbon nanotubes (SWCNTs) and multi-walled carbon nanotubes (MWCNTs) have displayed distinguishable properties within these battery atmospheres, however, limited studies address the effect of CNT's diameter on the cathode's performance [292-295]. In this chapter, battery performance is examined using SWCNTs, herringbone carbon nanotubes (HRCNTs) and MWCNTs, to determine CNT's diameter effect on the cathode, during cycling.

5.2 Results and Discussion

5.2.1 Cyclic Voltammetry and Charge/Discharge Cycling

CNT fillers were purchased from Sigma-Aldrich and Tokyo Chemical Industry. Table 10 illustrates the diameter, length, purity and manufacturer of each CNT filler during experimentation. A cross sectional view of the CNT shows that adjacent graphene layers are reportedly 0.34 nm apart in MWCNTs, according to multiple reports [296, 297]. Pristine carbon-cloths (CC, purchased from Fuel Cell Earth) were punched into 0.5" discs then dipped into their respective CNT solutions and dried for 30 minutes at 100°C. Cathode loadings were established by repeatedly dipping and drying until a 0.1 mg loading of CNT was measured on a digital scale. After fabrication, cells were allowed to rest under argon (a minimum 10 hours) before analytical testing.

CNT Filler	Diameter	Length	Layers	Purity	Surface Area
MW_1CNT	5-20 nm	5 µm	14-59	>95% carbon	95-430 m^2/g
MW_2CNT	20-40 nm	5-15 µm	59-118	>85% carbon	50-120 m^2/g
SWCNT	1-3 nm	Above 5 µm	1	>85% carbon	1315 m^2/g
HRCNT	10-20 nm	5-15 µm	30-60	>85% carbon	150-296 m^2/g

Table 10. Respective diameters and lengths for each CNT filler type [297-299].

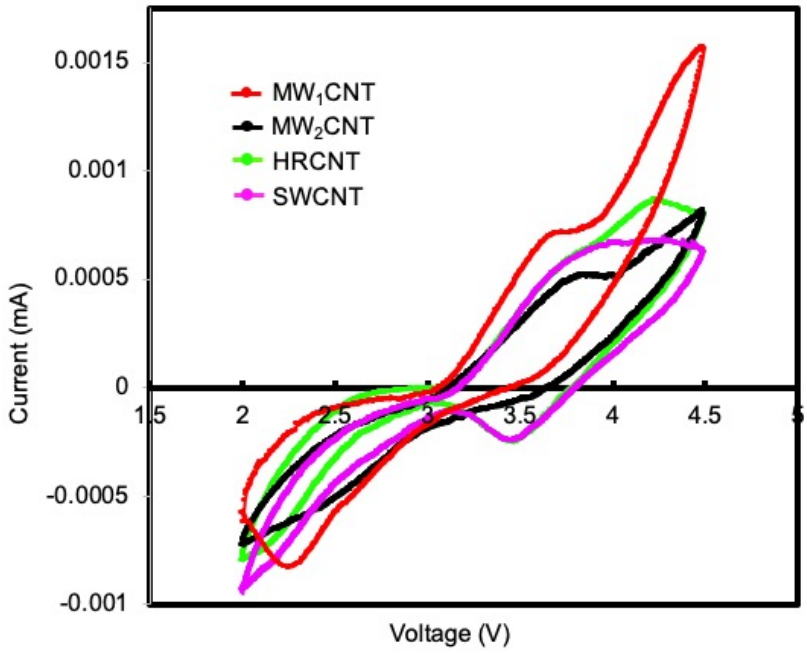

Figure 35. Comparison CV of cells prepared using various CNTs in the cathodes. Scan rate was 5 mV/s.

Cyclic voltammetry in Figure 35 illustrates the current range areas of each filler type between 2.0-4.5 V voltage window. CV concluded that MW_1CNTs operated significantly better during charge (OER) while the SWCNTs had a slightly deeper discharge (ORR) than the other CNT fillers. This means that the MW_1CNTs are able to recharge the battery more efficiently than the other CNTs. The redox potential of Li-O_2 (3.85-4.09 V *vs.* Li/Li^+) [232] sits right in between the potentials of I^-/I_3^- (-3.5 V) and I_3^-/I_2 (-4.25 V). Therefore, it is energetically favorable for O_2 to be chemically reduced by I^- and for Li_2O_2 to be chemically oxidized by I_2 [233]. During charge, peaks at approximately 3.5-3.7 V and 4.0-4.4 V correspond to oxygen (O_2) evolution and iodine (I_2) evolution reactions, respectively. It can be noted that significant iodine evolution only occurred in MWCNT cells. MW_1CNTs had the steepest charge versus voltage, accounting for its improved stability

over the other CNT loadings. During discharge, peaks at 3.5 V and 2.4 V correspond to lithium-iodide (LiI) and lithium-peroxide (Li_2O_2) reduction reactions, respectively. Figure 35 illustrates 2 peaks during OER for MWCNTs cells, confirming that LiI RM did not completely oxidize the Li_2O_2 at 3.5 V, and completed oxidation at 4.4 V. Figure 35 also illustrates 2 peaks during ORR for SWCNT and HRCNT cells, confirming that LiI RM did not completely reduce the Li_2O_2 at 3.5 V, and instead, completed Li_2O_2 reduction at 2.1 V [185].

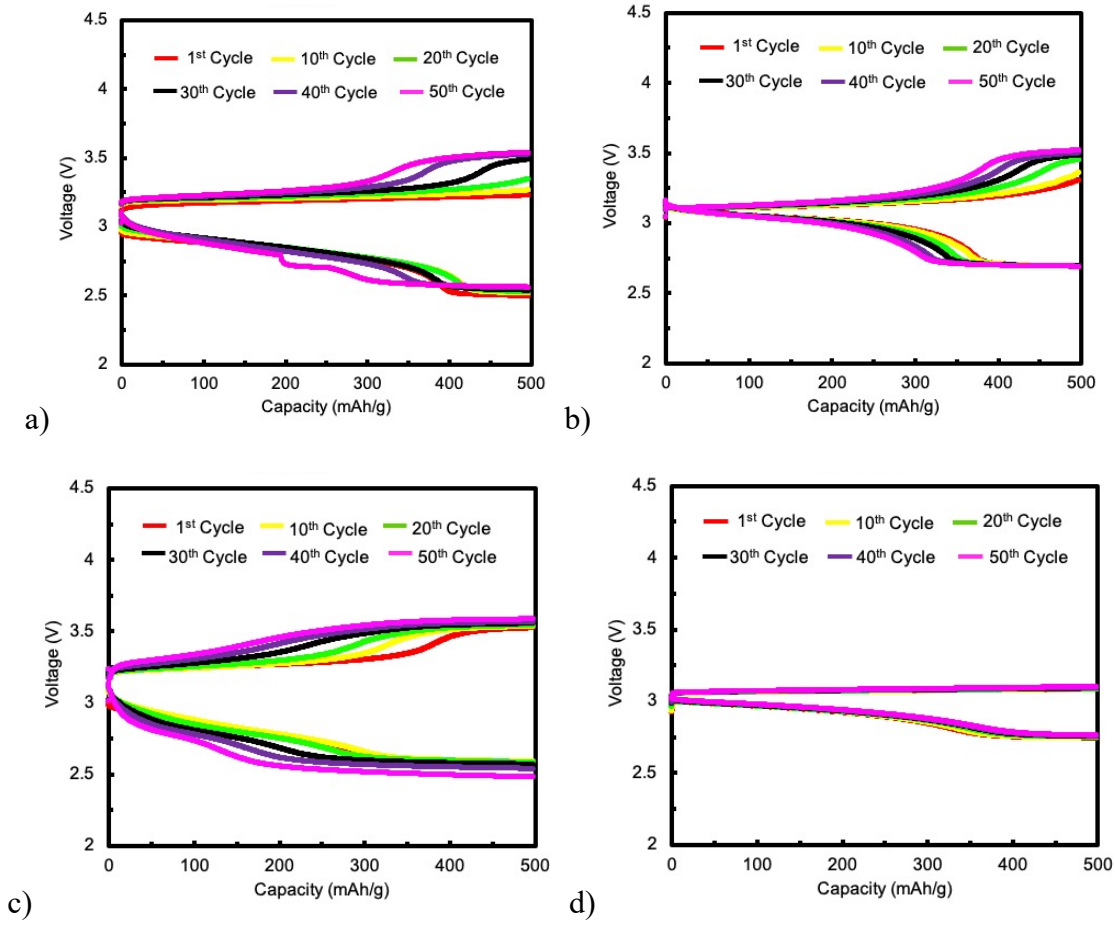

Figure 36. CCD plots of a) HRCNT, b) MW_2CNT, c) SWCNT and d) MW_1CNT up to the 50th cycle. Current capacity was set to 500 mAh/g with a voltage window of 2.0-4.5 V.

Cyclic charge/discharge, as seen in Figure 36, was completed under capacity 500 mAh/g. MW_1CNT operated significantly better over its initial 50 cycle span, producing an overpotential of 0.4 V, which is less than half the potentials of HRCNT (1 V), SWCNT (1 V) and MW_2CNT (0.8 V) during the same duration. From the graphs, it can be seen that MW_1CNT had a stable reaction during OER (charge), while additional (unwanted) reactions occurred significantly in the other CNT fillers, indicated by the sudden charge potential increase. Data suggests filler geometry affects cell performance being that SWCNT (single concentric) and HRCNT (rectangular scales) had more noticeable potential increases during cycling. Data also illustrates that cells with smaller cathode-filler diameters, specifically SWCNT (< 3 nm) and MW_1CNT (5-20 nm), reacted more stably and had fewer potential fluctuations in both OER and ORR. Fluctuations of potential are reduced in both MWCNT cells, suggesting that the MWCNT design (layered concentric) operates more reactively (illustrated by reactivity peaks in Figure 35) with LiI redox, allowing for increased stability in highly corrosive settings (illustrated by stable potential in Figure 36). Being that the SWCNT also had a significantly larger surface area than MWCNT (Table 10), any oxide reactivity would produce significantly more corrosion and surface defects, accounting for rapid cathode pore clogging and deterioration, despite having a reduced filler diameter. It should be noted that MW_1CNT cycled considerably longer than its counterparts, producing 401 cycles, while HRCNT, MW_2CNT and SWCNT completed at 75, 92 and 111 cycles, respectively, confirming reduced filler diameter and concentric layering are important in optimized Li-O_2 cell systems.

5.2.2 Electrochemical Impedance Spectroscopy

EIS measurements investigated the cell potentiostatic properties during cycling at a rate of 5 mV/s. R_b (initial point) corresponds to the resistance of the cell, R_{int} (semi-circle length) is the resistance between the electrode/electrolyte surfaces and R_{ion} refers to the ionic transfer resistance in the cell system [81, 104, 173, 180, 239, 240, 265]. Values of R_b, R_{int} and R_{ion} were determined and plotted for up to 50 cycles in Figure 38.

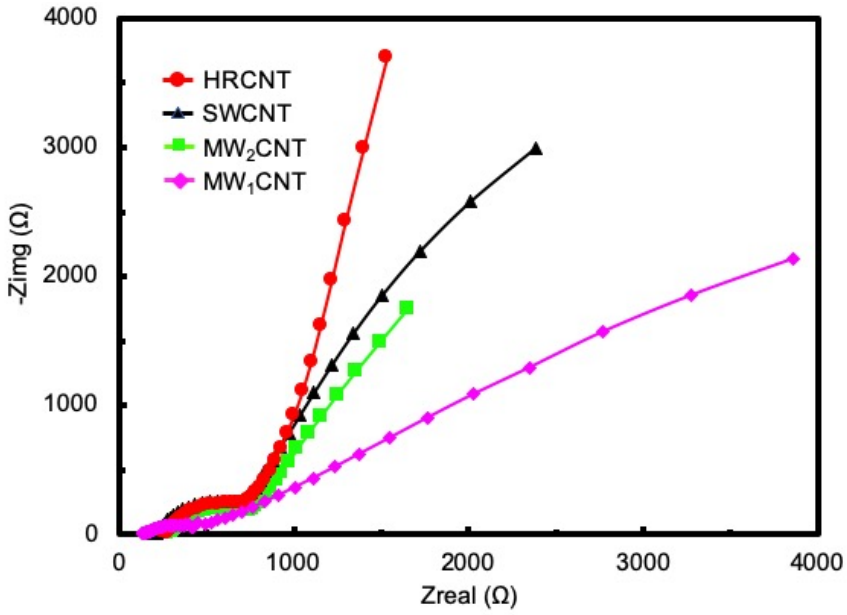

Figure 37. Nyquist plots of cells with various CNT cathodes before the 1st discharge cycle.

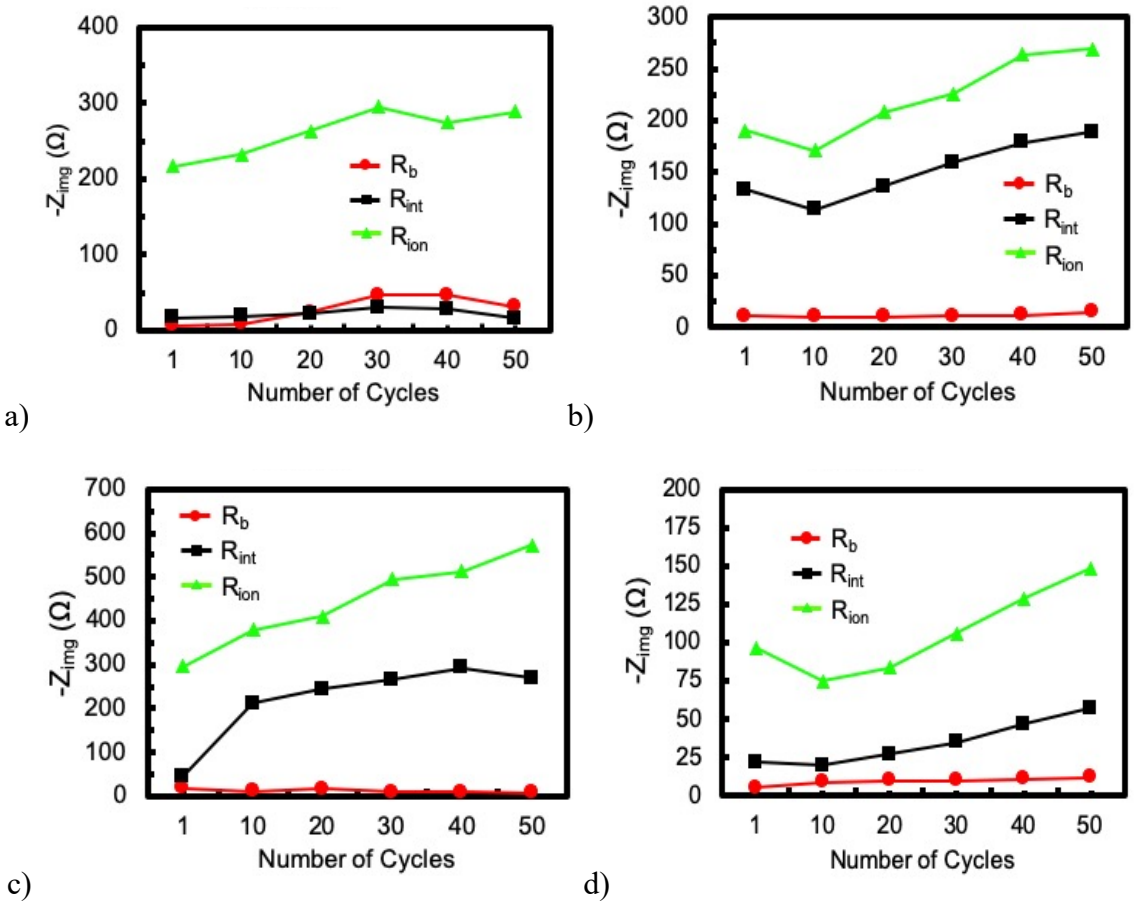

Figure 38. Evolution of resistances obtained using an EIS study of cells with cathodes containing a) HRCNT, b) MW_2CNT, c) SWCNT and d) MW_1CNT for the first 50 cycles.

Resistance shifts primarily increased linearly for R_{int} and R_{ion} for all 4 CNTs, indicating their proportionality to the increasing cycle number. This increase is attributed to the byproduct formation clogging the cathode pores and forming on the cell surfaces, as cycling continued [173, 239, 265]. SWCNTs (Figure 38 plot c) had the greatest increase in R_{int} and R_{ion}, indicating that both MWCNTs and HRCNTs are stronger and more conductive in highly corrosive cell environments. This could be due to more O_2 and Li^+ being captured within the conductive CNT wall layers, forming more Li_2O_2 during ORR. Additionally, during OER, redox mediation is speculated to assist in capturing additional

oxygen radicals, increasing Li_2O_2 formation, thus stabilizing the cell and ultimately extending cell lifetime. This can be seen in Figure 37 (significantly smaller semicircle diameter of MW_1CNT cell) indicating greater charge transfer kinetics due to decreased R_{int} resistance. EIS measurements indicated that smaller diameters in MWCNT systems (MW_1CNT specifically) operated almost 2x better than its counterparts, when determining R_{ion}. Wang *et al.* [300] reported that SWCNTs are less resistant to electrochemical oxidation than MWCNTs. SWCNTs had a larger increase of capacitive current indicating a higher oxidation degree of carbon with potential over a holding time. SWCNT possess higher and more accessible surface areas than MWCNTs. Wang *et al.* reported [301] that increasing carbon surface area correlates to increased corrosion rates, therefore higher surface areas result in more corrosivity defects. According to Lu *et al.* [302], smaller tube diameters should increase the oxidation rates, since the local strain energy will be raised along the entire length of the tube due to the decreased radius of curvature. Compared with the diameter of 5-20 nm for MWCNTs in this study, the diameter of SWCNTs is less than 3 nm (Table 10), thus, a higher local strain energy would occur on the SWCNT, resulting in higher corrosion rates [302]. These results confirm SWCNTs are less resistant to electrochemical oxidation (more corrosive) than MWCNTs.

5.2.3 Raman Spectroscopy

After CCD failure, cathodes were examined for byproduct formation to better characterize Li_2O_2 and Li_2CO_3 formation. Figure 39 shows that all CNT cathodes had a low amount of Li_2O_2 and Li_2CO_3 byproducts (Raman bands at 820 cm^{-1} and 1082 cm^{-1}, respectively) clogging the cathode pores, attributing to LiI RM assistance in the cathode.

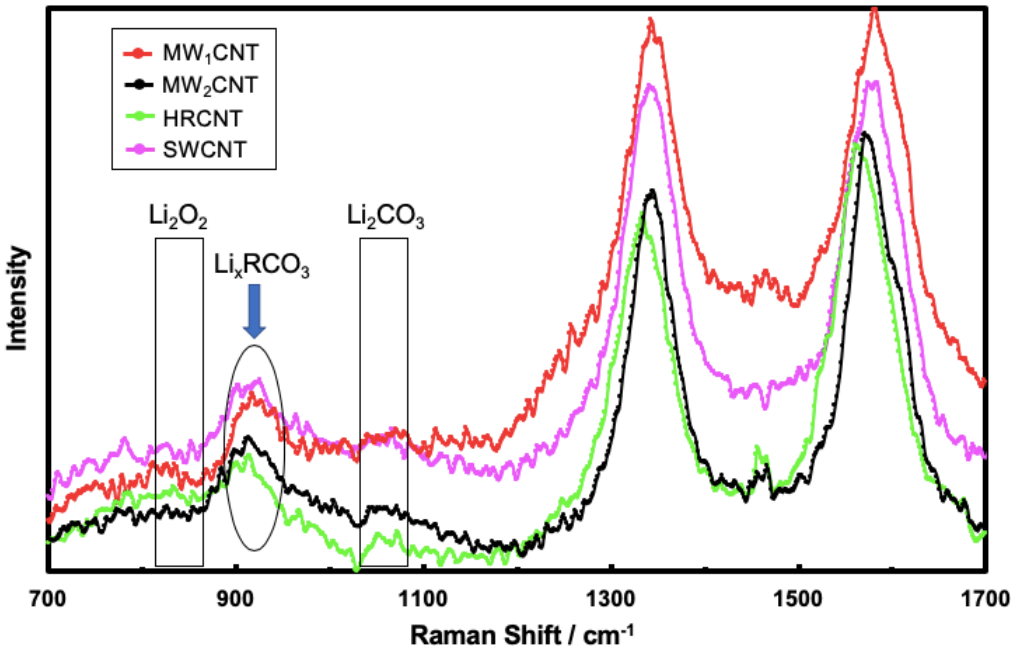

Figure 39. Comparison Raman spectra between 700-1700 cm^{-1} of CNT cathodes after failure.

Raman peaks between 900-950 cm^{-1} in CNT cathodes suggest possible formation of a different byproduct specie causing failure. Reports indicate possible formation of a phosphate (PO_4^{-3}) species [242, 303], which is 45 times less conductive than carbonate (CO_3^{-2}) species, thus confirming Li_2PO_4 would have more of a negative impact on the cells in regard to reducing electrochemical performance due to increased reactivity, oxide corrosion and cathode pore clogging. However, due to the nature of this study, phosphate contamination is highly unlikely despite CNT purity being > 95%. Further review of Raman peaks between 850-930 cm^{-1} indicate possible PVDF-β reactivity [272]. Different phases exist in PVDF depending on various parameters like solvent type and volatility, polymer fillers, and loading in solution. Despite the many improvements PVDF has on the cell system (light weight, larger chain flexibility, good mechanical properties, chemical

and electrical resistance, etc.), high dissipation (loss of energy) and dielectric loss due to electrochemical cycling and glass microfiber reactivity reduces cathode conductivity, resulting in failure [271]. Based on this knowledge, it could be theorized that PVDF reactivity caused CNT loading defects due to byproduct layer formation at the cathode/cGPE interface. This could create potential side product (LiOH, Li_2CO_3 and LiF) and oxide/superoxide (Li_2O or LiO_2) formations, however the nature of this is still undetermined due to very few solvent-side product/ superoxide Raman correlation studies for Li-O_2 batteries [171]. Furthermore, cell failure and CNT cathode defects are more likely due to radical R-ions (carbon or hydrogen) in the system reacting with Li_2O_2 or Li_2CO_3, resulting in insoluble, Li_xRCO_3 byproducts (Raman peak at 920 cm^{-1}).

5.3 Conclusion

This work assesses how CNT diameter and geometry effect Li-O_2 battery performance. Cells were constructed using LiI RM (at the CNT cathode) and cGPE (as the electrolyte). CV concluded that MW_1CNTs operated significantly better during OER and was less reactive during ORR, resulting in a more stable and improved rechargeability. The impedance spectra showed that the ionic resistance of cells with MW_1CNT operated approximately 2x better than the other fillers in its first 50 cycles. HRCNT, SWCNT, MW_1CNT and MW_2CNT cells completed 75, 111, 92 and 401 cycles before failure, respectively, before Raman was completed. Raman spectroscopy indicated low Li_2O_2 and Li_2CO_3 formation (Raman bands at 820 cm^{-1} and 1082 cm^{-1}, respectively) on the CNT cathodes and noticeable peaks between 850-950 cm^{-1}, resulting in a high amount of Li_xRCO_3 byproduct species, leading to cell failure. Analyses confirm thin, concentric

CNTs (SWCNT and MWCNT) operate better than tiled CNTs (HRCNT), however, thin, layered-concentric cells (specifically MW_1CNT) minimized undesirable reactivity with cell components. MW_1CNTs minimized the rate of clogging at cathode active sites better than SWCNTs. Results demonstrated improved roundtrip cyclic efficiency and system stability, and reduced resistance (ionic and interfacial) and charge potentials, for thin, layered-concentric fillings suggesting MW_1CNTs (d= 5-20 nm) operate best overall in Li-O_2 battery systems under the current conditions and concentrations.

6 CONCLUSIONS AND FUTURE WORK

This dissertation has shown the importance of cGPE in the development of a dual-enhancement system, consisting of loaded CNT fillers and LiI RM. This system can significantly optimize the energy density, improve lifetime and reduce overpotential, while maintaining a mechanically and electrochemically stable cell structure with minimal resistance up to 3.7 V in Li-O_2 batteries. Efficient cell operation was dependent upon precision cell construction. Due to its hand-made development within the Swagelok cell, every battery constructed had potential error ranging from: (1) total amount of applied solution, (2) Swagelok cell tightening pressure, (3) cell-rod pressing, (4) lithium foil brushing and steel rod sand-paper cleansing, (5) cell resting/stabilization time, (6) Swagelok cell O_2 tube connection and (7) potential fluctuating atmospheric conditions in the room (during testing).

Accelerated cell deterioration was observed to occur beyond 3.7 V charge, where the systematic oxidation effects of the LiI redox becomes negligible. However, LiI's ability to assist cell potential during charge drastically improved cell lifetime by capturing radical oxygen ions, forming an abundance of Li_2O_2 compounds. This reaction reduced both electrolyte and electrode decomposition due to potential growth. cGPE's unique polymer composition provided additional anode protection and stability, while minimizing R_{ion}, R_b, R_{int} in the electrolyte and improving ionic conduction. Variating CNT loading from 0.1 - 0.5 mg (operating at 500 mAh/g current density) optimized ionic conductivity without exceeding threshold, however, organic-species oxidation at the cathode eventually

continued to form Li_xRCO_3, causing cathode pore clogging, byproduct layering and loss of dielectric properties. Studies using various CNTs (HRCNT, SWCNT and MWCNTs) determined that MWCNTs (specifically MW_1CNT, d= 5-20 nm) operated significantly better during charge (OER) with an ionic resistance approximately 2x better than the other CNT fillers in its first 50 cycles. This was due to the LiI redox being activated electromagnetically during charge cycles, allowing for a reduced overpotential during discharge cycles. Results suggest thin, layered-concentric CNT fillers improve roundtrip cyclic efficiency and system stability, while reducing resistance and charge potentials in Li-O_2 battery systems.

In conclusion, maximized Li-O_2 cells returned 201 cycles for GPE and 423 cycles for cGPE. Cycles consisted of 2 hours of charge and 2 hours of discharge, with 20 minutes of rest after each half cycle. Optimizations resulted in 800% (47 cycles → 423 cycles) and 737% (24 cycles → 201 cycles) increases in battery lifetimes for cGPE and GPE cells, respectively, and an astounding 1663% cycling performance increase for maximized cGPE cells, when compared to the control GPE (24 cycles → 423 cycles). These observations suggest that research should focus more on cathode and electrolyte filler micro-structuring, as well as their reactions to variable redox mediators/catalysts, to extend the lifetime and energy density of future Li-O_2 batteries.

Future work should consider: (1) optimizing CNT loading parameters and single dimensional micro-structuring techniques, (2) variating cathode materials including carbon cloth, Ni foam, etc., (3) creating a conductive, polymer electrolyte that eliminates the need

for a PVDF binder, (4) implementing an additional mediator to minimize the formation of organic oxides, and (5) creating an all-in-one system that contains electrolyte (preferably a composite), cathode filler loading and redox mediation in a single disk. Improvements upon these suggestions will likely improve Li-O_2's scalability, offering potential commercializing and patentable applications in future Li-O_2 battery technology.

BIBLIOGRAPHY

1. Reddy, T.B., *Linden's handbook of batteries*. Vol. 4. 2011, New York: McGraw-Hill.

2. Armand, M. and J. Tarascon, *Building better batteries.* Nature, 2008. **451**(7179): p. 652-657.

3. Tarascon, J. and M. Armand, *Issues and challenges facing rechargeable lithium batteries.* Nature, 2001. **414**(6861): p. 359-367.

4. Bruce, P., B. Scrosati, and J. Tarascon, *Nanomaterials for rechargeable lithium batteries.* Angewandte Chemie-International Edition, 2008. **47**(16): p. 2930-2946.

5. Schiffer, M.B., *Draw the lightning down: Benjamin Franklin and electrical technology in the age of enlightenment*. 2006: University of California Press.

6. Piccolino, M., *Animal electricity and the birth of electrophysiology: The legacy of Luigi Galvani.* Brain Research Bulletin, 1998. **46**(5): p. 381-407.

7. Piccolino, M., *Luigi Galvani and animal electricity: two centuries after the foundation of electrophysiology (vol 20, pg 443, 1997).* Trends in Neurosciences, 1997. **20**(12): p. 577-577.

8. Volta, A., *XVII. On the electricity excited by the mere contact of conducting substances of different kinds. In a letter from Mr. Alexander Volta, FRS Professor of Natural Philosophy in the University of Pavia, to the Rt. Hon. Sir Joseph Banks, Bart. KBPR S.* 1800, Philosophical transactions of the Royal Society of London 90. p. 403-431.

9. Peck, R.L., *Ionic semiconductor materials and applications thereof*, U.S.P. Office, Editor. 1991: United States of America.

10. Grove, W.R., *XXIV. On voltaic series and the combination of gases by platinum*. 1839, The London, Edinburgh, and Dublin Philosophical Magazine and Journal of Science. p. 127-130.

11. Kurzweil, P., *Gaston Planté and his invention of the lead–acid battery- The genesis of the first practical rechargeable battery*. 2010, Journal of Power Sources. p. 4424-4434.

12. Vincent, C. and B. Scrosati, *Modern batteries*. 1997: Elsevier.

13. Oakes, M., *A brief history of Batteries and Stored Energy*. 2006, Neta World. p. 1-6.

14. Mertens, J., *From the lecture room to the workshop: John Frederic Daniell, the constant battery and electrometallurgy around 1840.* Annals of Science, 1998. **55**(3): p. 241-261.

15. Pop, V., et al., *Battery management systems: Accurate state-of-charge indication for battery-powered applications*. Vol. 9. 2008: Springer Science & Business Media.

16. Tichenor, R.L., *Nickel Oxides-Relation Between Electrochemical and Foreign Ion Content*. 1952, Industrial & Engineering Chemistry. p. 973-977.

17. Perlin, J., *Silicon solar cell turns 50*. 2004, National Renewable Energy Lab: Golden, Colorado, United States.

18. AUBORN, J., et al., *LITHIUM ANODE CELLS OPERATING AT ROOM-TEMPERATURE IN INORGANIC ELECTROLYTIC SOLUTIONS.* Journal of the Electrochemical Society, 1973. **120**(12): p. 1613-1619.

19. BASU, S., et al., *SYNTHESIS AND PROPERTIES OF LITHIUM-GRAPHITE INTERCALATION COMPOUNDS.* Materials Science and Engineering, 1979. **38**(3): p. 275-283.

20. ZANINI, M., S. BASU, and J. FISCHER, *ALTERNATE SYNTHESIS AND REFLECTIVITY SPECTRUM OF STAGE 1 LITHIUM-GRAPHITE INTERCALATION COMPOUND.* Carbon, 1978. **16**(3): p. 211-212.

21. MIZUSHIMA, K., et al., *LIXCOO2 (O LESS-THAN X LESS-THAN-OR-EQUAL-TO 1) - A NEW CATHODE MATERIAL FOR BATTERIES OF HIGH-ENERGY DENSITY.* Solid State Ionics, 1981. **3-4**(AUG): p. 171-174.

22. YAZAMI, R. and P. TOUZAIN, *A REVERSIBLE GRAPHITE LITHIUM NEGATIVE ELECTRODE FOR ELECTROCHEMICAL GENERATORS.* Journal of Power Sources, 1983. **9**(3-4): p. 365-371.

23. Yoshino, A., K. Sanechika, and T. Nakajima, *Secondary Battery*, U.P. Office, Editor. 1987: United States of America.

24. Thackeray, M., C. Wolverton, and E. Isaacs, *Electrical energy storage for transportation-approaching the limits of, and going beyond, lithium-ion batteries.* Energy & Environmental Science, 2012. **5**(7): p. 7854-7863.

25. Goriparti, S., et al., *Review on recent progress of nanostructured anode materials for Li-ion batteries.* Journal of Power Sources, 2014. **257**: p. 421-443.

26. Blomgren, G., *The Development and Future of Lithium Ion Batteries.* Journal of the Electrochemical Society, 2017. **164**(1): p. A5019-A5025.

27. Bruce, P., et al., *Li-O-2 and Li-S batteries with high energy storage (vol 11, pg 19, 2012).* Nature Materials, 2012. **11**(2).

28. Karagulian, F., et al., *Contributions to cities' ambient particulate matter (PM): A systematic review of local source contributions at global level.* Atmospheric Environment, 2015. **120**: p. 475-483.

29. (IEA), I.E.A., *CO2 Emissions from Fuel Combustion* in *Highlights 2015 Edition*. 2015, International Energy Agency: Paris, France.

30. ., I.E.A.I., *Global EV Outlook 2016*, in *Beyond One Million Electric Cars*. 2016, International Energy Agency: Paris, France.

31. Sims, R., et al., *Transport Climate Change 2014: Mitigation of Climate Change.*, in *Contribution of Working Group III to the Fifth Assessment Report of the Intergovernmental Panel on Climate Change*, O. Edenhofer, Editor. 2014, Cambridge University Press: Cambridge and New York.

32. Hawkins, T., et al., *Comparative environmental life cycle assessment of conventional and electric vehicles (vol 17, pg 53, 2013).* Journal of Industrial Ecology, 2013. **17**(1): p. 158-160.

33. Sankhla, M., et al., *Heavy metals contamination in water and their hazardous effect on human health-a review*. 2016, Int. J. Curr. Microbiol. App. Sci p. 759-766.

34. Nitta, N., et al., *Li-ion battery materials: present and future.* Materials Today, 2015. **18**(5): p. 252-264.

35. Dunn, J., et al., *The significance of Li-ion batteries in electric vehicle life-cycle energy and emissions and recycling's role in its reduction.* Energy & Environmental Science, 2015. **8**(1): p. 158-168.

36. Placke, T., et al., *Lithium ion, lithium metal, and alternative rechargeable battery technologies: the odyssey for high energy density.* Journal of Solid State Electrochemistry, 2017. **21**(7): p. 1939-1964.

37. Sun, H., et al., *Control of electrochemical properties of nickel-rich layered cathode materials for lithium ion batteries by variation of the manganese to cobalt ratio.* Journal of Power Sources, 2015. **275**: p. 877-883.

38. Brain, M., C.W. Bryant, and C. Pumphrey, *How batteries work*. 2000, How Stuff Works.

39. McKenna, E., et al., *Economic and environmental impact of lead-acid batteries in grid-connected domestic PV systems.* Applied Energy, 2013. **104**: p. 239-249.

40. Notter, D., et al., *Contribution of Li-Ion Batteries to the Environmental Impact of Electric Vehicles (vol 44, pg 6550, 2010).* Environmental Science & Technology, 2010. **44**(19): p. 7744-7744.

41. Peters, J., et al., *The environmental impact of Li-Ion batteries and the role of key parameters - A review.* Renewable & Sustainable Energy Reviews, 2017. **67**: p. 491-506.

42. McManus, M., *Environmental consequences of the use of batteries in low carbon systems: The impact of battery production.* Applied Energy, 2012. **93**: p. 288-295.

43. Steffan, J., et al., *The effect of soil on human health: an overview.* European Journal of Soil Science, 2018. **69**(1): p. 159-171.

44. Deckers, J. and E. Steinnes, *STATE OF THE ART ON SOIL-RELATED GEO-MEDICAL*. Advances in Agronomy, ed. D.L. Sparks. Vol. 84. 2004: Academic Press. 332.

45. Balabanova, B., et al., *Quantitative assessment of metal elements using moss species as biomonitors in downwind area of lead-zinc mine.* Journal of Environmental Science and Health Part a-Toxic/hazardous Substances & Environmental Engineering, 2017. **52**(3): p. 290-301.

46. Filippelli, G. and M. Laidlaw, *THE ELEPHANT IN THE PLAYGROUND confronting lead-contaminated soils as an important source of lead burdens to urban populations.* Perspectives in Biology and Medicine, 2010. **53**(1): p. 31-45.

47. Li, P., et al., *Contamination and health risks of soil heavy metals around a lead/zinc smelter in southwestern China.* Ecotoxicology and Environmental Safety, 2015. **113**: p. 391-399.

48. Haefliger, P., et al., *Mass Lead Intoxication from Informal Used Lead-Acid Battery Recycling in Dakar, Senegal.* Environmental Health Perspectives, 2009. **117**(10): p. 1535-1540.

49. Lo, Y., et al., *Childhood Lead Poisoning Associated with Gold Ore Processing: a Village-Level Investigation-Zamfara State, Nigeria, October-November 2010.* Environmental Health Perspectives, 2012. **120**(10): p. 1450-1455.

50. Hanna-Attisha, M., et al., *Elevated Blood Lead Levels in Children Associated With the Flint Drinking Water Crisis: A Spatial Analysis of Risk and Public Health Response.* American Journal of Public Health, 2016. **106**(2): p. 283-290.

51. Laidlaw, M., et al., *Children's blood lead seasonality in flint, Michigan (USA), and soil-sourced lead hazard risks.* 2016, International journal of environmental research and public health. p. 358.

52. Liu, G., et al., *An ecological risk assessment of heavy metal pollution of the agricultural ecosystem near a lead-acid battery factory.* Ecological Indicators, 2014. **47**: p. 210-218.

53. Bhangu, B., et al., *Nonlinear observers for predicting state-of-charge and state-of-health of lead-acid batteries for hybrid-electric vehicles.* Ieee Transactions on Vehicular Technology, 2005. **54**(3): p. 783-794.

54. Cerdas, F., et al., *Exploring the Effect of Increased Energy Density on the Environmental Impacts of Traction Batteries: A Comparison of Energy Optimized Lithium-Ion and Lithium-Sulfur Batteries for Mobility Applications.* Energies, 2018. **11**(1).

55. Nordberg, G., et al., *Risk assessment of effects of cadmium on human health (IUPAC Technical Report).* Pure and Applied Chemistry, 2018. **90**(4): p. 755-808.

56. Hunter, P., *A toxic brew we cannot live without*. 2008. p. 15-18.

57. Masse, A., E. Solorzano, and N. Olgado, *Charging the Battery Power Revolution.*, J.A. Chiarelli, Editor. 2019, Worcester Polytechnic Institute: Chamber of Industry of Costa Rica.

58. Moura, P., et al. *Demand Response and Energy Storage for Zero Energy Residential Buildings*. in *8th International Conference on Energy Efficiency in Domestic Appliances and Lighting (EEDAL'15)*. 2015. Lucerne, Switzerland.

59. Faria, R., et al., *Primary and secondary use of electric mobility batteries from a life cycle perspective.* Journal of Power Sources, 2014. **262**: p. 169-177.

60. Assuncao, A., P. Moura, and A. de Almeida, *Technical and economic assessment of the secondary use of repurposed electric vehicle batteries in the residential sector to support solar energy.* Applied Energy, 2016. **181**: p. 120-131.

61. Madlener, R. and A. Kirmas, *Economic viability of second use electric vehicle batteries for energy storage in residential applications*. 2017, Energy Procedia. p. 3806-3815.

62. Santos, J., P. Moura, and A. de Almeida, *Technical and economic impact of residential electricity storage at local and grid level for Portugal.* Applied Energy, 2014. **128**: p. 254-264.

63. Lin, C., et al. *Battery management system with dual-balancing mechanism for LiFePO 4 battery module*. in *In TENCON 2011-2011 IEEE Region 10 Conference*. 2011. Bali, Indonesia: IEEE.

64. Haq, I., et al., *Development of battery management system for cell monitoring and protection*, in *2014 international conference on electrical engineering and computer science (ICEECS)*. 2014, IEEE. p. 203-208.

65. Kozak, T., et al. *Influence of ambient temperature on the amount of electric energy produced by solar modules*. in *2009 MIXDES-16th International Conference Mixed Design of Integrated Circuits & Systems*. 2009. Lodz, Poland: IEEE.

66. Javaid, M., et al., *Estimation of Solar Power Efficiency in Day Time at Different Temperatures*. 2011, International Journal of Electrical & Computer Sciences. p. 48-52.

67. Girishkumar, G., et al., *Lithium - Air Battery: Promise and Challenges.* Journal of Physical Chemistry Letters, 2010. **1**(14): p. 2193-2203.

68. Fiori, C., K. Ahn, and H. Rakha, *Power-based electric vehicle energy consumption model: Model development and validation.* Applied Energy, 2016. **168**: p. 257-268.

69. Kane, M. *All-Electric Car Range, Price & More Compared For U.S. – July 2019*. 2019 [cited 2019 August 29]; Available from: https://insideevs.com/news/361157/electric-car-compared-us-july-2019/.

70. Zubi, G., et al., *The lithium-ion battery: State of the art and future perspectives.* Renewable & Sustainable Energy Reviews, 2018. **89**: p. 292-308.

71. Chung, D., E. Elgqvist, and S. Santhanagopalan, *Automotive lithium-ion cell manufacturing: Regional cost structures and supply chain considerations* 2016, National Renewable Energy Lab (NREL): Golden, CO (United States).

72. Chemali, E., et al., *Electrochemical and Electrostatic Energy Storage and Management Systems for Electric Drive Vehicles: State-of-the-Art Review and Future Trends.* Ieee Journal of Emerging and Selected Topics in Power Electronics, 2016. **4**(3): p. 1117-1134.

73. Imanishi, N. and APA, *The lithium air battery: fundamentals*, ed. A.C. Luntz. 2014, New York: Springer.

74. Amanchukwu, C., et al., *Understanding the Chemical Stability of Polymers for Lithium-Air Batteries.* Chemistry of Materials, 2015. **27**(2): p. 550-561.

75. Li, Y., et al., *Recent Advances in Non-Aqueous Electrolyte for Rechargeable Li-O-2 Batteries.* Advanced Energy Materials, 2016. **6**(18).

76. Yi, J., et al., *Status and prospects of polymer electrolytes for solid-state Li-O-2 (air) batteries.* Energy & Environmental Science, 2017. **10**(4): p. 860-884.

77. Hummelshoj, J., et al., *Communications: Elementary oxygen electrode reactions in the aprotic Li-air battery.* Journal of Chemical Physics, 2010. **132**(7).

78. Debart, A., et al., *alpha-MnO2 nanowires: A catalyst for the O-2 electrode in rechargeable lithium batteries.* Angewandte Chemie-International Edition, 2008. **47**(24): p. 4521-4524.

79. Read, J., *Characterization of the lithium/oxygen organic electrolyte battery.* Journal of the Electrochemical Society, 2002. **149**(9): p. A1190-A1195.

80. Abraham, K. and Z. Jiang, *A polymer electrolyte-based rechargeable lithium/oxygen battery.* Journal of the Electrochemical Society, 1996. **143**(1): p. 1-5.

81. Zhang, D., et al., *Novel composite polymer electrolyte for lithium air batteries.* Journal of Power Sources, 2010. **195**(4): p. 1202-1206.

82. Wang, Y. and H. Zhou, *A lithium-air battery with a potential to continuously reduce O-2 from air for delivering energy.* Journal of Power Sources, 2010. **195**(1): p. 358-361.

83. Zhang, S., D. Foster, and J. Read, *Discharge characteristic of a non-aqueous electrolyte Li/O-2 battery.* Journal of Power Sources, 2010. **195**(4): p. 1235-1240.

84. Ren, X., et al., *Oxygen reduction reaction catalyst on lithium/air battery discharge performance.* Journal of Materials Chemistry, 2011. **21**(27): p. 10118-10125.

85. Lu, Y., H. Gasteiger, and Y. Shao-Horn, *Catalytic Activity Trends of Oxygen Reduction Reaction for Nonaqueous Li-Air Batteries.* Journal of the American Chemical Society, 2011. **133**(47): p. 19048-19051.

86. Lu, Y., et al., *Platinum-Gold Nanoparticles: A Highly Active Bifunctional Electrocatalyst for Rechargeable Lithium-Air Batteries.* Journal of the American Chemical Society, 2010. **132**(35): p. 12170-12171.

87. Black, R., et al., *The Role of Catalysts and Peroxide Oxidation in Lithium-Oxygen Batteries.* Angewandte Chemie-International Edition, 2013. **52**(1): p. 392-396.

88. Debart, A., et al., *An O-2 cathode for rechargeable lithium batteries: The effect of a catalyst.* Journal of Power Sources, 2007. **174**(2): p. 1177-1182.

89. McCloskey, B., et al., *Solvents' Critical Role in Nonaqueous Lithium-Oxygen Battery Electrochemistry.* Journal of Physical Chemistry Letters, 2011. **2**(10): p. 1161-1166.

90. Freunberger, S., et al., *Reactions in the Rechargeable Lithium-O-2 Battery with Alkyl Carbonate Electrolytes.* Journal of the American Chemical Society, 2011. **133**(20): p. 8040-8047.

91. Peng, Z., et al., *Oxygen Reactions in a Non-Aqueous Li+ Electrolyte.* Angewandte Chemie-International Edition, 2011. **50**(28): p. 6351-6355.

92. Veith, G., et al., *Spectroscopic Characterization of Solid Discharge Products in Li-Air Cells with Aprotic Carbonate Electrolytes.* Journal of Physical Chemistry C, 2011. **115**(29): p. 14325-14333.

93. Xu, W., et al., *Effects of Nonaqueous Electrolytes on the Performance of Lithium/Air Batteries.* Journal of the Electrochemical Society, 2010. **157**(2): p. A219-A224.

94. Mizuno, F., et al., *Rechargeable Li-Air Batteries with Carbonate-Based Liquid Electrolytes.* Electrochemistry, 2010. **78**(5): p. 403-405.

95. Xiao, J., et al., *Investigation of the rechargeability of Li-O-2 batteries in non-aqueous electrolyte.* Journal of Power Sources, 2011. **196**(13): p. 5674-5678.

96. Zhang, T. and H. Zhou, *From Li-O-2 to Li-Air Batteries: Carbon Nanotubes/Ionic Liquid Gels with a Tricontinuous Passage of Electrons, Ions, and Oxygen.* Angewandte Chemie-International Edition, 2012. **51**(44): p. 11062-11067.

97. Chamaani, A., et al., *Stabilizing effect of ion complex formation in lithium-oxygen battery electrolytes.* Journal of Electroanalytical Chemistry, 2018. **815**: p. 143-150.

98. Lu, Y., et al., *Lithium-oxygen batteries: bridging mechanistic understanding and battery performance.* Energy & Environmental Science, 2013. **6**(3): p. 750-768.

99. Gao, X., et al., *A rechargeable lithium-oxygen battery with dual mediators stabilizing the carbon cathode.* Nature Energy, 2017. **2**(9).

100. Lu, J., et al., *A lithium-oxygen battery based on lithium superoxide.* Nature, 2016. **529**(7586): p. 377-+.

101. Carter, E., A. Carley, and D. Murphy, *Evidence for O-2(-) radical stabilization at surface oxygen vacancies on polycrystalline TiO2.* Journal of Physical Chemistry C, 2007. **111**(28): p. 10630-10638.

102. STANLEY, J., *REACTIONS OF SUPEROXIDE WITH PEROXIDES.* Journal of Organic Chemistry, 1980. **45**(8): p. 1413-1418.

103. FRIMER, A. and I. ROSENTHAL, *CHEMICAL-REACTIONS OF SUPEROXIDE ANION RADICAL IN APROTIC-SOLVENTS.* Photochemistry and Photobiology, 1978. **28**(4-5): p. 711-719.

104. Laoire, C., et al., *Influence of Nonaqueous Solvents on the Electrochemistry of Oxygen in the Rechargeable Lithium-Air Battery.* Journal of Physical Chemistry C, 2010. **114**(19): p. 9178-9186.

105. Rogers, E., et al., *Investigating the Mechanism and Electrode Kinetics of the Oxygen vertical bar Superoxide (O-2 vertical bar O-2(center dot-)) Couple in Various Room-Temperature Ionic Liquids at Gold and Platinum Electrodes in the Temperature Range 298-318 K.* Journal of Physical Chemistry C, 2009. **113**(41): p. 17811-17823.

106. Islam, M. and T. Ohsaka, *Roles of ion pairing on electroreduction of dioxygen in imidazolium-cation-based room-temperature ionic liquid.* Journal of Physical Chemistry C, 2008. **112**(4): p. 1269-1275.

107. Barnes, A., et al., *Unusual voltammetry of the reduction of O-2 in [C(4)dmim][N(Tf)(2)] reveals a strong interaction of O-2(center dot-) with the [C(4)dmim](+) cation.* Journal of Physical Chemistry C, 2008. **112**(35): p. 13709-13715.

108. De Giorgio, F., F. Soavi, and M. Mastragostino, *Effect of lithium ions on oxygen reduction in ionic liquid-based electrolytes.* Electrochemistry Communications, 2011. **13**(10): p. 1090-1093.

109. Allen, C., et al., *Oxygen Electrode Rechargeability in an Ionic Liquid for the Li-Air Battery.* Journal of Physical Chemistry Letters, 2011. **2**(19): p. 2420-2424.

110. PEARSON, R., *HARD AND SOFT ACIDS AND BASES.* Chemistry in Britain, 1967. **3**(3): p. 103-&.

111. Zhang, T. and H. Zhou, *A reversible long-life lithium-air battery in ambient air.* Nature Communications, 2013. **4**.

112. McCloskey, B., et al., *Twin Problems of Interfacial Carbonate Formation in Nonaqueous Li-O-2 Batteries.* Journal of Physical Chemistry Letters, 2012. **3**(8): p. 997-1001.

113. Gallant, B., et al., *Chemical and Morphological Changes of Li-O-2 Battery Electrodes upon Cycling.* Journal of Physical Chemistry C, 2012. **116**(39): p. 20800-20805.

114. Mitchell, R., et al., *All-carbon-nanofiber electrodes for high-energy rechargeable Li-O-2 batteries.* Energy & Environmental Science, 2011. **4**(8): p. 2952-2958.

115. Aurbach, D., et al., *Advances in understanding mechanisms underpinning lithium-air batteries.* Nature Energy, 2016. **1**.

116. Adams, B., et al., *Current density dependence of peroxide formation in the Li-O-2 battery and its effect on charge.* Energy & Environmental Science, 2013. **6**(6): p. 1772-1778.

117. Horstmann, B., et al., *Rate-Dependent Morphology of Li2O2 Growth in Li-O-2 Batteries.* Journal of Physical Chemistry Letters, 2013. **4**(24): p. 4217-4222.

118. Aetukuri, N., et al., *Solvating additives drive solution-mediated electrochemistry and enhance toroid growth in non-aqueous Li-O-2 batteries.* Nature Chemistry, 2015. **7**(1): p. 50-56.

119. Johnson, L., et al., *The role of LiO2 solubility in O-2 reduction in aprotic solvents and its consequences for Li-O-2 batteries.* Nature Chemistry, 2014. **6**(12): p. 1091-1099.

120. Grande, L., et al., *The Lithium/Air Battery: Still an Emerging System or a Practical Reality?* Advanced Materials, 2015. **27**(5): p. 784-800.

121. Feng, N., P. He, and H. Zhou, *Critical Challenges in Rechargeable Aprotic Li-O-2 Batteries.* Advanced Energy Materials, 2016. **6**(9).

122. Assary, R., et al., *The Effect of Oxygen Crossover on the Anode of a Li-O2 Battery using an Ether-Based Solvent: Insights from Experimental and Computational Studies.* Chemsuschem, 2013. **6**(1): p. 51-55.

123. Younesi, R., et al., *The SEI layer formed on lithium metal in the presence of oxygen: A seldom considered component in the development of the Li-O-2 battery.* Journal of Power Sources, 2013. **225**: p. 40-45.

124. Shui, J., et al., *Reversibility of anodic lithium in rechargeable lithium-oxygen batteries.* Nature Communications, 2013. **4**.

125. Lee, H., et al., *Chemical aspect of oxygen dissolved in a dimethyl sulfoxide-based electrolyte on lithium metal.* Electrochimica Acta, 2014. **123**: p. 419-425.

126. Kim, B., et al., *A Moisture-and Oxygen-Impermeable Separator for Aprotic Li-O-2 Batteries.* Advanced Functional Materials, 2016. **26**(11): p. 1747-1756.

127. Liu, Q., et al., *Artificial Protection Film on Lithium Metal Anode toward Long-Cycle-Life Lithium-Oxygen Batteries (vol 27, pg 5241, 2015).* Advanced Materials, 2015. **27**(40): p. 6089-6089.

128. Hassoun, J., et al., *A Metal-Free, Lithium-Ion Oxygen Battery: A Step Forward to Safety in Lithium-Air Batteries.* Nano Letters, 2012. **12**(11): p. 5775-5779.

129. Hirshberg, D., et al., *Feasibility of Full (Li-Ion)-O-2 Cells Comprised of Hard Carbon Anodes.* Acs Applied Materials & Interfaces, 2017. **9**(5): p. 4352-4361.

130. Ye, L., et al., *Lithium-Air Batteries: Performance Interplays with Instability Factors.* Chemelectrochem, 2015. **2**(3): p. 312-323.

131. Thotiyl, M., et al., *The Carbon Electrode in Nonaqueous Li-O-2 Cells.* Journal of the American Chemical Society, 2013. **135**(1): p. 494-500.

132. Peng, Z., et al., *A Reversible and Higher-Rate Li-O-2 Battery.* Science, 2012. **337**(6094): p. 563-566.

133. Wu, B., et al., *Carbon-Free CoO Mesoporous Nanowire Array Cathode for High-Performance Aprotic Li-O-2 Batteries.* Acs Applied Materials & Interfaces, 2015. **7**(41): p. 23182-23189.

134. Thotiyl, M., et al., *A stable cathode for the aprotic Li-O-2 battery.* Nature Materials, 2013. **12**(11): p. 1049-1055.

135. Sharon, D., et al., *The importance of solvent selection in Li-O-2 cells.* Chemical Communications, 2017. **53**(22): p. 3269-3272.

136. Sharon, D., et al., *Mechanistic Role of Li+ Dissociation Level in Aprotic Li-O-2 Battery.* Acs Applied Materials & Interfaces, 2016. **8**(8): p. 5300-5307.

137. Yao, X., et al., *Why Do Lithium-Oxygen Batteries Fail: Parasitic Chemical Reactions and Their Synergistic Effect.* Angewandte Chemie-International Edition, 2016. **55**(38): p. 11344-11353.

138. Balaish, M., A. Kraytsberg, and Y. Ein-Eli, *A critical review on lithium-air battery electrolytes.* Physical Chemistry Chemical Physics, 2014. **16**(7): p. 2801-2822.

139. Jung, K., et al., *A quasi-solid-state rechargeable lithium-oxygen battery based on a gel polymer electrolyte with an ionic liquid.* Chemical Communications, 2014. **50**(41): p. 5458-5461.

140. Leng, L., et al., *A novel stability-enhanced lithium-oxygen battery with cellulose-based composite polymer gel as the electrolyte.* Electrochimica Acta, 2015. **176**: p. 1108-1115.

141. Yi, J., et al., *Novel Stable Gel Polymer Electrolyte: Toward a High Safety and Long Life Li-Air Battery.* Acs Applied Materials & Interfaces, 2015. **7**(42): p. 23798-23804.

142. McCloskey, B., et al., *Mechanistic insights for the development of Li-O-2 battery materials: addressing Li2O2 conductivity limitations and electrolyte and cathode instabilities.* Chemical Communications, 2015. **51**(64): p. 12701-12715.

143. Shao, Y., et al., *Making Li-Air Batteries Rechargeable: Material Challenges.* Advanced Functional Materials, 2013. **23**(8): p. 987-1004.

144. Chawla, N., et al., *Palladium-Filled Carbon Nanotubes Cathode for Improved Electrolyte Stability and Cyclability Performance of Li-O-2 Batteries.* Journal of the Electrochemical Society, 2017. **164**(1): p. A6303-A6307.

145. Xu, J., et al., *Tailoring deposition and morphology of discharge products towards high-rate and long-life lithium-oxygen batteries.* Nature Communications, 2013. **4**.

146. Liu, Q., et al., *Flexible lithium-oxygen battery based on a recoverable cathode.* Nature Communications, 2015. **6**.

147. Freunberger, S., et al., *The Lithium-Oxygen Battery with Ether-Based Electrolytes.* Angewandte Chemie-International Edition, 2011. **50**(37): p. 8609-8613.

148. Elia, G., et al., *Role of the Lithium Salt in the Performance of Lithium-Oxygen Batteries: A Comparative Study.* Chemelectrochem, 2014. **1**(1): p. 47-50.

149. Nishikami, Y., et al., *Oxygen-enriched electrolytes based on perfluorochemicals for high-capacity lithium-oxygen batteries.* Journal of Materials Chemistry a, 2015. **3**(20): p. 10845-10850.

150. Safa, M., et al., *Polymeric Ionic Liquid Gel Electrolyte for Room Temperature Lithium Battery Applications.* Electrochimica Acta, 2016. **213**: p. 587-593.

151. Zhu, Y., et al., *A Composite Gel Polymer Electrolyte with High Performance Based on Poly(Vinylidene Fluoride) and Polyborate for Lithium Ion Batteries.* Advanced Energy Materials, 2014. **4**(1).

152. Long, L., et al., *Polymer electrolytes for lithium polymer batteries.* Journal of Materials Chemistry a, 2016. **4**(26): p. 10038-10069.

153. Chai, J., et al., *A high-voltage poly(methylethyl alpha-cyanoacrylate) composite polymer electrolyte for 5 V lithium batteries.* Journal of Materials Chemistry a, 2016. **4**(14): p. 5191-5197.

154. Luo, W., et al., *A hybrid gel-solid-state polymer electrolyte for long-life lithium oxygen batteries.* Chemical Communications, 2015. **51**(39): p. 8269-8272.

155. Liu, T., et al., *Cable-Type Water-Survivable Flexible Li-O-2 Battery.* Small, 2016. **12**(23): p. 3101-3105.

156. Liu, Q., et al., *A Flexible and Wearable Lithium-Oxygen Battery with Record Energy Density achieved by the Interlaced Architecture inspired by Bamboo Slips.* Advanced Materials, 2016. **28**(38): p. 8413-8418.

157. Le, H., et al., *Composite Gel Polymer Electrolyte Based on Poly(vinylidene fluoride-hexafluoropropylene) (PVDF-HFP) with Modified Aluminum Doped Lithium Lanthanum Titanate (A-LLTO) for High-Performance Lithium Rechargeable Batteries.* Acs Applied Materials & Interfaces, 2016. **8**(32): p. 20710-20719.

158. Elia, G. and J. Hassoun, *A gel polymer membrane for lithium-ion oxygen battery.* Solid State Ionics, 2016. **287**: p. 22-27.

159. Croce, F., et al., *Role of the ceramic fillers in enhancing the transport properties of composite polymer electrolytes.* Electrochimica Acta, 2001. **46**(16): p. 2457-2461.

160. Ma, C., et al., *Cross-linked branching nanohybrid polymer electrolyte with monodispersed TiO2 nanoparticles for high performance lithium-ion batteries.* Journal of Power Sources, 2016. **317**: p. 103-111.

161. Zhou, D., et al., *SiO2 Hollow Nanosphere-Based Composite Solid Electrolyte for Lithium Metal Batteries to Suppress Lithium Dendrite Growth and Enhance Cycle Life.* Advanced Energy Materials, 2016. **6**(7).

162. Zhang, P., et al., *Enhanced electrochemical and mechanical properties of P(VDF-HFP)-based composite polymer electrolytes with SiO2 nanowires.* Journal of Membrane Science, 2011. **379**(1-2): p. 80-85.

163. Do, N., et al., *Influence of Fe2O3 Nanofiller Shape on the Conductivity and Thermal Properties of Solid Polymer Electrolytes: Nanorods versus Nanospheres.* Journal of Physical Chemistry C, 2012. **116**(40): p. 21216-21223.

164. Liu, W., et al., *Ionic Conductivity Enhancement of Polymer Electrolytes with Ceramic Nanowire Fillers.* Nano Letters, 2015. **15**(4): p. 2740-2745.

165. Wang, M., et al., *Improved performances of lithium-ion batteries with a separator based on inorganic fibers.* Journal of Materials Chemistry a, 2017. **5**(1): p. 311-318.

166. Pfaffenhuber, C., et al., *Soggy-sand effects in liquid composite electrolytes with mesoporous materials as fillers.* Journal of Materials Chemistry a, 2013. **1**(40): p. 12560-12567.

167. Yi, J., et al., *Interfacial construction of Li2O2 for a performance-improved polymer Li-O-2 battery.* Journal of Materials Chemistry a, 2016. **4**(7): p. 2403-2407.

168. Wang, S., et al., *Immobilization of Anions on Polymer Matrices for Gel Electrolytes with High Conductivity and Stability in Lithium Ion Batteries.* Acs Applied Materials & Interfaces, 2016. **8**(23): p. 14776-14787.

169. Chamaani, A., et al., *One-Dimensional Glass Micro-Fillers in Gel Polymer Electrolytes for Li-O-2 Battery Applications.* Electrochimica Acta, 2017. **235**: p. 56-63.

170. Wang, H., et al., *A Composite Polymer Electrolyte Protect Layer between Lithium and Water Stable Ceramics for Aqueous Lithium-Air Batteries.* Journal of the Electrochemical Society, 2013. **160**(4): p. A728-A733.

171. Gittleson, F., et al., *Raman Spectroscopy in Lithium-Oxygen Battery Systems.* Chemelectrochem, 2015. **2**(10): p. 1446-1457.

172. Mirzaeian, M. and P. Hall, *Characterizing capacity loss of lithium oxygen batteries by impedance spectroscopy.* Journal of Power Sources, 2010. **195**(19): p. 6817-6824.

173. Kichambare, P., et al., *Electrochemical performance of highly mesoporous nitrogen doped carbon cathode in lithium-oxygen batteries.* Journal of Power Sources, 2011. **196**(6): p. 3310-3316.

174. Bieker, G., M. Winter, and P. Bieker, *Electrochemical in situ investigations of SEI and dendrite formation on the lithium metal anode.* Physical Chemistry Chemical Physics, 2015. **17**(14): p. 8670-8679.

175. Miao, R., et al., *A new ether-based electrolyte for dendrite-free lithium-metal based rechargeable batteries.* Scientific Reports, 2016. **6**.

176. Lu, Y., et al., *Stable Cycling of Lithium Metal Batteries Using High Transference Number Electrolytes.* Advanced Energy Materials, 2015. **5**(9).

177. Kim, S., et al., *Mechanically compliant and lithium dendrite growth-suppressing composite polymer electrolytes for flexible lithium-ion batteries.* Journal of Materials Chemistry a, 2013. **1**(16): p. 4949-4955.

178. Schweikert, N., H. Hahn, and S. Indris, *Cycling behaviour of Li/Li4Ti5O12 cells studied by electrochemical impedance spectroscopy.* Physical Chemistry Chemical Physics, 2011. **13**(13): p. 6234-6240.

179. Kim, H., et al., *Enhanced Electrochemical Stability of Quasi-Solid-State Electrolyte Containing SiO2 Nanoparticles for Li-O-2 Battery Applications.* Acs Applied Materials & Interfaces, 2016. **8**(2): p. 1344-1350.

180. Knudsen, K., et al., *An Electrochemical Impedance Study of the Capacity Limitations in Na-O-2 Cells.* Journal of Physical Chemistry C, 2016. **120**(20): p. 10799-10805.

181. Bardenhagen, I., et al., *In situ investigation of pore clogging during discharge of a Li/O-2 battery by electrochemical impedance spectroscopy.* Journal of Power Sources, 2015. **278**: p. 255-264.

182. Yi, J. and H. Zhou, *A Unique Hybrid Quasi-Solid-State Electrolyte for Li-O-2 Batteries with Improved Cycle Life and Safety.* Chemsuschem, 2016. **9**(17): p. 2391-2396.

183. Huang, X., et al., *Carbon Nanotube-Encapsulated Noble Metal Nanoparticle Hybrid as a Cathode Material for Li-Oxygen Batteries.* Advanced Functional Materials, 2014. **24**(41): p. 6516-6523.

184. Shao, Y., et al., *Electrocatalysts for Nonaqueous Lithium-Air Batteries: Status, Challenges, and Perspective.* Acs Catalysis, 2012. **2**(5): p. 844-857.

185. Kundu, D., et al., *A Highly Active Low Voltage Redox Mediator for Enhanced Rechargeability of Lithium-Oxygen Batteries.* Acs Central Science, 2015. **1**(9): p. 510-515.

186. Arenas, L., et al., *The characteristics and performance of hybrid redox flow batteries with zinc negative electrodes for energy storage.* Renewable & Sustainable Energy Reviews, 2018. **90**: p. 992-1016.

187. Chamaani, A., et al., *Composite Gel Polymer Electrolyte for Improved Cyclability in Lithium-Oxygen Batteries.* Acs Applied Materials & Interfaces, 2017. **9**(39): p. 33819-33826.

188. Knudsen, K., et al., *An Electrochemical Impedance Spectroscopy Study on the Effects of the Surface- and Solution-Based Mechanisms in Li-O-2 Cells.* Journal of the Electrochemical Society, 2016. **163**(9): p. A2065-A2071.

189. Markus, I., G. Jones, and J. Garcia, *Investigation of Electrolyte Concentration Effects on the Performance of Lithium-Oxygen Batteries.* Journal of Physical Chemistry C, 2016. **120**(11): p. 5949-5957.

190. Jeong, S., et al., *Suppression of dendritic lithium formation by using concentrated electrolyte solutions.* Electrochemistry Communications, 2008. **10**(4): p. 635-638.

191. Rahner, D., *The role of anions, solvent molecules and solvated electrons in layer formation processes on anode materials for rechargeable lithium batteries.* Journal of Power Sources, 1999. **81**: p. 358-361.

192. Sagane, F., T. Abe, and Z. Ogumi, *Li+-Ion Transfer through the Interface between Li+-Ion Conductive Ceramic Electrolyte and Li+-Ion-Concentrated Propylene Carbonate Solution.* Journal of Physical Chemistry C, 2009. **113**(46): p. 20135-20138.

193. Giffin, G., et al., *Complex Nature of Ionic Coordination in Magnesium Ionic Liquid-Based Electrolytes: Solvates with Mobile Mg2+ Cations.* Journal of Physical Chemistry C, 2014. **118**(19): p. 9966-9973.

194. Suo, L., et al., *FT-Raman spectroscopy study of solvent-in-salt electrolytes.* Chinese Physics B, 2016. **25**(1).

195. Lassegues, J., et al., *Spectroscopic Identification of the Lithium Ion Transporting Species in LiTFSI-Doped Ionic Liquids.* Journal of Physical Chemistry a, 2009. **113**(1): p. 305-314.

196. Umebayashi, Y., et al., *Lithium ion solvation in room-temperature ionic liquids involving bis(trifluoromethanesulfonyl) imide anion studied by Raman Spectroscopy and DFT calculations.* Journal of Physical Chemistry B, 2007. **111**(45): p. 13028-13032.

197. Gunasekara, I., et al., *A Study of the Influence of Lithium Salt Anions on Oxygen Reduction Reactions in Li-Air Batteries.* Journal of the Electrochemical Society, 2015. **162**(6): p. A1055-A1066.

198. Xu, W., et al., *The stability of organic solvents and carbon electrode in nonaqueous Li-O-2 batteries.* Journal of Power Sources, 2012. **215**: p. 240-247.

199. Zhang, Z., et al., *Increased Stability Toward Oxygen Reduction Products for Lithium-Air Batteries with Oligoether-Functionalized Silane Electrolytes.* Journal of Physical Chemistry C, 2011. **115**(51): p. 25535-25542.

200. Liu, B., et al., *Enhanced Cycling Stability of Rechargeable Li-O-2 Batteries Using High-Concentration Electrolytes.* Advanced Functional Materials, 2016. **26**(4): p. 605-613.

201. Giordani, V., et al., *High Concentration Lithium Nitrate/Dimethylacetamide Electrolytes for Lithium/Oxygen Cells.* Journal of the Electrochemical Society, 2016. **163**(13): p. A2673-A2678.

202. Li, F., et al., *Enhanced Cycling Performance of Li-O2 Batteries by the Optimized Electrolyte Concentration of LiTFSA in Glymes.* Advanced Energy Materials, 2013. **3**(4): p. 532-538.

203. Huang, Q., et al., *Reversible chemical delithiation/lithiation of LiFePO4: towards a redox flow lithium-ion battery.* Physical Chemistry Chemical Physics, 2013. **15**(6): p. 1793-1797.

204. Pan, F., et al., *Redox Targeting of Anatase TiO2 for Redox Flow Lithium-Ion Batteries.* Advanced Energy Materials, 2014. **4**(15).

205. Jennings, J., Q. Huang, and Q. Wang, *Kinetics of LixFePO4 Lithiation/Delithiation by Ferrocene-Based Redox Mediators: An Electrochemical Approach.* Journal of Physical Chemistry C, 2015. **119**(31): p. 17522-17528.

206. Jia, C., et al., *High-energy density nonaqueous all redox flow lithium battery enabled with a polymeric membrane.* Science Advances, 2015. **1**(10).

207. Visco, S., et al., *Aqueous and nonaqueous lithium-air batteries enabled by water-stable lithium metal electrodes.* Journal of Solid State Electrochemistry, 2014. **18**(5): p. 1443-1456.

208. Kuboki, T., et al., *Lithium-air batteries using hydrophobic room temperature ionic liquid electrolyte.* Journal of Power Sources, 2005. **146**(1-2): p. 766-769.

209. Scrosati, B. and J. Garche, *Lithium batteries: Status, prospects and future.* Journal of Power Sources, 2010. **195**(9): p. 2419-2430.

210. Safa, M., et al., *Capacity Fading Mechanism in Lithium-Sulfur Battery using Poly(ionic liquid) Gel Electrolyte.* Electrochimica Acta, 2017. **258**: p. 1284-1292.

211. Chawla, N., *Recent advances in non-flammable electrolytes for safer lithium-ion batteries*, N. Bharti, Editor. 2019, Batteries.

212. Chawla, N., *Nanocatalysts in lithium oxygen batteries*. 2018, *Nano Science Nano Technology. An Indian Journal*

213. Chawla, N., *Mechanism of Ionic Impedance Growth for Palladium-Containing CNT Electrodes in Lithium-Oxygen Battery Electrodes and its Contribution to Battery Failure*, A. Chamaani, Editor. 2019, Batteries. p. 15.

214. Lau, K., et al., *Electronic Structure of Lithium Peroxide Clusters and Relevance to Lithium-Air Batteries.* Journal of Physical Chemistry C, 2012. **116**(45): p. 23890-23896.

215. Bruce, P., et al., *Li-O-2 and Li-S batteries with high energy storage.* Nature Materials, 2012. **11**(1): p. 19-29.

216. Gallagher, K., et al., *Quantifying the promise of lithium-air batteries for electric vehicles.* Energy & Environmental Science, 2014. **7**(5): p. 1555-1563.

217. Kumar, B., et al., *A Solid-State, Rechargeable, Long Cycle Life Lithium-Air Battery.* Journal of the Electrochemical Society, 2010. **157**(1): p. A50-A54.

218. Schiraldi, D., *Perfluorinated polymer electrolyte membrane durability.* Polymer Reviews, 2006. **46**(3): p. 315-327.

219. Weng, G., et al., *Unlocking the capacity of iodide for high-energy-density zinc/polyiodide and lithium/polyiodide redox flow batteries.* Energy & Environmental Science, 2017. **10**(3): p. 735-741.

220. Zhao, Y., L. Wang, and H. Byon, *High-performance rechargeable lithium-iodine batteries using triiodide/iodide redox couples in an aqueous cathode.* Nature Communications, 2013. **4**.

221. Chen, H., Y. Zhou, and Y. Lu, *Lithium Organic Nanocomposite Suspension for High-Energy-Density Redox Flow Batteries.* Acs Energy Letters, 2018. **3**(8): p. 1991-1997.

222. Li, Z., et al., *A high-energy and low-cost polysulfide/iodide redox flow battery.* Nano Energy, 2016. **30**: p. 283-292.

223. Chen, H., et al., *Sulphur-impregnated flow cathode to enable high-energy-density lithium flow batteries.* Nature Communications, 2015. **6**.

224. Weng, G., et al., *Investigations of High Voltage Vanadium-Metal Hydride Flow Battery toward kWh Scale Storage with 100 cm(2) Electrodes.* Journal of the Electrochemical Society, 2016. **163**(1): p. A5180-A5187.

225. Greatbatch, W., et al., *The solid-state lithium battery: a new improved chemical power source for implantable cardiac pacemakers*. 1971, IEEE Transactions of Biomedical Engineering. p. 317-324.

226. Izutsu, K., *Electrochemistry in nonaqueous solutions*. 2 ed. 2009: John Wiley & Sons. 432.

227. Reichardt, C., *Solvents and solvent effects: An introduction.* Organic Process Research & Development, 2007. **11**(1): p. 105-113.

228. Bockris, J.O.M., *Modern electrochemistry 2B: electronics in chemistry, engineering, biology and environmental science*, A.K. Reddy, Editor. 2000, Springer Science & Business Media.

229. Han, S., et al., *Electrolyte Solvation and Ionic Association V. Acetonitrile-Lithium Bis(fluorosulfonyl)imide (LiFSI) Mixtures.* Journal of the Electrochemical Society, 2014. **161**(14): p. A2042-A2053.

230. Bard, A.J., *Fundamentals and applications*, L.R. Faulkner, Editor. 2001, Electrochemical Methods. p. 580-632.

231. Huang, Q., et al., *A redox flow lithium battery based on the redox targeting reactions between LiFePO4 and iodide.* Energy & Environmental Science, 2016. **9**(3): p. 917-921.

232. Liang, Z. and Y. Lu, *Critical Role of Redox Mediator in Suppressing Charging Instabilities of Lithium-Oxygen Batteries.* Journal of the American Chemical Society, 2016. **138**(24): p. 7574-7583.

233. Kuss, C., et al., *Kinetics of Heterosite Iron Phosphate Lithiation by Chemical Reduction.* Journal of Physical Chemistry C, 2014. **118**(34): p. 19524-19528.

234. Bryantsev, V., et al., *Predicting Solvent Stability in Aprotic Electrolyte Li-Air Batteries: Nucleophilic Substitution by the Superoxide Anion Radical (O-2(center dot-)).* Journal of Physical Chemistry a, 2011. **115**(44): p. 12399-12409.

235. Bryantsev, V. and F. Faglioni, *Predicting Autoxidation Stability of Ether- and Amide-Based Electrolyte Solvents for Li-Air Batteries.* Journal of Physical Chemistry a, 2012. **116**(26): p. 7128-7138.

236. Bryantsev, V., *Predicting the stability of aprotic solvents in Li-air batteries: pK(a) calculations of aliphatic C-H acids in dimethyl sulfoxide.* Chemical Physics Letters, 2013. **558**: p. 42-47.

237. Yu, M., et al., *Integrating a redox-coupled dye-sensitized photoelectrode into a lithium-oxygen battery for photoassisted charging.* Nature Communications, 2014. **5**.

238. Wu, F., et al., *Lithium Iodide as a Promising Electrolyte Additive for Lithium-Sulfur Batteries: Mechanisms of Performance Enhancement.* Advanced Materials, 2015. **27**(1): p. 101-108.

239. Cecchetto, L., et al., *Study of a Li–air battery having an electrolyte solution formed by a mixture of an ether-based aprotic solvent and an ionic liquid*. 2012, Journal of Power Sources. p. 233-238.

240. Hojberg, J., et al., *Reactions and SEI Formation during Charging of Li-O-2 Cells.* Ecs Electrochemistry Letters, 2015. **4**(7): p. A63-A66.

241. Zhai, D., et al., *Raman Evidence for Late Stage Disproportionation in a Li-O-2 Battery.* Journal of Physical Chemistry Letters, 2014. **5**(15): p. 2705-2710.

242. Crane, N., et al., *Raman spectroscopic evidence for octacalcium phosphate and other transient mineral species deposited during intramembranous mineralization.* Bone, 2006. **39**(3): p. 434-442.

243. Zhang, Y., et al., *High-Performance Lithium-Air Battery with a Coaxial-Fiber Architecture.* Angewandte Chemie-International Edition, 2016. **55**(14): p. 4487-4491.

244. Lim, H., et al., *Superior Rechargeability and Efficiency of Lithium-Oxygen Batteries: Hierarchical Air Electrode Architecture Combined with a Soluble Catalyst.* Angewandte Chemie-International Edition, 2014. **53**(15): p. 3926-3931.

245. Gittleson, F., W. Ryu, and A. Taylor, *Operando Observation of the Gold-Electrolyte Interface in Li-O-2 Batteries.* Acs Applied Materials & Interfaces, 2014. **6**(21): p. 19017-19025.

246. Ryu, W., et al., *A New Design Strategy for Observing Lithium Oxide Growth-Evolution Interactions Using Geometric Catalyst Positioning.* Nano Letters, 2016. **16**(8): p. 4799-4806.

247. Yang, J., et al., *Evidence for lithium superoxide-like species in the discharge product of a Li-O-2 battery.* Physical Chemistry Chemical Physics, 2013. **15**(11): p. 3764-3771.

248. Zhai, D., et al., *Disproportionation in Li-O-2 Batteries Based on a Large Surface Area Carbon Cathode.* Journal of the American Chemical Society, 2013. **135**(41): p. 15364-15372.

249. Olivares-Marin, M., et al., *Spatial Distributions of Discharged Products of Lithium-Oxygen Batteries Revealed by Synchrotron X-ray Transmission Microscopy.* Nano Letters, 2015. **15**(10): p. 6932-6938.

250. Schaltin, S., et al., *A QCM study of ORR-OER and an in situ study of a redox mediator in DMSO for Li-O-2 batteries.* Physical Chemistry Chemical Physics, 2015. **17**(19): p. 12575-12586.

251. Adams, B., et al., *Towards a Stable Organic Electrolyte for the Lithium Oxygen Battery.* Advanced Energy Materials, 2015. **5**(1).

252. Yue, L., et al., *All solid-state polymer electrolytes for high-performance lithium ion batteries.* 2016(5): p. 139-164.

253. Lin, Y., et al., *A wider temperature range polymer electrolyte for all-solid-state lithium ion batteries.* Rsc Advances, 2013. **3**(27): p. 10722-10730.

254. Gittleson, F., et al., *Oxygen solubility and transport in Li-air battery electrolytes: establishing criteria and strategies for electrolyte design.* Energy & Environmental Science, 2017. **10**(5): p. 1167-1179.

255. Porcarelli, L., et al., *Super Soft All-Ethylene Oxide Polymer Electrolyte for Safe All-Solid Lithium Batteries.* Scientific Reports, 2016. **6**.

256. Bhattacharyya, A. and J. Maier, *Second phase effects on the conductivity of non-aqueous salt solutions: "Soggy sand electrolytes".* Advanced Materials, 2004. **16**(9-10): p. 811-+.

257. Osinska, M., et al., *Study of the role of ceramic filler in composite gel electrolytes based on microporous polymer membranes.* Journal of Membrane Science, 2009. **326**(2): p. 582-588.

258. Bhattacharyya, A., et al., *New class of soft matter electrolytes obtained via heterogeneous doping: Percolation effects in "soggy sand" electrolytes.* Solid State Ionics, 2006. **177**(26-32): p. 2565-2568.

259. Liao, Y., et al., *Improvement in ionic conductivity of self-supported P(MMA-AN-VAc) gel electrolyte by fumed silica for lithium ion batteries.* Electrochimica Acta, 2009. **54**(26): p. 6396-6402.

260. Gentili, V., et al., *Composite gel-type polymer electrolytes for advanced, rechargeable lithium batteries.* Journal of Power Sources, 2007. **170**(1): p. 185-190.

261. Srivastava, S., et al., *25th Anniversary Article: Polymer-Particle Composites: Phase Stability and Applications in Electrochemical Energy Storage.* Advanced Materials, 2014. **26**(2): p. 201-233.

262. Bhattacharyya, A., *Ion Transport in Liquid Salt Solutions with Oxide Dispersions: "Soggy Sand" Electrolytes.* Journal of Physical Chemistry Letters, 2012. **3**(6): p. 744-750.

263. Chawla, N. and M. Safa, *Sodium Batteries: A Review on Sodium-Sulfur and Sodium-Air Batteries.* Electronics, 2019. **8**(10).

264. Kundu, D., et al., *A highly active nanostructured metallic oxide cathode for aprotic Li-O-2 batteries.* Energy & Environmental Science, 2015. **8**(4): p. 1292-1298.

265. Eswaran, M., N. Munichandraiah, and L. Scanlon, *High Capacity Li-O-2 Cell and Electrochemical Impedance Spectroscopy Study.* Electrochemical and Solid State Letters, 2010. **13**(9): p. A121-A124.

266. Nanda, J., et al., *Anomalous Discharge Product Distribution in Lithium-Air Cathodes.* Journal of Physical Chemistry C, 2012. **116**(15): p. 8401-8408.

267. Takechi, K., T. Shiga, and T. Asaoka, *A Li-O-2/CO2 battery.* Chemical Communications, 2011. **47**(12): p. 3463-3465.

268. Takechi, K., et al., *Li-air flow battery for accelerated separation of O2 reduction reaction and discharge product storage.* Abstracts of Papers of the American Chemical Society, 2016. **252**.

269. Ogasawara, T., et al., *Rechargeable Li2O2 electrode for lithium batteries.* Journal of the American Chemical Society, 2006. **128**(4): p. 1390-1393.

270. McCloskey, B., et al., *On the Efficacy of Electrocatalysis in Nonaqueous Li-O-2 Batteries.* Journal of the American Chemical Society, 2011. **133**(45): p. 18038-18041.

271. Qi, Y., et al., *Investigation on FT-IR spectra and dielectric property of PVDF/inorganic composites.* Journal of Materials Science-Materials in Electronics, 2013. **24**(5): p. 1446-1450.

272. Singh, P., et al., *Ferroelectric polymer-ceramic composite thick films for energy storage applications.* Aip Advances, 2014. **4**(8).

273. Maurin, G., et al., *Electrochemical lithium intercalation into multiwall carbon nanotubes: a micro-Raman study.* Solid State Ionics, 2000. **136**: p. 1295-1299.

274. Maurin, G., et al., *Lithium doping of multiwalled carbon nanotubes produced by catalytic decomposition.* Nano Letters, 2001. **1**(2): p. 75-79.

275. Xiong, Z., Y. Yun, and H. Jin, *Applications of Carbon Nanotubes for Lithium Ion Battery Anodes.* Materials, 2013. **6**(3): p. 1138-1158.

276. Yang, X., P. He, and Y. Xia, *Preparation of mesocellular carbon foam and its application for lithium/oxygen battery.* Electrochemistry Communications, 2009. **11**(6): p. 1127-1130.

277. Seman, R., M. Azam, and A. Mohamad, *Systematic gap analysis of carbon nanotube-based lithium-ion batteries and electrochemical capacitors.* Renewable & Sustainable Energy Reviews, 2017. **75**: p. 644-659.

278. Liu, H., et al., *Porous Carbon Composites for Next Generation Rechargeable Lithium Batteries.* Advanced Energy Materials, 2017. **7**(24).

279. Zhang, Y., et al., *An Ultra-flexible Silicon–Oxygen Battery Fiber with High Energy Density*. 2017, Angewandte Chemie International Edition. p. 13741-13746.

280. Safa, M., et al., *Poly(Ionic Liquid)-Based Composite Gel Electrolyte for Lithium Batteries.* Chemelectrochem, 2019. **6**(13): p. 3319-3326.

281. Maurin, G., et al., *Electrochemical intercalation of lithium into multiwall carbon nanotubes.* Chemical Physics Letters, 1999. **312**(1): p. 14-18.

282. Bulusheva, L., et al., *Electrochemical properties of nitrogen-doped carbon nanotube anode in Li-ion batteries.* Carbon, 2011. **49**(12): p. 4013-4023.

283. Chen, S., et al., *Chemical-free synthesis of graphene-carbon nanotube hybrid materials for reversible lithium storage in lithium-ion batteries.* Carbon, 2012. **50**(12): p. 4557-4565.

284. Landi, B., et al., *Carbon nanotubes for lithium ion batteries.* Energy & Environmental Science, 2009. **2**(6): p. 638-654.

285. Byon, H., et al., *Role of Oxygen Functional Groups in Carbon Nanotube/Graphene Freestanding Electrodes for High Performance Lithium Batteries.* Advanced Functional Materials, 2013. **23**(8): p. 1037-1045.

286. Avery, A., et al., *Tailored semiconducting carbon nanotube networks with enhanced thermoelectric properties.* Nature Energy, 2016. **1**.

287. Yin, J., et al., *Synergy Between Metal Oxide Nanofibers and Graphene Nanoribbons for Rechargeable Lithium-Oxygen Battery Cathodes.* Advanced Energy Materials, 2015. **5**(4).

288. Thomas, M. and B. Corry, *A computational assessment of the permeability and salt rejection of carbon nanotube membranes and their application to water desalination.* Philosophical Transactions of the Royal Society a-Mathematical Physical and Engineering Sciences, 2016. **374**(2060).

289. Pascal, T., W. Goddard, and Y. Jung, *Entropy and the driving force for the filling of carbon nanotubes with water.* Proceedings of the National Academy of Sciences of the United States of America, 2011. **108**(29): p. 11794-11798.

290. Fornasiero, F., et al., *pH-Tunable Ion Selectivity in Carbon Nanotube Pores.* Langmuir, 2010. **26**(18): p. 14848-14853.

291. Li, B., et al., *Ambipolar zinc-polyiodide electrolyte for a high-energy density aqueous redox flow battery.* Nature Communications, 2015. **6**.

292. Chew, S., et al., *Flexible free-standing carbon nanotube films for model lithium-ion batteries.* Carbon, 2009. **47**(13): p. 2976-2983.

293. Claye, A., et al., *Solid-state electrochemistry of the Li single wall carbon nanotube system.* Journal of the Electrochemical Society, 2000. **147**(8): p. 2845-2852.

294. Zang, J. and Y. Zhao, *Silicon nanowire reinforced by single-walled carbon nanotube and its applications to anti-pulverization electrode in lithium ion battery.* Composites Part B-Engineering, 2012. **43**(1): p. 76-82.

295. Jiang, K., et al., *Superaligned Carbon Nanotube Arrays, Films, and Yarns: A Road to Applications.* Advanced Materials, 2011. **23**(9): p. 1154-1161.

296. Yamabe, T., K. Fukui, and K. Tanaka, *The Science and Technology of Carbon Nanotubes*, ed. K. Tanaka and S. Iijima. 1999: Elsevier. 750.

297. Peigney, A., et al., *Specific surface area of carbon nanotubes and bundles of carbon nanotubes.* Carbon, 2001. **39**(4): p. 507-514.

298. Cheng, X., et al., *Robust growth of herringbone carbon nanofibers on layered double hydroxide derived catalysts and their applications as anodes for Li-ion batteries.* Carbon, 2013. **62**: p. 393-404.

299. Moyseowicz, A., A. Sliwak, and G. Gryglewicz, *Influence of structural and textural parameters of carbon nanofibers on their capacitive behavior.* Journal of Materials Science, 2016. **51**(7): p. 3431-3439.

300. Wang, H., et al., *Electrochemical durability investigation of single-walled and multi-walled carbon nanotubes under potentiostatic conditions.* Journal of Power Sources, 2008. **176**(1): p. 128-131.

301. Wang, J., et al., *Effect of carbon black support corrosion on the durability of Pt/C catalyst.* Journal of Power Sources, 2007. **171**(2): p. 331-339.

302. Lu, X., et al., *Scanning electron microscopy study of carbon nanotubes heated at high temperatures in air.* Journal of Applied Physics, 1999. **86**(1): p. 186-189.

303. Bouhaouss, A., et al., *Effect of chemical treatments on the ionic conductivity of carbonate apatite.* International Journal of Inorganic Materials, 2001. **3**(6): p. 437-441.

APPENDICES

7.1 Solution Preparations

1) 1M Electrolyte Solution Materials: lithium bis(trifluoromethanesulfonyl)imide (LiTFSI, MW=287.8 g) salt, tetraethylene glycol dimethyl ether (TEGDME) solvent

Measurements (1 ml): LiTFSI (.287 g) + TEGDME (1 mL) ~ Ratio: 80% LiTFSI and 20% TEGDME

2) Polymer Solution Materials: Ethoxylated trimethylolpropane triacrylate (ETPTA, MW= 428 Dal) monomer, 2-hydroxy-2-methyl-1-phenyl-1-propanon (HMPP, photo-initiator to be cured with λ=365 nm)

Measurements: ETPTA (2 g) + HMPP (.02 g) ~ Ratio: 99% ETPTA and 1% HMPP

3) PDMS Template Solution Materials: Sylgard 184 Monomer Base, Sylgard 184 Curing Agent

Measurements (0.25 g): Sylgard 184 Base (10 g) + Sylgard 184 Curing Agent (1 g)

*Spread uniformly over a glass slide then cure on a hot plate. Peel PDMS template off, then puncture 0.5" holes, and reconfigure evenly back onto glass slide to make GPE/cGPE polymerization mold templates.

PDMS Template Calculation:

$V_{GLASS} = (X * Y)_{GLASS} * Z_{PDMS}$ (thickness) $\quad$ $Density_{PDMS}$ (P) $= M_{PDMS} * V_{GLASS}$

Figure 40. Illustration of a PDMS template used for GPE/cGPE disc polymerization.

4) 1M GPE Solution Materials: lithium bis(trifluoromethanesulfonyl)imide (LiTFSI) salt, tetraethylene glycol dimethyl ether (TEGDME) solvent, Ethoxylated trimethylolpropane triacrylate (ETPTA, MW= 428 Dal) monomer, 2-hydroxy-2-methyl-1-phenyl-1-propanon (HMPP, photo-initiator to be cured with λ= 365 nm)

Measurements (1 g): 1M Electrolyte (.8 g) + Polymer (.2 g)

5) 1M cGPE-1% Solution Materials: lithium bis(trifluoromethanesulfonyl)imide (LiTFSI) salt, tetraethylene glycol dimethyl ether (TEGDME) solvent, Ethoxylated trimethylolpropane triacrylate (ETPTA, MW= 428 Dal) monomer, 2-hydroxy-2-methyl-1-phenyl-1-propanon (HMPP, photo-initiator to be cured with λ=365 nm), glass fibers

Measurements (1 g):

Glass (.01 g) + 1M GPE Solution [Electrolyte (.8 g) + Polymer (.2 g)]

*Cure both GPE/cGPE templates under UV light in an Argon-filled glove box for 10 minutes. Keep a magnetic spinner twisting in solution at all times in between use (or solution may polymerize due to glovebox atmospheric changes i.e. poor vacuuming, temperature changes, chemical contact, etc.)

a) 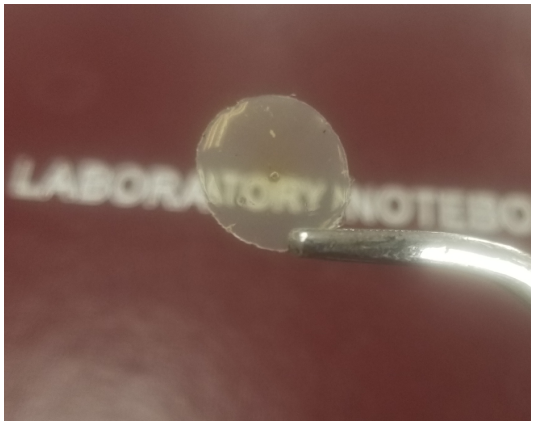 b) 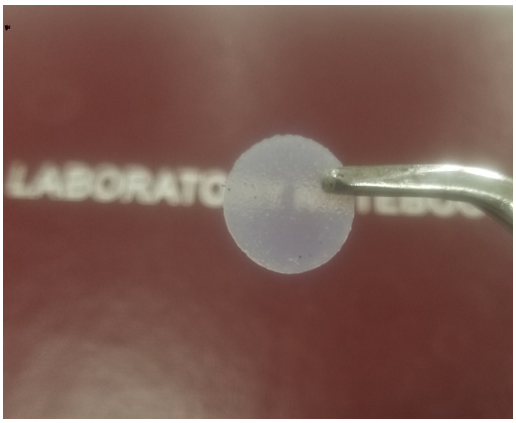

Figure 41. Illustrations of pristine a) 1M GPE and b) 1M cGPE-1% disks. A clear difference in visibility can be seen in the cGPE-1% due to the glass fibers.

6) 0.05M LiI Redox Mediator Materials: Lithium Iodide (LiI) powder, tetraethylene glycol dimethyl ether (TEGDME) solvent

Measurements (1 mL): LiI powder (6.692 mg) + TEGDME (1 mL)

N= m*V, m= # of mol_{WANTED}/L V= # of L_{WANTED} N= # of mol_{NEEDED}

$$N\ x\ \frac{molecular\ weight}{mol} = grams$$

.05M LiI → MW= 133.84 g, V= 1mL= .001 L →N= mV= .00005 mol. Put into equation:

N x (MW/ mol) = .00005 mol x (133.84 /mol) = .006692 g LiI= 6.692 mg LiI

7) Carbon Nanotube (CNT) Solution Materials: Carbon cloth, CNT fillers, N-methylpyrrolidine (NMP) solvent and polyvinylidene fluoride (PVDF) polymer

Measurements (6mL): 90% CNT (1 g) + 10% PVDF (.1 g) + 6 mL NMP

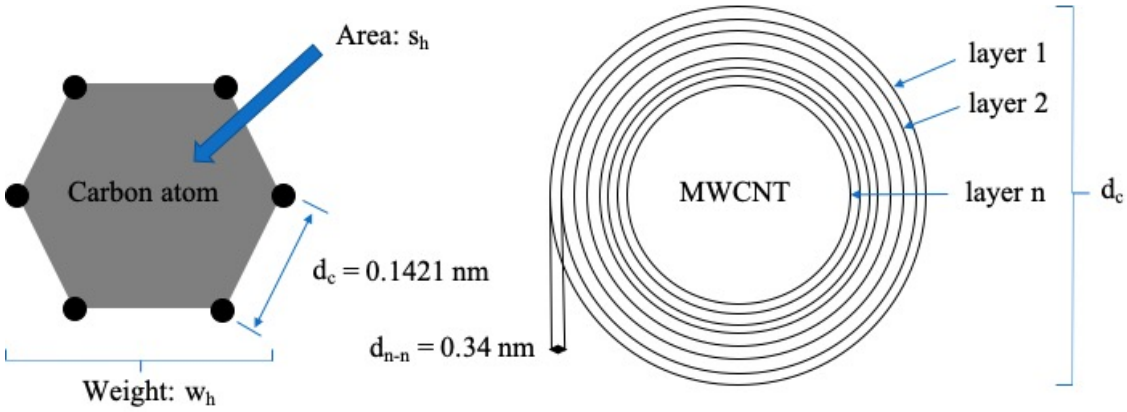

Figure 42. Schematic arrangement of carbon within graphene layers [297].

The CNT surface area calculations are based on the following hypotheses: (i) all CNTs are closed (only the external surface of each CNT is considered) (ii) the length of the C-C bonds in the curved graphene sheets is the same as in the planar sheet i.e. $d_{c\text{-}c} = 0.1421$ nm, (iii) the MWCNTs are composed of concentric layers with a wall-distance of $d_{n\text{-}n} = 0.34$ nm, (iv) the aspect ratio of CNTs is sufficiently high (0.1) to neglect the area of the tip surfaces in comparison to the area of the cylindrical surfaces [297].

$$\text{SWCNT}_{SA} = \frac{s_h}{w_h} = \frac{3d_{c-c}^2\frac{\sqrt{3}}{2}}{2\frac{Mc}{\mathcal{N}}} = \frac{5.246\ x\ 10^{-20} m^2}{3.988\ x\ 10^{-23} g} = 1315\ \frac{m^2}{g}$$

s_h corresponds to two carbon atoms whose weight, w_h, takes into account the atomic weight of carbon (M_c = 12.01 g / mol) and the Avogadro number ($\mathcal{N}$ = 6.0233 x 10^{23}/mol) for one side of a graphene sheet. For MWCNT, external diameter is d_c, length is L, and number of layers is n. SA is an acronym for surface area [297].

$$\text{MWCNT}_{SA} = \frac{s_{MW}}{w_{MW}} = \frac{\pi L d_c}{\left(\frac{1}{SWCNT_{SA}}\right) x \left(\pi L\left[nd_c - 2d_{n-n}\sum_{i-1}^{n-1} i\right]\right)} = \frac{1315 d_c}{nd_c - 0.68\left[\sum_{i-1}^{n-1} i\right]}$$

7.2 Experimental Methodology

1. Deconstruct and clean the Swagelok cell using soap, water and electrolysis.
2. Dry components (capsule, spring, stainless steel mesh, steel rod) on hot plate.
3. Use 2400-4000 p sandpaper to clean the steel rod and Swagelok spring surfaces, then press the springs into their respective capsules using the steel rod and tighten to construct Swagelok ½ cell.
4. Pour PDMS solution onto glass slide, spread solution to make a thin, even coating then cure on a hot plate.
5. Peel the PDMS template off and puncture 0.5” holes into template.
6. Clean and dry/wipe the hole puncher.
7. Reconfigure the punctured template onto the glass slide.
8. Cut out a section of Carbon cloth and puncture 0.5” holes in the section.
9. Clean and dry/wipe the hole puncher.
10. Weigh the Carbon cloth on a digital scale and record data.

11. Dip the Carbon cloth punctures into the CNT solution, remove any drippage, and cure in the vacuum oven at 225 °F until dry.
12. Weigh the Carbon cloth (now with CNT loading, Carbon cathode) on a digital scale and subtract Carbon cloth weight to determine CNT loading weight.
13. Place constructed Swagelok ½ cells, 0.5" punctured PDMS templates (on glass slide), Carbon cathodes, and stainless-steel mesh into "evacuation/release" chamber of Argon-filled glove box.
14. Slowly pull lever towards Evacuate for 30 seconds, then release for 30 seconds to minimize outside atmosphere content in glove box. Perform at least 3 times for best results.
15. Place all materials in chamber into the glove box and prepare for GPE/cGPE disk creation.
16. Shake and swirl the GPE/cGPE solution mix to ensure proper mixing
17. Use a pipette to extract GPE/cGPE solution and place 1-2 drops into each 0.5" puncture of the PDMS template slide and spread until the punctures are evenly coated.
18. Once the GPE/cGPE solutions are spread in the desired number of punctures, turn off the main glove box light and use UV light for 10 minutes to polymerize the GPE/cGPE disks.
19. Once the timer is complete, turn off the UV light, turn on the main glove box light, and peel off the PDMS template leaving only the 0.5" GPE/cGPE disks on the slides.
20. Take Lithium foil out of its sealed container and unravel the Lithium foil as needed.

21. Puncture 0.5” holes into the Lithium foil and gently press (using a steel rod with a cleansed sheet over end) the 0.5” Lithium foil disk into the Swagelok ½ cell.
22. Use a razor to peel off a GPE/cGPE disk from the glass slide.
23. Dip/soak the 0.5” GPE/cGPE disk into the 1M LiTFSI-TEGDME electrolyte, then align evenly and gently press the GPE/cGPE disk into the Swagelok ½ cell.
24. Use a razor to peel off a Carbon cathode from the glass slide.
25. Evenly align and gently press the Carbon cathode into the Swagelok ½ cell.
26. At this point, use a micro pipette to evenly soak cathode with 20 uL 1M LiTFSI-TEGDME electrolyte OR 30 uL 0.05 M LiI redox mediator (most optimized concentrations and volumes pertaining to our experimentation).
27. Align and gently press a stainless-steel mesh onto the cathode to act as a current collector for the Swagelok cell.
28. Seal and tighten the Swagelok cell ½ components to make 1 cell, then tighten metal bands at the anode and cathode ends of the Swagelok cell for banana clip gripping.
29. Repeat steps (20-28) for the desired amount of Swagelok cells.
30. Allow to rest straight up (for stabilization) overnight at least 10 hours before measuring OCV and performing CV, CCD, EIS, Raman and SEM analyses.

7.3 Battery History

Date-Inventor	Significance
1748- Benjamin Franklin	The term "battery" was used to describe an array of charged glass plates.
1780s- Luigi Galvani	First electric based demonstration of nerve impulses.
1800- Alessandro Volta	Voltaic Pile was considered the first wet cell battery constructed of alternating discs of zinc and copper with soaked cardboard in between creating the first practical method of generating electricity.
1836- John F. Daniell	The Daniell Cell produced ~ 1.1 V using a dual electrolyte system consisting of copper sulfate and zinc sulfate.
1839- William Robert Grove	Created the first ever electrical fuel cell by using hydrogen and oxygen.
1859- Gaston Plante	First practical, rechargeable storage lead-acid battery (commonly used in cars) is invented.
1866- Georges Leclanche	The Leclanche cell created the first dry-cell battery by sealing its packaging and substituting the electrolyte with ammonium chloride.
1881- J.A. Thiebaut	First battery with both the negative electrode and porous pot placed in a zinc cup was patented.
1881- Carl Gassner	Invention of the first commercially practical dry-cell battery constructed using zinc and carbon.
1899- Waldemar Jungner	The first nickel-cadmium rechargeable battery was invented.
1901- Thomas Alva Edison	The alkaline storage battery was invented.

1949- Lew Urry	Development of an alkaline battery with a 5x-8x performance upgrade than zinc-carbon cells.
1954- Gerald Pearson, Calvin Fuller and Daryl Chapin	The first solar battery was developed allowing the sun's energy to be converted to electricity.
1964- Samuel Ruben and Phillip Mallory	Duracell was incorporated.
1973- Adam Heller	Invention of the lithium thionyl chloride battery capable of high energy densities, temperature endurance and shelf life, necessary for medical devices and defense systems.
1977- Samar Basu (University of Pennsylvania)	Demonstrated the forward electrochemical reaction of lithium and graphite leading to a workable electrode (LiC_6), providing an alternative to the lithium metal electrode battery.
1979- Stanford University and Oxford University	Invention of a 4V rechargeable lithium-lithium cobalt oxide ($LiCoO_2$) cell capable of making Li batteries commercial.
1980- Rachid Yazami	Demonstrated the reverse electrochemical mechanism of a lithium-graphite electrode, leading to the most commercial lithium-ion graphite electrode as of 2011.
1985- Akira Yoshino	A prototype cell using a pro-Li ion carbon electrode and lithium cobalt oxide ($LiCoO_2$) electrode was developed allowing for the first air stable and safe, industrial scale cell production creating the birth of lithium-ion batteries.

Table 11. Timeline of batteries from 1740s to 1980s [5-23].

7.4 Characteristic Tables

Lithium bis(trifluoromethanesulfonyl)imide (LiTFSI salt)
High Battery Performance
High Chemical and Thermal Stability
Low Cost to Lifetime
High Solubility in TEGDME

Tetraethylene glycol dimethyl ether (TEGDME solvent)
Low DN (Base) following the Li_2O_2 Surface Phase Mechanism
Low Discharge Capacity
Good Cyclability
Most Stable with LiTFSI (High DN Salt)

Trimethylolpropane ethoxylate triacrylate (ETPTA polymer)
Electrochemical Stability in the Voltage Range of 2.0-4.5 V
High Mechanical Properties (Flexible, Anode Protection)
Electrolyte Insulating Properties
Compatible with Li-O_2 battery components

Table 12. Characteristic tables of GPE components used in this study.

Glass Microfibers (cGPE fillers- electrolyte)
Maintains Thin, Flexible structure of GPE
Thermally, Chemically and Mechanically Stable
Good Li-ion Conductor and Electronic Insulator
Chemically Compatible with Electrodes
High Oxygen Solubility
Minimizes Charge Accumulation and Concentration Polarization
Conductive Composites Improve Ionic Transport

Carbon Nanotubes (CNT fillers- cathode)
High Specific Surface Area
Good Chemical Stability
High Electrical Conductivity
Large Accessibility of Active Sites
Intrinsic Pore Structure
Improves Electron Transfer

Table 13. Characteristic tables of fillers used in this study.

Polyvinylidene fluoride (PVDF polymer- cathode)
Excellent Mechanical Properties
High Dielectric strength
High Purity
Chemically and Electrically Stable
Low Volatility
Low Moisture Absorbing
Low Deformation (Creep)
High Dissipation (Energy Lost) *con
Low Glass Fiber Reinforcement (Initiates Decomposition) *con

N-Methyl-2-Pyrrolidone (NMP solvent- cathode)
Low Volatility
Low Viscosity
Polar Aprotic
Good Solvency
Miscible (mixes well) with H_2O
High Chemical and Thermal Stability
Low Surface Tension (doesn't attract particles that reduce surface area)

Table 14. Characteristic tables of cathode components used in this study.

Lithium-Iodide (LiI redox mediator- cathode)
Thermally Stable
Assists Cathode (Oxidation) during Charge
Improves Electron Transport
Reduces Overpotential of Cell
Improves Roundtrip Cycle Efficiency

Table 15. Characteristic tables of redox mediators used in this study.

VITA

MARCUS CARLTON HERNDON

EDUCATION

2016-2020	Doctor of Philosophy Florida International University Miami, Florida, USA
2014-2016	Master of Science Florida International University Miami, Florida, USA
2009-2013	Bachelor of Science Kennesaw State University Kennesaw, Georgia, USA

PUBLICATIONS AND PRESENTATIONS

Chamaani, A., Safa, M., Chawla, N., Herndon, M., & El-Zahab, B. (2018). Stabilizing effect of ion complex formation in lithium–oxygen battery electrolytes. Journal of Electroanalytical Chemistry.

Chawla, N., Chamaani, A., Safa, M., Herndon, M., & El-Zahab, B. (2019). Mechanism of Ionic Impedance Growth for Palladium-Containing CNT Electrodes in Lithium-Oxygen Battery Electrodes and its Contribution to Battery Failure. Batteries, 5(1), 15

Diong, B., Tippens, S., Francis, T., & Herndon, M. (2015, June). A New Photovoltaic Module Design Paradigm: Cell Strands That Track the Sun. In ASME 2015 9th International Conference on Energy Sustainability collocated with the ASME 2015 Power Conference, the ASME 2015 13th International Conference on Fuel Cell Science, Engineering and Technology, and the ASME 2015 Nuclear Forum (pp. V002T11A005). American Society of Mechanical Engineers.

Herndon, M. (2016). Choosin- The Game of Choices (Card Game). Copyright.

Herndon, M. “Effect of Thermal Depolymerization of Wasted Food Extracts on Alternate Fuel Production.” In ASME 2016 10th International Conference on Energy Sustainability collocated with the ASME 2016 Power Conference and the ASME 2016 14th International Conference on Fuel Cell Science, Engineering and Technology (pp. V001T02A006). American Society of Mechanical Engineers. June 2016.

Herndon, M. “Food Waste Utilization as a Viable Alternative Energy Generating Feedstock (Review).” In International Conference for Renewable Energy and Conservation. Perth, Western Australia, Australia, June 2017.

Safa, M., Adelowo, E., Chamaani, A., Chawla, N., Baboukani, A.R., Herndon, M., Wang, C. and El-Zahab, B., 2019. Poly (Ionic Liquid)-Based Composite Gel Electrolyte for Lithium Batteries. ChemElectroChem, 6(13), pp.3319-3326.